DOCTORAL (Ph.D.) DISSERTATION

HydroGIS-based watershed management using land cover mapping and hydrological modeling for urban water balance assessment

Douraied Guizani

Ph.D. candidate

Dissertation supervisor:

Prof. Dr. Attila Nagy

UNIVERSITY OF DEBRECEN

Doctoral School of Food Sciences

Debrecen, 2026

HYDROGIS-BASED WATERSHED MANAGEMENT USING LAND COVER MAPPING AND HYDROLOGICAL MODELING FOR URBAN WATER BALANCE ASSESSMENT

Dissertation submitted in partial fulfilment of the requirements for the doctoral (PhD) degree in Food Sciences

Written by Douraied Guizani, certified MSc in Agricultural Water management Engineering

Prepared in the framework of the Doctoral School of Food Sciences of the University of Debrecen

(Food Sciences program)

Dissertation supervisor: Prof Dr. Attila Nagy

The official opponents of the dissertation:

.....

.....

.

The evaluation board:

Chairperson:

.....

members:

.....

.....

.....

The date and venue of the dissertation defence:

....., 2026. .....

List of Abbreviations

Abbreviation	Full Term
LC	Land Cover
L8	Landsat 8
S2	Sentinel 2
NDVI	Normalized Difference Vegetation Index
CLC	Corine Land Cover
RO	Runoff
ET	Evapotranspiration
ET_o	Reference evapotranspiration
ETcn	Evapotranspiration for each LC class
K_c	Crop coefficients
I	Infiltration
PMM	Mean annual precipitation
RS	Remote Sensing
ML	Machine Learning
MLC	Maximum Likelihood Classification
SVM	Support Vector Machine
RF	Random Forest
T_c	Time of Concentration
DEM	Digital Elevation Model
WRS	Worldwide Reference System
TD	Transformed Divergence
JM	Jeffries–Matusita
OA	Overall Accuracy
K	Kappa index
PA	Producer's Accuracy
UA	User's Accuracy
Q	Quantity Disagreement
A	Allocation Disagreement
GE	Google Earth

List of Figures

List of Tables

Contents

1. INTRODUCTION

Water is one of the most essential natural resources, fundamental to sustaining ecosystems, driving economic development, and supporting human well-being (Michelle et al., 2021). Although water covers over 70% of the Earth's surface, freshwater especially accessible and usable forms is limited and unevenly distributed (Frank and Benon, 2016) Increasing demands, coupled with environmental pressures and mismanagement, have intensified the global water crisis (Srivastav et al., 2022). Over the past six decades, population growth, intensified agriculture, industrialization, and, most significantly, rapid urbanization have drastically increased pressure on water resources (Kintu et al., 2019). Simultaneously, climate change has changed hydrological regimes, increased the frequency and severity of extreme weather events, and created significant uncertainty in water availability and planning (Caldwell et al., 2012).

Urbanization has a significant impact on natural water-related processes in a drastic manner (Ma et al., 2009). The fact that cities are growing cause that permeable natural surfaces are increasingly replaced by impervious materials like asphalt, concrete, and rooftops (Weng and Lu, 2008). The consequences of these actions are the disruption of the water cycle through increasing surface RO, lowering infiltration, changing ET patterns, and decreasing water quality (Dams et al., 2013). The consequences are far-reaching and they may cause water scarcity, urban flooding, exhaustion of groundwater recharge, and rising of water infrastructure stress (Smerdon et al., 2009). As a result, cities face significant challenges in managing storm water, preserving freshwater ecosystems, and ensuring reliable water supply for their growing populations.

Effective water management under these dynamic urban settings requires accurate, high-resolution, and frequently updated land cover (LC) data (Banjara et al., 2024). Traditional datasets like Urban Atlas and the Corine Land Cover (CLC) provide valuable baselines but are limited by their long update cycles and low temporal resolution (Poleman, 2018). These limitations hinder timely responses to rapidly changing urban landscapes. To bridge this gap, remote sensing (RS) and Hydro-GIS technologies provide strong tools for rapid, spatially explicit, and cost-effective LC monitoring and hydrological modeling (Schott, 2002; Chemak et al., 2022). In particular, combining satellite imagery such as Landsat 8 (L8) and Sentinel-2 (S2) with machine learning techniques, such as, the Support

Vector Machine (SVM), Maximum Likelihood Classifier (MLC), and Random Forest (RF), enhances the accuracy and efficiency of LC classification efforts (Al Kafy 2023).

Additionally, RS is good for multi-temporal analysis as it allows for the detection and measurement of LC changes over the course of time (Jensen, 2000). This capability is essential in assessing the impacts of urban expansion on agricultural land and hydrological systems. They are antecedent to a thorough comprehension of the water balance components' modelling such as surface runoff, evapotranspiration, and infiltration besides providing environmental and infrastructure inputs (Qingyan et al., 2021). Introducing these changes into hydrological models hence results in an improved understanding of the effects of urbanization on the water cycle.

This is why Debrecen in Hungary, the second-largest city after the capital and a regional hub of development, is thus a representative case for LC transformation resulting from urban growth and its consequent hydrological processes (Tamás et al., 2019). Since 2018 to the present, Debrecen has seen tremendous industrial and urban development, which is evidenced by the growth of residential and commercial areas and the introduction of new manufacturing facilities (Guizani et al., 2024). Along with that came the direct conversion of agricultural and natural lands into built-up areas. The space was cleared of natural vegetation, and the new impervious surfaces caused changes in the drainage patterns, increased the flood risk, the degradation of water and soil quality, as well as the reduction of agricultural productivity, among others (Tamás et al., 2019).

Urban landscapes are an important factor in meteorological and hydrological conditions (Qingyan et al., 2021). Once within a watershed, urbanization starts to change the local microclimatic and hydrological systems of a city. LC changes, mostly through the rapid expansion of impervious surfaces such as roads and rooftops, decrease infiltration and evapotranspiration rates, and increase surface RO (Dams et al., 2013; Weng and Lu, 2008). Ramier et al. (2011) observed during a 38-month study in Nantes, France, the contribution of these surfaces to increased runoff levels. Another alteration, in surface characteristics, is closely associated with changes in hydrographic systems, either natural or man-made, if these changes raise the potentials for occurrences of flash floods and urban microclimate extremes including intensified urban heat island (UHI) manifestation (Vrebos et al., 2014; Manandhar et al., 2023). Furthermore, Al Kafy (2022) demonstrated how neural network models can effectively analyze the influence of urban expansion on

surface heat island intensity, suggesting that similar techniques could be applied to study the hydrological impacts of LC changes in rapidly urbanizing regions.

Understanding these changes requires a detailed examination of the region's watershed characteristics, especially at the sub-watershed level. Morphometric parameters like watershed shape, size, slope, and drainage density influence the hydrological response of an area (Guizani et al., 2022). Furthermore, the time of concentration the time it takes for runoff to travel from the most distant point in the watershed to the outlet is a critical factor in forecasting peak flow and flood potential(Guizani et al., 2022). By defining and analysing sub-watersheds in Debrecen, this study integrates physiographic variables and hydrological parameters into a comprehensive modeling framework, enhancing the accuracy of water balance estimation under urbanizing conditions.

Additionally, the rapid loss of crop-covered areas in Debrecen poses significant threats to local food security (Pénzes et al., 2023). The city's ability to produce fresh food is reduced as fertile agricultural lands are turned into impermeable urban surfaces (Molnár and Kozma, 2018; Iváncsics and Kovács, 2021). This research presents a multidisciplinary framework that combines LC classification, watershed analysis, hydrological modeling, and urban agriculture. The findings aim to support data-driven planning, enhance urban water management strategies, and promote sustainable food production in rapidly developing regions (Figure 1).

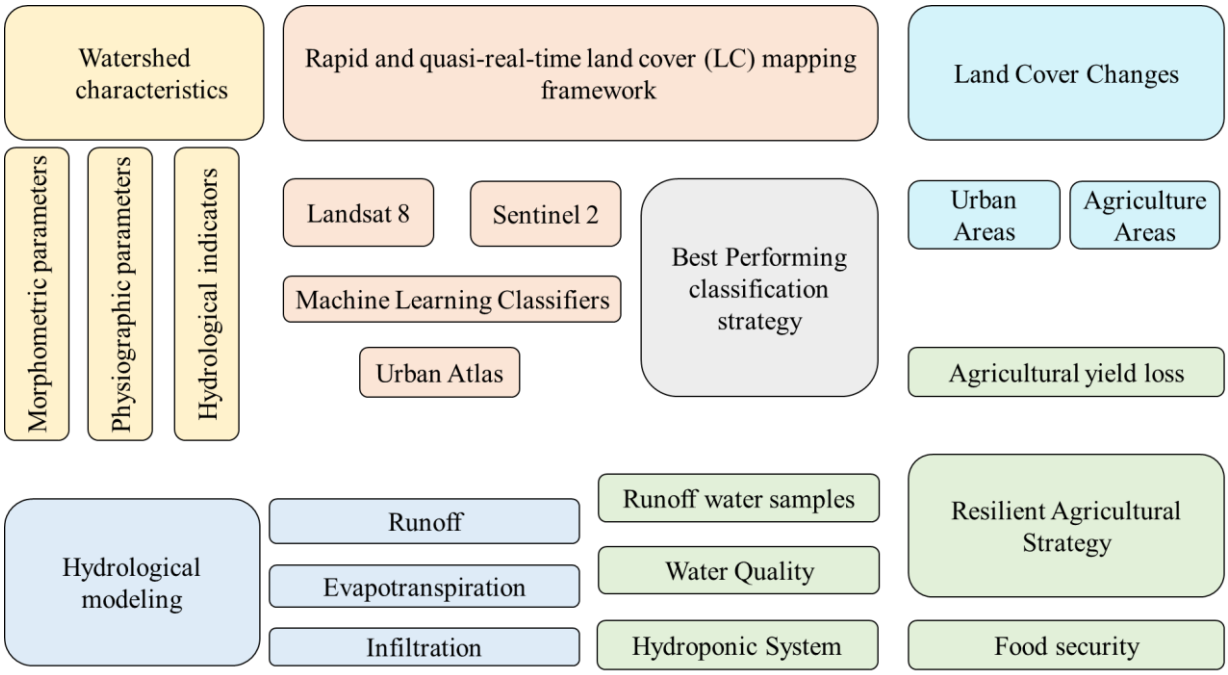

Figure 1. Overview of the research framework addressing urban hydrology, LC dynamics, and sustainable resource management (Source: Author, 2025).

In this context, the research is guided by the following aims:

1. To develop and test a robust and adaptable framework for rapid and quasi-real-time LC mapping in fast-developing urban environments, using Debrecen as a model city.
   - Design a replicable LC mapping workflow based on the MLC method.
   - Evaluate the adaptability and transferability of the proposed framework to other urban contexts.
2. To assess the effectiveness of multi-sensor remote sensing data combined with machine learning algorithms in enhancing the accuracy of LC classification in dynamic urban landscapes.
   - Investigate the contribution of multi-sensor satellite data to enhancing the accuracy and spatial detail of LC classification in urban environments.
   - Compare the performance of various machine learning algorithms and identify the most suitable classification method in enhancing classification outcomes across dynamic urban areas.

3. To develop an integrated hydrological modeling framework by assessing watershed characteristics and incorporating LC dynamics for enhanced urban water balance estimation in the Debrecen region.

- Evaluate the morphometric and physiographic attributes of the Debrecen watershed and its sub-watersheds to strengthen hydrological modeling and analysis.
- Integrate classified LC maps into pixel-scale hydrological modeling in order to refine water balance estimation temporally and spatially across urban and peri-urban landscapes.

4. To quantify LC changes and related hydrological and crop yield parameters in Debrecen, with a particular focus on urban expansion and the associated decline of agricultural areas, in response to rapid urbanization dynamics observed between 2018 and 2022.

- Conduct multi-temporal LC change detection to identify and map spatial patterns of urban expansion and agricultural land loss between 2018 and 2022.
- Quantify the extent and rate of LC transitions, highlighting the impact of urban growth on the surrounding agricultural landscape.
- Identifying yield loss due to urbanization

2. LITERATURE REVIEW

2.1 Urbanization and its effect on watershed

Urbanization profoundly alters natural landscapes and environmental systems (Caldwell et al., 2012). Driven by population growth, infrastructure development, and land use change, this complex process produces notable and frequently long-lasting environmental impacts (Srivastav et al., 2022). By 2050, 68% of the world's population is expected to reside in urban areas, up from 56% currently (United Nations, 2022). Such concentrated urban development, particularly in the developing nations, strains local ecosystems, atmospheric conditions, and water supplies, often outpacing the ability of cities to mitigate the environmental consequences (Kintu et al., 2019). (Figure 2)

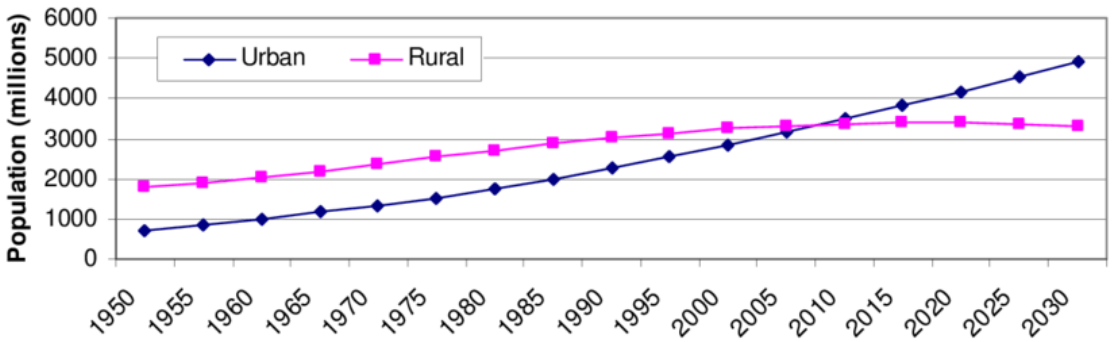

Figure 2. The world's urban and rural population trends between 1950 and 2030 (Source: UN 2005)

Urbanization has one of its biggest influences on a watershed's hydrology (Kintu et al., 2019; Bueno-Suárez and Coq-Huelva, 2020). A watershed is a natural catchment system that collects, infiltrates, stores, and conveys water through different hydrological pathways. Hydrologic pathways include evapotranspiration, surface runoff and subsurface flow or groundwater flow (Heath, R. C. 1983). These pathways depend on elements of LC, soil characteristics, climate, and terrain (Su et al., 2025). As urbanization occurs and once natural surfaces are converted to hard surfaces (concrete, asphalt and roofing), areas that were once characterized by significant infiltration now experience little to no infiltration and the likelihood of increasing surface RO (Hung et al., 2018). For example, once a watershed becomes fully urbanized, it is possible for 70% of precipitation to become direct runoff, where in forested or agricultural watersheds only 10–20% is RO (Schueler, 1997). Because of the changes made to hydrology in urban

centers, the potential for urban flooding created by RO increases as does the degree to which water quality can be degraded through the introduction of pollutants and sediments from urban RO in water bodies (Manandhar et al., 2023).

Soil sealing can significantly restrict water infiltration (movement through the ground), decreasing groundwater recharge, which is crucial for aquifers and baseflow to rivers in dry times. As groundwater levels decrease, cities are often faced with water scarcity, which is exacerbated during heatwaves or drought (Banjara et al., 2024; Mengistu et al., 2022). To combat this, many cities are now implementing solutions using green infrastructure, looking to restore some level of natural hydrological function (Corrigan, 2023). Cities are increasingly implementing strategies utilizing green roofs, rain gardens, bioswales, and permeable pavements (and many other strategies and systems). These systems allow for better infiltration while lowering urban temperatures, improving air quality, and increasing biodiversity (Liao et al., 2017).

Figure 3. Sustainable Urban Drainage Solutions for Resilient Cities. (Source: EPA, 2020)

ET is an additional important facet of the hydrological cycle that modifies in response to urbanization (Bueno-Suárez and Coq-Huelva, 2020). Urbanization moves vegetation

from areas and potential ET is reduced with a corresponding loss in the land's ability to return moisture to the atmosphere, thus, changing local humidity and temperature patterns (Gaffin et al., 2006). These changes help intensify the UHI effect (Lee et al., 2017). An UHI occurs when urban areas reach temperatures much higher than their rural counterparts, caused by the basic principles of heat retention by artificial surfaces and the loss of ET (Zhang et al., 2023). The UHI can alter local climate dynamics, increase energy loads for cooling, increase smog formation, and exacerbate heat stress in urban areas, especially for vulnerable populations (Liu et al., 2021; Parsons et al., 2021; Wu et al., 2025). In cities such as Phoenix and Los Angeles, the UHI intensity can be over 7°C in the evening (Brazel et al., 2000). Further, in cities like Tokyo and Seoul urban core locations demonstrate average temperature differences of 3–5°C over adjacent rural areas, during the warmer summer months (Choi et al., 2014). The microclimatic changes associated with UHI can also affect atmospheric circulation, precipitation, and thunderstorm events. Urban areas can trigger localized convective storms, and studies in Guangzhou, China, and São Paulo, Brazil, have recorded up to 10–20% increases to rainfall (urban rain) against surrounding rural areas (Jimenez et al., 2025).

The urban form and spatial layout are fundamentally important and impact urban hydrology and microclimate. For instance, high-density, high-rise cities (Hong Kong, Singapore) experience a different microclimatic effect than low-density, sprawling metropolitan areas like Houston and Atlanta (Yong and Lim, 2020; Wong et al., 2022). Singapore is a prime example of sustainable urban design and development. The city-state has numerous and integrated metrics of green infrastructure, from rooftop gardens to vertical and climbing forests, to park networks to adapt to UHI effects and manage storm water (Wong et al., 2022). Informal and rapid urbanization in cities such as Kinshasa and Peshawar has created significant environmental challenges because of poor planning, limited storm water drainage, and poor vegetation cover.

Urbanization poses historical and contemporary problems in Central Europe. While the growing speed is slower than in the Global South, post-socialist cities are transforming with new land uses changed and urban forms in the last thirty years (Aalbers et al., 2023). In Hungary, urban areas represented no more than 72% of the population with major cities of Budapest, Szeged, and Debrecen undergoing dynamic LC changes (Szilassi, 2017; Kovács et al., 2019).

Urban LC change has consequences for more than local climate. It affects flood regime, water quality, urban habitability and resilience to extreme weather (Caldwell et al., 2012). Thus, productive future urban sustainability planning consistently integrates LC monitoring, RS, hydrological modeling and urban planning. Initiatives such as the Tisza River Project, which captures the precise relationship between hydrology and spatial complexity to create innovative climate adaptation strategies for cities in Hungary, represent practical examples of this approach (Lóczy et al., 2009; Tamás et al., 2019). This experience from Debrecen adds to a wider understanding, common to cities across Europe, that retaining green space, sustainable drainage, and integrated situational adjustments, can help to eliminate or mitigate broadly the negative effects of urban LC change on watershed function or microclimate (Qingyan et al., 2021). As cities grow on global and regional scales, we need to understand the connections between urban expansion, hydrological change, and microclimate change not only as a matter of academic inquiry but as a necessary underpinning to design livable, climate-resilient cities (Rahman et al., 2022; Ramier et al., 2011). In prime examples of high-density, vertical urbanism (Singapore) and expansive, horizontal practices (the suburban experience of Central Europe), the insights of urban hydrology and LC change need to be shifted into practical applications of planning, policy reform, and infrastructure development that promote ecological harmony, human health and wellness, and ultimately sustainability for the future (Mudereri et al., 2023; Shi and Li, 2021).

2.2 LC Classification in Urban Environments

Urban planning and environmental monitoring have also used LC classification, especially in light of growing urbanisation and its effects on water resources (Weng and Lu, 2008). Accurate and updated LC data is necessary for spatial processes, environmental change assessment, and effective planning for sustainable land and water resource management (Mengistu et al., 2022). Over the past few decades, LC data collection, processing, and analysis have advanced significantly, providing information that is temporally consistent, spatially continuous, and economical (Zhao et al., 2023; Banjara et al., 2024).

Accurate LC data are vital because hydrological parameters: RO, infiltration, and ET, are directly derived from LC classes. Studies show that LC errors can significantly distort hydrological outputs, underscoring the need to link LC accuracy with model reliability.

Urbanization further amplifies this sensitivity, with projected stream flows varying from a 26% increase to a 16% decrease, indicating greater extremes and potential impacts on human and natural systems (Botero-Acosta et al., 2025).

Having high to moderate spatial resolution, multi-spectral perception, and frequent visits; the S2 and L8 are the two most significant of the several RS systems. Furthermore, the L8 offers multi-temporal LC studies due to its temporal stability and wide monitoring ability of large areas of interest with 30-meter resolution and 16-day return interval (Roy et al., 2014). Given its 5-day return period and 10- to 20-meter resolution, objects being changed on a fine scale, especially in a variety of urban settings, could be monitored using S2 data (Acharki, 2022). They provide a medium for researchers to observe LC changes, which can be traced, monitored, and classified, particularly those changes that include urbanisation, industrialisation, and conversion to farmland (Basheer et al., 2022).

To interpret imagery from satellites and create LC maps, a variety of classification techniques have been applied. Because of their accuracy and adaptability, machine learning techniques including SVM, RF, and MLC are frequently employed (Belgiu and Drăguţ, 2016). Research has shown that SVM performs well with limited training sets and big-dimensional data, which is useful in urban settings where spectral overlap across classes is frequent. As an ensemble learning technique, RF can manage big datasets while avoiding overfitting (Adugna et al., 2022). Despite being a more conventional statistical classifier, MLC is nonetheless appropriate given its simplicity and probabilistic character, especially in cases when class distributions are widely separated (Talukdar et al., 2020).

In LC classification, selecting and evaluating training data as well as assessing classification accuracy are very important processes. To demonstrate the reliability of classification results, metrics such as Overall Accuracy (OA), Kappa coefficient (K), F1 score, and disagreement measures (Quantity Disagreement and Allocation Disagreement) are required (Pontius and Millones, 2011). In order to assess distinction of LC classes during training and improve classification performance, spectral separability indices like Transformed Divergence (TD) and Jeffries-Matusita (J-M) distance are applied. (Jensen, 2000).

The importance of LC classification in urban hydrological modelling and water planning has been highlighted by recent studies. Accurate LC maps are essential for calculating important hydrologic parameters such as R, I, ET, and storage (Zhu et al., 2016). RS for

LC classification is a helpful addition to process modelling and supports policies related to urban resilience, water conservation, and climate adaptation (Zhou et al., 2022).

Additionally, by monitoring the spatiotemporal dynamics of urban growth and LC change, multi-temporal LC analysis provides researchers with deeper understanding of the causes and consequences of these changes. More understanding of the interaction between water and landscape in urbanising areas can be gained by merging LC data with datasets on precipitation, soil moisture, and topography (Mengistu et al., 2022; Banjara et al., 2024).

Therefore, RS based LC classification is a valuable tool for environmental change assessment, particularly in the urban hydrological interface. Advances in satellite technology and classifier methods continue to enhance our capacity to monitor and model urban expansion and its implications for water management. Using the potential of satellites such as L8 and S2, combined with robust classification algorithms and accuracy assessments, ensures that decision-makers and researchers are equipped with the spatial intelligence necessary to guide sustainable development and mitigate the negative impacts of urbanisation on water systems.

2.2.1 Machine Learning in LC Classification

The integration of machine learning (ML) techniques into LC classification has significantly enhanced accuracy, scalability, and automation in RS applications. These techniques offer adaptive, data driven approaches that can learn sophisticated patterns in spectral data, particularly in heterogeneous environments such as cities. Among the most widely applied techniques in RS are SVM, RF, and MLC, with varying strengths and weaknesses.

- **Support Vector Machines (SVMs)** serve as robust supervised learning tools that are optimized for classification problems. Nonetheless, SVMs are also used to analyze regression and classification problems. SVM main focus is to find an optimal hyperplane (or decision boundary) that clearly separates the LC classes, while minimizing the number of classification errors, in a high-dimensional feature space. In order to achieve this goal, SVM has to maximize a margin (area distance) that is the distance between this hyperplane and the nearest data point (the support vectors).The idea is to ideally maximize this

margin/area, as it can improve the overall performance of the classification (Deilmai et al., 2014; Talukdar et al., 2020) (Figure 4a).

- **Maximum Likelihood Classification (MLC)** is a probabilistic method. MLC relies on statistical theory, and it assumes the spectral data for each LC class is normal in the feature space (Deilmai et al., 2014). Using Bayes' theorem, MLC assigns a pixel to the class option that has the greatest probability resulting from the statistical properties of the training samples (Norovsuren et al., 2019) (Figure 4b).
- **Random Forest (RF)** is an ensemble ML algorithm that generates predictions through the aggregating the predictions of a number of decision trees (Breiman, 2001). Each tree is built using a random sample of the dataset and features, leading to a heterogeneity of classifiers that collectively enhance model robustness and generalization (Figure 4c). When classifying a new data point, it passes through all trees, and the majority class predicted by all trees becomes the final output (Pal, 2005; Xie et al., 2019).

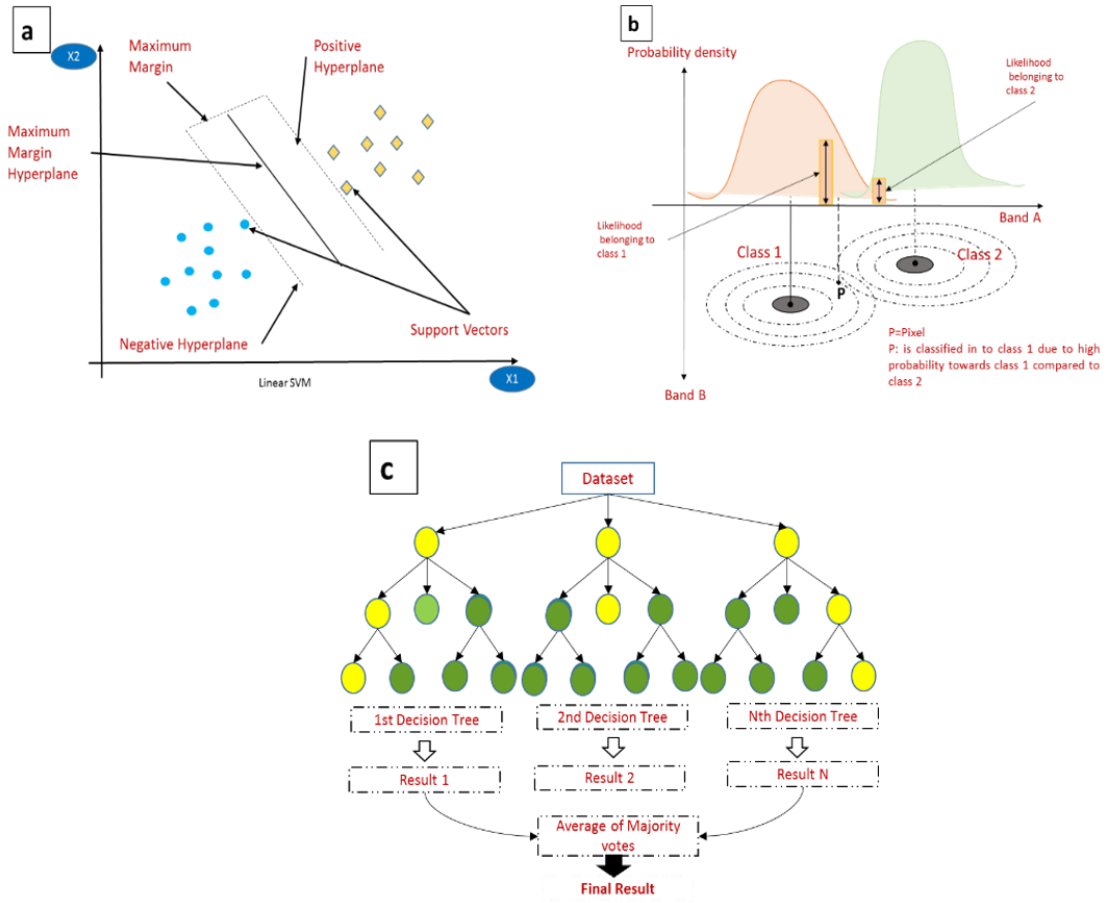

Figure 4. (a) Conceptual diagram of the SVM algorithm depicts the optimal hyperplane and support vectors; (b) MLC based on probability density functions is illustrated; and (c) schematic diagram of the RF algorithm (Source: Author, 2025).

2.2.2 LC Change Detection and Urban Expansion

Urbanization has an enormous effect on LC patterns, fundamentally changing hydrologic processes and urban water management systems. As urban areas expand, there is an increase in impervious surfaces, a loss in vegetative cover, and an increase in industrial and housing activity. Natural hydrologic functions, including I, ET, and groundwater recharge are changed. Understanding and detecting LC change is critical to determine the effects of LC change on hydrology, especially in urban areas that are rapidly growing.

Urban sprawl is the horizontal expansion of built-up areas. When urban areas sprawl often occurs at the expense of natural vegetation, agricultural lands, and water bodies. Under these changes, urban flooding risks will increase and water scarcity and water quality concerns will worsen (Liu et al., 2018). Rapid and unplanned urbanization in metropolitan areas, like Shanghai and lagoons, has been linked to frequent flood events and dropping

water table levels in these growing region, caused by impermeable surfaces and natural drainage lost.

Industrialization, often occurring alongside urban expansion, poses additional challenges to urban water systems. The establishment of industrial zones contributes to point and non-point source pollution, with harmful effluents entering rivers, streams, and groundwater reservoirs. For example, the development of industrial estates and factories in places like Debrecen has increased the pollution load of surface waters, which includes values for nutrients, heavy metals, and organic contaminants (Kovács 2011; Kovács et al., 2019). Pollution from urban and industrial development alters levels in a way that not only threatens life in aquatic environments but the pollution impacts the water quality for human consumption, agricultural production, recreation, and other uses. Integrated urban planning that accounts for industrial impacts is therefore essential for maintaining hydrological and ecological balance.

Urban green spaces offer vital ecosystem services, which are reduced significantly when vegetated areas converted to impervious surfaces. Vegetation is critical for I, ET, biodiversity, and microclimate maintenance. When vegetative areas are lost, urban water storage capacity decreases and the UHI effect becomes exacerbated, which further modifies local atmospheric moisture dynamics and influences rainfall patterns (Lauer et al., 2023). Green infrastructure, such as urban parks, permeable pavements, green roofs, and retention basins, can mitigate these effects by reinstating the important hydrologic functions and overall resilience for urban consequences of climate extremes.

RS techniques, particularly multi-temporal satellite imagery and ML classification techniques, have become essential for detecting LC change in urban areas. Comparing both despite classification change, and change vector analysis have allowed for robust analyses and quantitative understanding of LC change spatially and temporally (Johnson et al., 1998; Zhang et al., 2021). These results provide important data necessary for urban hydrological modeling, and water management planning and assessment for environmental effects.

2.3 Hydrological Modeling in urban areas

Hydrological modeling is critical at the watershed scale for understanding and managing water resources given LC changes, climate change, and urban growth. Hydrological models describe processes like surface runoff (R), infiltration (I), and evapotranspiration (ET) and can help understand water availability, flood risks, and ground water recharge. Accurate and up-to-date modeling has become increasingly important throughout urbanization, including consideration of declining water tables, increasing water demand, and altered hydrological cycles. Several hydrological models have been widely adopted in watershed-scale assessments:

- SWAT (Soil and Water Assessment Tool): For long-term watershed simulation, this semi-distributed model works especially well in mixed-land use and agricultural environments (Gassman et al., 2007).
- WEAP (Water Evaluation and Planning System): An integrated water resources planning tool that integrates demand analysis and water allocation (Bañares et al., 2024).
- HEC-HMS (Hydrologic Engineering Center Hydrologic Modeling System): A widely used model for simulating runoff-precipitation interactions, particularly in urbanised basins (Guduru and Mohammed, 2024).

The models performance is largely founded upon the accuracy of provided inputs. These include knowledge of current LC maps, soil detections, meteorological records and topography. High resolution remote sensing (RS) data provided from sources such as S2 and L8 allow us to update LC classifications without significant lag time. These classifications directly inform our hydrological predictions. Furthermore, the last decade has made significant gains with machine learning (ML) and object based image analysis to improve the accuracy of LC mapping. Thus we have made more spatially explicit hydrological models that are pixel based (Kim et al., 2022).

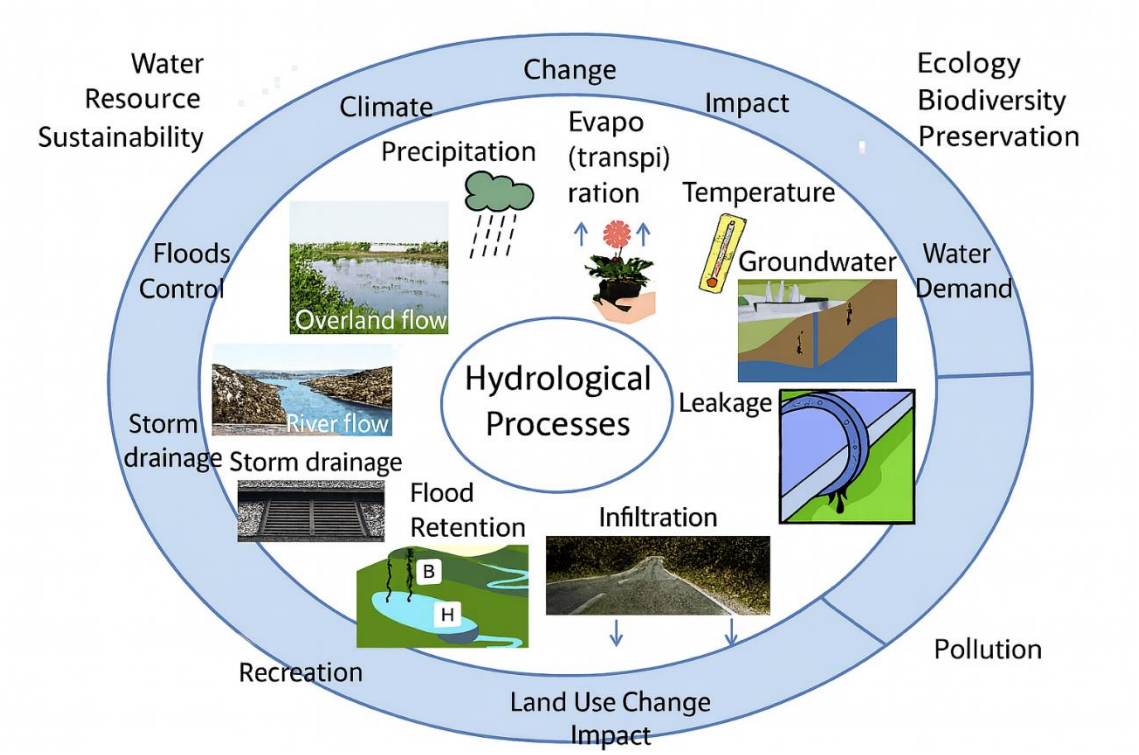

Figure 5. Integrated Hydrological Processes and Water Sustainability Framework (Patle, P., and Sharma, A. 2025)

Urbanization tends to increase impervious LC which changes natural hydrology. For example, Jakarta, Indonesia is seeing land subsidence of 20 cm a year because of excess groundwater extraction to meet increasing urban water demand. This is contributing to extreme flood risk. Partly related to this issue, in Telangana, India, although over 75 mm of rain fell in April 2025 (over the seasonal average), the groundwater levels remained alarmingly low at about 20 meters below ground level. The situation in Telangana was attributed to short duration, high intensity precipitation events, deforestation, and over-extraction driven by urban growth (Wakode, 2018).

The complex relationship between natural systems and human alterations is increasingly understood and predicted with the use of hydrological models. In the Pu River Basin, China, the hydrological model HEC-HMS was used to assess the impact of urbanization, with results revealing significantly greater peak discharge and increased flood risk due to changes in the runoff process (Zhang et al., 2023). In a second study of Xiamen City, China, the WEAP model was used to assess water supply/demand from 2015 to 2050, taking population growth, industrial changes, and climate variability into account. The study highlighted a need to develop long-term water sustainability models through

hydrological modeling of urban planning to safeguard water in the future (Kou et al., 2018).

Similar examples are present throughout Europe, for example using HEC-HMS modeling in the Wirynka River catchment in Poland to identify the effects of the suburbanization process on flooding and flow patterns. In Pakistan's Central Indus Basin, WEAP modelling provided useful information around potential water futures when assessing the impacts of growth and climatic change. The model found that if no action is taken, water demand could be greater than supply by 40% by 2050 (Asghar et al., 2019).

Urbanization alters both large-scale hydrological shifts, but it also affects localized hydrological performance metrics such as time of concentration (Tc), which is defined as the time it takes for water to travel from the farthest point in the watershed to the outlet. Tc is an important parameter in stormwater design, and urbanization can drastically reduce a watershed's Tc via impervious surfaces, which may increase flash flood potential (Welle and Woodward, 1986). Initially, empirical models, which are based on the NRCS curve number or Kirpich equation, were used in urban settings, but now there has been more use of spatially distributed data inputs, like slope gradient, and high-resolution LULC inputs to make the models more applicable in urban watersheds (Mehta et al., 2022).

Morphometric analysis of watersheds is also vital in hydrologic modeling because it quantifies their physical characteristics, such as drainage density, bifurcation ratios, and slope, to identify hydrologically sensitive areas and assess vulnerability to erosion, sediment transport, and floods (Bashar, 2023). In rapidly urbanizing sub-watersheds, it helps locate areas of infrastructure development that interfere with slope-driven flow regimes, or exacerbate hydrological hazards (Benzougagh et al., 2022).

LC dynamics is especially vital to quantify infiltration capacity, ET, and runoff in urban areas. Using pixel-based modelling approaches with LC maps, soil variables, slope, and meteorological variables, all with a spatial resolution at the pixel level, cities can begin to predict hydrology in a more localized way (Grimmond et al., 2010). Planners can quantify the hydrological changes related to the change in LC (impacts, directly and indirectly to LC change) and specify nature-based alternatives, or solutions in relation to land development and land use changes, like green infrastructure, or rainwater harvesting systems. Hydrological modeling provides the scientific foundation that gives a broader

overview of how to manage the impacts happening on water resources from accelerated urbanization. While there are multitude tools to test and simulate yield losses due to accelerated urbanization. There are examples all over the globe in many world cities - think Jakarta and its subsidence or India's groundwater crisis; the demand for spatially-explicit dimensions of water management is not going away. As urbanized land continues to expand and climatic variability becomes a constant, an enhanced understanding of the spatial-temporal relationships between, and effects of, LC and the hydrological cycle will hold more prominent value for reducing water scarcity, reducing flooding, or general sustainable development management (Elmqvist et al., 2013).

2.4 Alternative water resources and utilization of run off

The increasing stress on global freshwater resources from population growth, climate change, and urbanization increases the need for other water resources critical to maintain agriculture and food production in regions already experiencing water stress. These resources include treated wastewater, rainwater harvesting, greywater reuse, and desalinated water to close the loop in the water cycle and recycle water in urban areas where water is highly demanded and freshwater supplies are being overexploited. According to the Food and Agriculture Organization (FAO), approximately 4% of global irrigated land is presently irrigated through non-conventional sources such as treated wastewater and harvested rainwater, with expected increases as the demand on freshwater intensifies (FAO, 2020). In the Middle East and North African (MENA) region, more than 15% of irrigation water is sourced from alternative sources due to long-term water stress (Qadir et al., 2020). Urban agriculture is increasingly reliant on or suitable for these unconventional water sources to develop sustainable agricultural production.

Figure 6. Alternative Water Resources for Sustainable Water Management (Source: Author, 2025)

Urban agriculture has gained increasing attention as a sustainable strategy to address food insecurity, environmental degradation, and water scarcity within city settings. Among the methods utilized, hydroponics a soilless technique of growing plants has proved extremely efficient in the conservation of water and maximization of yield for growing in spatially constrained and soilless urban environments. Hydroponic systems provide a nutrient-water solution directly to the roots of plants, affording the grower complete control of growing conditions with minimal water loss due to evaporation and drainage. Hydroponic cultivation also requires 90% less water than traditional farming has a significantly higher productivity per square meter (Barbosa et al., 2015; Resh, 2013). For this reason, hydroponics could be extremely suitable for urban food production in areas where growing conditions are negatively affected by climate change-induced water stress.

As part of improving sustainability, treated wastewater (especially greywater from domestic use) can be used as a substitute irrigation method and water source in hydroponic systems. Treated greywater can be a nutrient-rich, safe, and plentiful water source when it is adequately treated, which lessens the demand on municipal supplies. Cities such as Tunis and Amman have conducted pilot-scale urban agriculture projects using treated greywater, and they provide good indications of productivity and water conservation (Paranychianakis et al., 2015). However, the monitoring of water quality and nutrient levels is critical to avoid contaminants entering the plants.

Therefore, linking hydroponics with urban runoff reuse systems, such as rainwater harvesting, can further promote sustainability and resilience in urban agriculture. Rainwater harvesting involves capturing and storing rainfall that lands on rooftops and other impervious surfaces and is utilized as a decentralized source of non-potable water for irrigation and household use. When rainwater is used in hydroponic systems, it has many advantages, such as less reliance on the municipal water system, increased reduction in stormwater runoff, and flooding control in urbanized areas (Campisano et al., 2017). In Melbourne, Australia and Berlin, Germany, urban rainwater harvesting has been linked to rooftop farming and community gardens with the aim of fostering sustainable food systems, increasing biodiversity, and limiting the UHI effect (Specht et al., 2014; Fletcher et al., 2015).

At the Nyírbátor experimental site, the lack of available natural surface water necessitates the use of alternative water resources. Such sources include excess water from adjacent

agricultural fields, treated fermentation sludge, and treated wastewaters. All these three sources are collected and transported to the common water reservoir having a total volume of 114,000 m^3 (Figure 7).

Figure 7. Main Water Reservoir for Storing Alternative Water Resources at the Nyírbátor Site (June 2025) (Source: Author, 2025)

The site has developed a strategic management system with the aim of optimizing the utilization of these alternative resources (Figure 8).

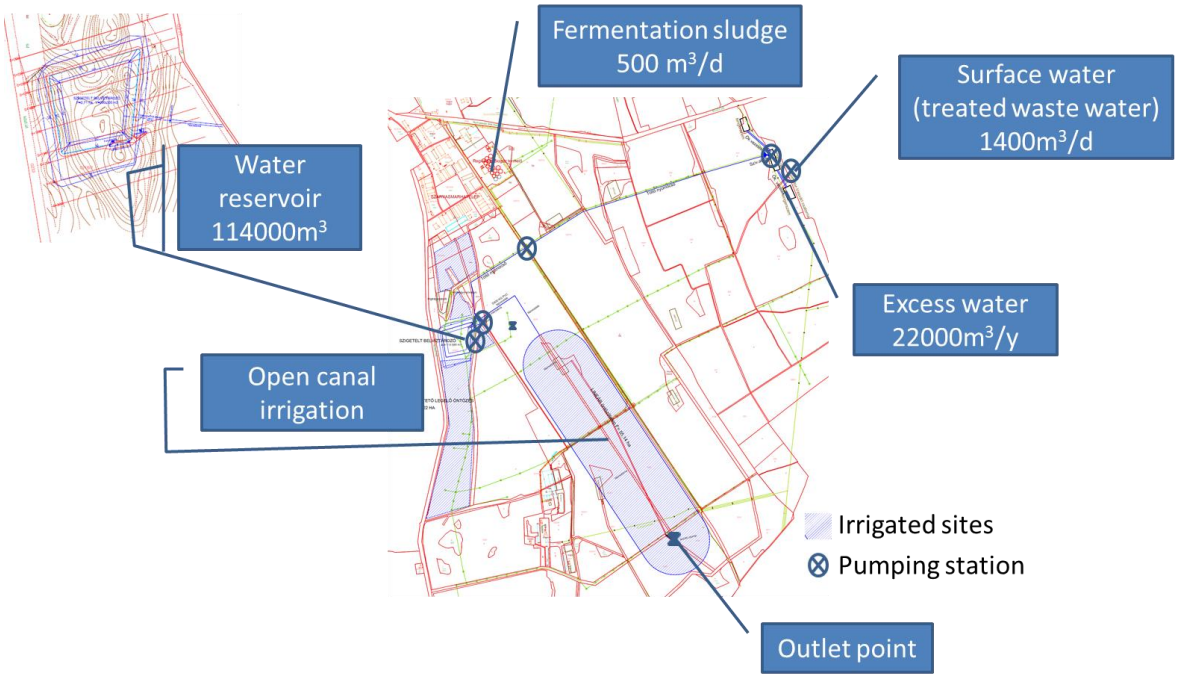

Figure 8. Strategic Management System of Alternative Water Resources at the Nyírbátor Site (Source: Author, 2025)

Excess water is primarily collected during early springtime, depending on seasonal conditions, from nearby agricultural lands. It is temporarily held in three surface reservoirs, with the annual volume of water that could be collected potential ranging between 10,000 and 30,000 m³. From this main central reservoir, water can be transferred further and pumped into the insulated storage reservoir for either irrigation or experimental use (Figure 9).

Figure 9. Irrigation System Pumping Water from the Reservoir to Agricultural Fields (May 2025) (Source: Author, 2025)

This type of integrated water management is a good example of sustainability in addressing water scarcity by creatively using available local resources.

This integrated strategy also advances the collective agenda of urban hydrological management by repurposing surplus runoff, commonly seen as a waste, as an asset towards developing localized food systems and green infrastructure. The reuse of urban runoff and treated water in hydroponics also allows for incorporation of nutrients and water to close the loop of urban metabolism, which is an important pathway to determining more circular and self-sufficient cities.

In addition to their environmental advantages, these systems also provide significant social and economic benefits. The systems are possible to become used in community gardens, schools, and homes to encourage local food production, provide food security, and decrease the reliance on long supply chains. It is also a significant opportunity for decreasing household water bills meaning more water is able to stay within the household and improving urban climate by increasing vegetation cover to cool an area to provide a heat buffer from the UHI effect, far away from traditional engineering solutions. Community-led hydroponics projects, possible through alternative water sources, develop to educational and capacity building locations of practice where the residents are

fully engaged in practicing sustainability and led to create a degree of ownership and responsibility towards the environment. The hydroponics systems facilitate this type of environment and are especially useful in low-resource or low-income contexts, thereby facilitating community development by increasing access to fresh produce and building resilience to socioeconomic and environmental stressors (Zhang et al., 2019; Specht et al, 2014).

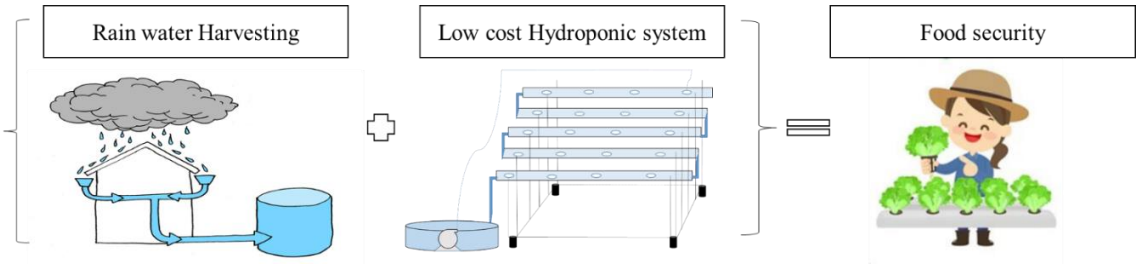

Figure 10. Rainwater Harvesting and Low-Cost Hydroponics for Food Security (Source: Author, 2025)

From a systems viewpoint, hydroponic systems, rainwater harvesting and runoff management, concomitantly exhibit a circular urban metabolism, by integrating and reinforcing productive loops from waste streams, for example, storm water, and treated greywater. It has implications for sustainable management of food and water, sustainable urban development, biodiversity enhanced, and adaptive capacity to climate change.

As cities grow rapidly and the area covered by impervious surfaces increases, the combination of LC based hydrological modeling with alternative urban farming techniques provides an opportunity to reduce environmental impacts while still allowing critical functions of a city to occur (McClintock et al., 2018). As cities continue urbanizing, and having pressured water and food resources, these integrated strategies can pave the road toward sustainability, equity, and integrity of the urban ecosystem. Cities like Cape Town (South Africa), Tunis (Tunisia), and Los Angeles (USA) are experimenting with urban agriculture systems enabled by treated and harvested water, where resource limitations are prompting unique innovations and resiliency.

According to Mougeot (2000), everything can almost be considered urban agriculture because it includes an enormous number of food or non-food production activities within the urban ecosystem. Therefore, urban agriculture, besides being a food security strategy, is pertinent for environmental quality and for building community resilience.

Figure 11. Aeroponic System Installed at the Institute of Water and Environmental Management, Faculty of Agricultural and Food Sciences and Environmental Management, University of Debrecen (Source: Author, 2025)

Urban farming plays a major role in food security, especially in low-and middle-income countries trained on data up to October 2022 by which buffer it helps households with nutrition and reduces reliance on food coming from outside the house (Zezza and Tasciotti, 2010). As urban farming promotes income and jobs especially around marginalized populations, women, and youth it also supports urban sustainability with environmental benefits such as carbon capture and storage, urban microclimate modification, storm water management, and biodiversity (FAO, 2014; Orsini et al., 2013). From a social sustainability position urban agriculture establishes a community and learning opportunity and subsequently mental health benefits, thus comes to influence urban living. Urban agriculture also contributes to more resilient urban food systems themselves as they shorten supply chains and lessen vulnerability to external shocks in global food supplies as demonstrated by the COVID-19 pandemic (Pulighe and Lupia, 2020).

Urban farming, however, can run into unavoidable difficulty with things like insecure tenure, competition for urban land, potential contamination from pollutants in soil or water, and limited access to resources such as water, land, capital and labour (Dubbeling et al., 2010; Hamilton et al., 2014). The integration of urban agriculture into many city planning processes is still wanted, but absent in most regions and institutional supports, such as policy mechanisms and instruments, are inconsistent. On the positive side, in recent years, there is an unprecedented level of collaboration among policy-makers, planning departments, institutional developers, food system researchers, non-profit organizations, and community organizations. Recent advances in remote sensing and GIS technologies, offer opportunities to facilitate land suitability analyses and monitor urban

agriculture while providing a new approach for data-informed decision making and spatial planning (Orsini et al., 2013).

3. MATERIAL AND METHODS

The methodological framework adopted in this study integrates spatial, climatic, hydrological, and remote sensing datasets to characterize land cover dynamics and assess their implications for urban water balance and agricultural productivity in Debrecen. The workflow begins with a detailed description of the study area (covering climatic, landscape, soil, and hydrographic characteristics) followed by watershed parametrization to establish the hydrological context. A rapid and quasi-real-time LC mapping framework was developed using the MLC method, complemented by machine learning algorithms for enhanced classification accuracy. Training datasets, validation procedures, and accuracy assessments were systematically implemented. Furthermore, an integrated tool was developed to compute hydrological coefficients essential for improving urban water balance estimations. Finally, LC change detection techniques and crop yield analyses were applied to evaluate the impacts of urban expansion on surrounding agricultural areas. The overall workflow is illustrated in Figure 12

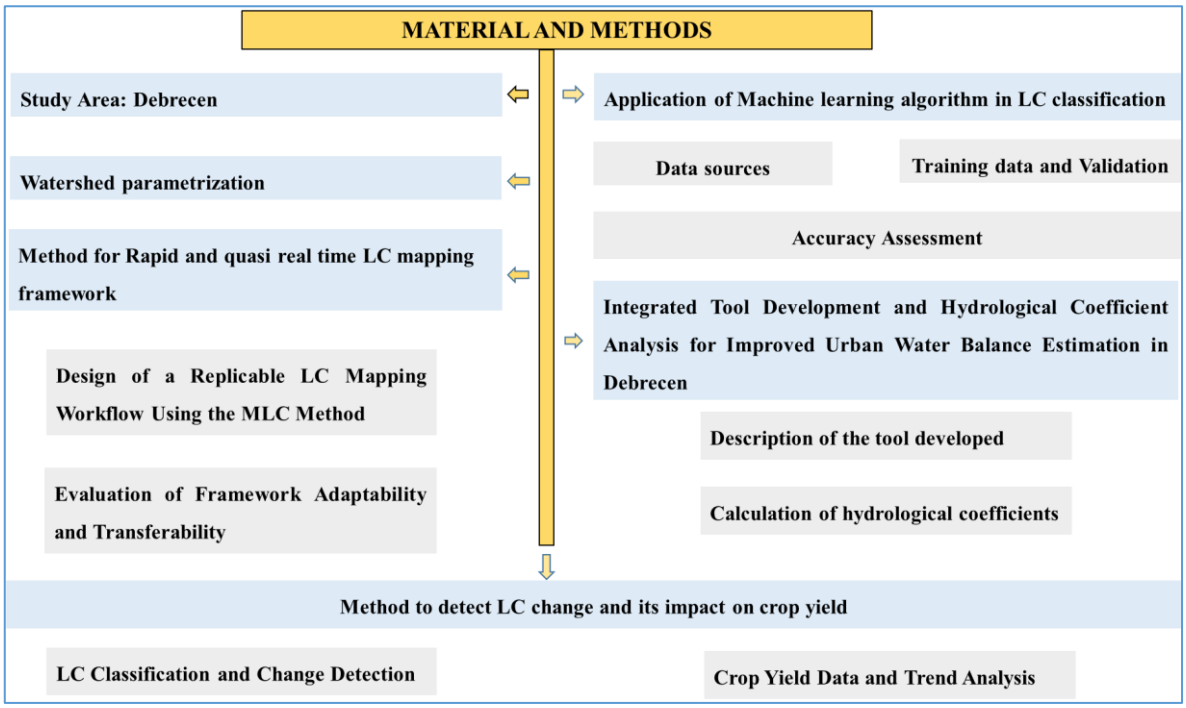

Figure 12. Workflow diagram for the Material and Methods structure (Source: Author, 2025).

3.1 Study Area

The second-biggest city in Hungary is Debrecen. It is home to between 203,000 and 207,000 people and has a total area of 461.25 km². According to urban development plans,

the population is expected to increase by 30,000 to 50,000 people by 2050 (STRATEGY 24). The Northern Great Plains region's regional capital, Debrecen, is located close to the EU's eastern border (Molnár and Kozma, 2018; Tamás et al., 2019). A medium-sized city, Debrecen serves as the commercial, cultural, administrative, and educational centre of eastern Hungary (Tamás et al., 2019).

In the past five years, over 1200 hectares of new industrial land have been allocated in Debrecen (Southern Industrial Park, North Western Economic Belt), where further development of the infrastructure is proceeding rapidly (Molnár and Kozma, 2018).

In the upcoming years, it is anticipated that the LC of dozens of hectares will alter. After the capital's constant expansion, Debrecen boasts Hungary's largest growing office capacity. In the same direction, the city's industrial parks are expanding in both area and diversity (Kozma and Molnár, 2018), leading to rapid development. The city's terrain and environment are dualistic, with large forest regions in the northeast and east and dense agricultural areas in the west. This distinction is what defines Debrecen's green space system.

The northern borders contain an important part of the forested lands. The city's dispersion is a result of Debrecen's substantial suburban and periurban population growth over the past few decades (Pénzes et al., 2023). The quick changes in Debrecen's hydrology are also a result of these processes. Furthermore, since 2019, significant LC alterations and other notable changes have been initiated as a result of intense industrial investments that have affected several regions of the city (Iváncsics and Kovács, 2021). Many of these transformations involve large water and labour-intensive automotive and battery industry developments, which significantly influence employment and contribute to population growth. Due to these significant LC and resource demand changes which have been still in progress, we targeted to define the temporal frame of this study between 2018 and 2022 when the changes in LC were dominant.

3.1.1 Climatic conditions

Analysis of a 29-year meteorological dataset (1991–2022) indicates that the hottest years occurred after the year 2000, with 2011 and 2012 being the two hottest years in the last decade of the previous century (Szalai et al., 2005). The climatic dataset was obtained from the NASA POWER Data Access Viewer (https://power.larc.nasa.gov/data-access-viewer/), an open-access meteorological database that provides daily records of low, high,

and mean temperatures, as well as solar radiation, relative humidity, wind speed, and sunshine duration. The period 1991–2022 was selected because NASA POWER offers continuous, homogenized, and quality-controlled climate observations for Debrecen starting from the early 1990s, ensuring a complete and consistent time series suitable for long-term climatic trend analysis. Debrecen's long-term average monthly temperatures from 1991 to 2022 show that August is the warmest month and January is the coldest. 22.7 °C is the average yearly temperature fluctuation (Figure 13a). Debrecen experiences a humid continental climate, with precipitation occurring throughout the year, even during the driest months. Among the climatic factors, precipitation has the largest variations. Between 1991 and 2022, the region recorded an average rainfall of 546 mm for each year. The minimum precipitation generally develops during the months of January to March, while precipitation from May to July exceeds twice as much as that in the dry months. The annual average global radiation reaching an elevation between 2001 and 2022 was measured at 4,631 MJ/m². Therefore, the maximum value appears in June and July, with more than 680 MJ/m² in July, whereas December and January have minimum values, with an approximate average of 100 MJ/m² per month (Figure 13b).

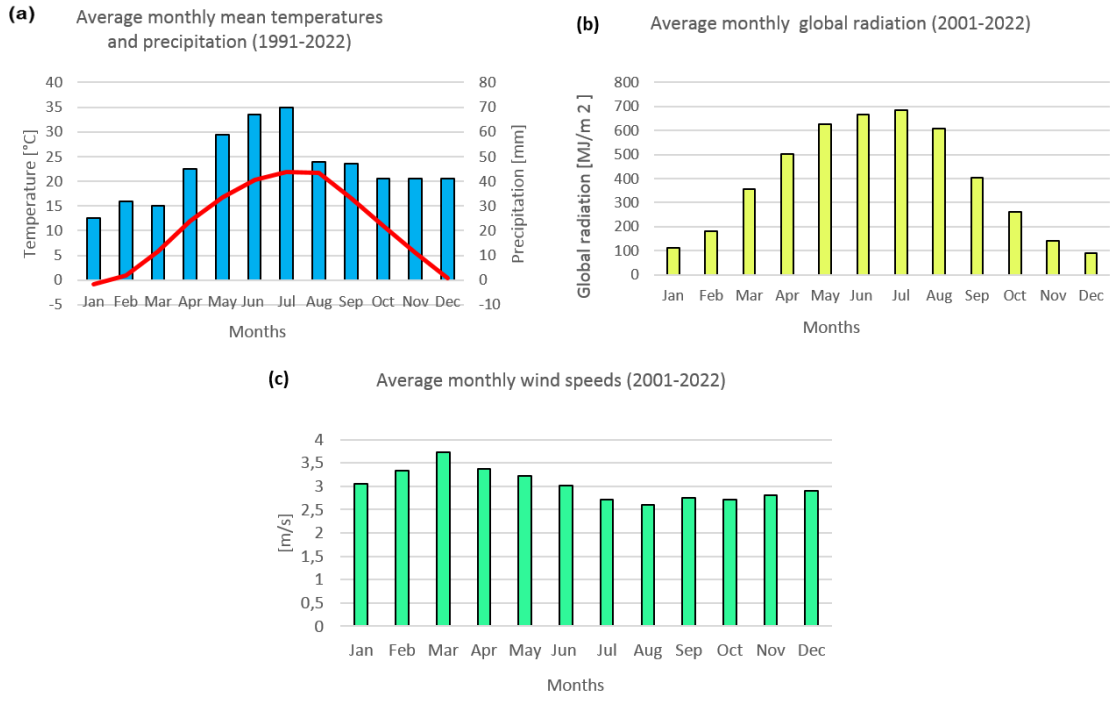

Figure 13. Climatic characteristics of Debrecen: (a) Average monthly temperatures and precipitation totals (1991–2022), (b) Average monthly amounts of global radiation values (2001–2022) and (c) Average monthly wind speeds (2001–2022) (Source: https://power.larc.nasa.gov/data-access-viewer/).

The average annual wind speed in Debrecen is 3.03 m/s. With an average of 3.71 m/s in March and the lowest recorded value of 2.62 m/s in August, the wind speed distribution throughout the year is characterised by a spring maximum (Figure 13c). Wind direction is predominantly from the northeast, accounting for 21% of occurrences, while the second-highest relative frequency is from the south (18%).

Debrecen provides useful examples of its relationship between urban city, microclimate and watershed processes, as the city folios pronounced spatial heterogeneity of LC, and urban form. The central districts of the city are composed of 60-80% artificial surfaces, which correspond with higher UHI intensity (Molnár and Kozma, 2018). MODIS (Moderate Resolution Imaging Spectroradiometer) thermal satellite observational data indicates that the winter temperature difference on any given night can be 3-6°C, between urban and rural zones in Debrecen, while summer temperature differences are typically between 0.5-1.5°C (Tamás et al., 2019) (Figure 14).

These differences are mainly due to variations in population density, building materials, green infrastructure, and urban form. For example, the Nagyerdő Forest in the northern portion of Debrecen with about 30% impervious surface coverage serves as a cooling zone or "urban oasis" within a metropolitan setting. In contrast, the southern industrial zone has large amounts of paved surfaces and little vegetation to cool the temperatures contributing to localized warming (Iváncsics and Kovács, 2021; STRATEGY 24, 2023). The east part of the city is experiencing similar suburban expansion but primarily at low densities with patchy green infrastructure while the west side is a collection of N–S linear apartment blocks (Pénzes et al., 2023). These differences in LC and urban design also affect areas such as temperature profiles across the city, promoting water runoff, infiltration potential, and air quality.

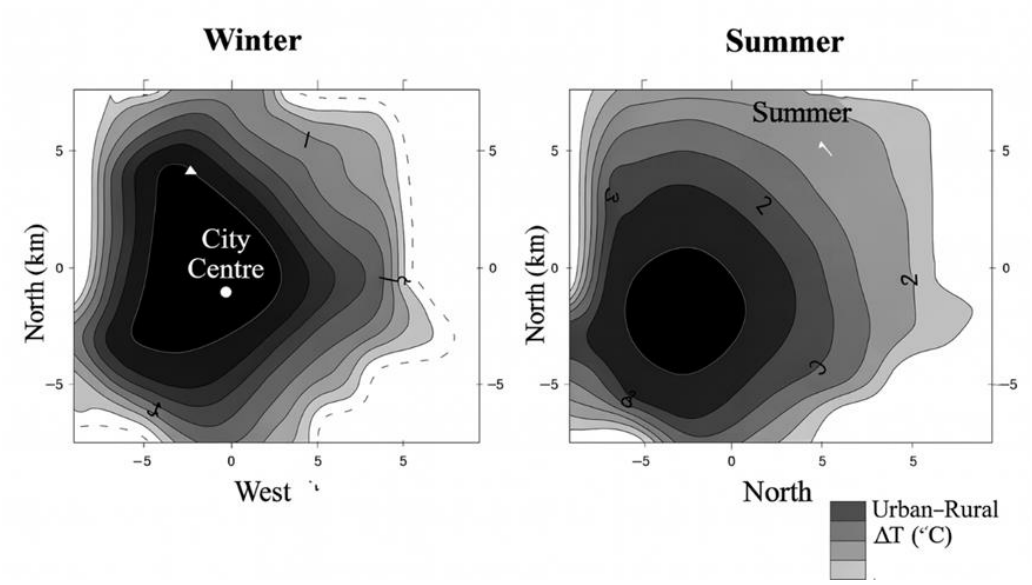

Figure 14. Mean UHI structure of Debrecen-based satellite measurements, (2002-2003, winter and summer) (source: Tamás et al., 2019)

3.1.2 Landscape and soil conditions of Debrecen

The city lies within a small landscape dominated by an alluvial fan plain with nearby flat areas coated with a thin cover of shifting sand. To the east lie distinct parabolic dunes, set on the other side of the Kondoros watercourse. Valleys running from north-northeast to south-southwest cut across the region horizontally, defining the special morphological features.

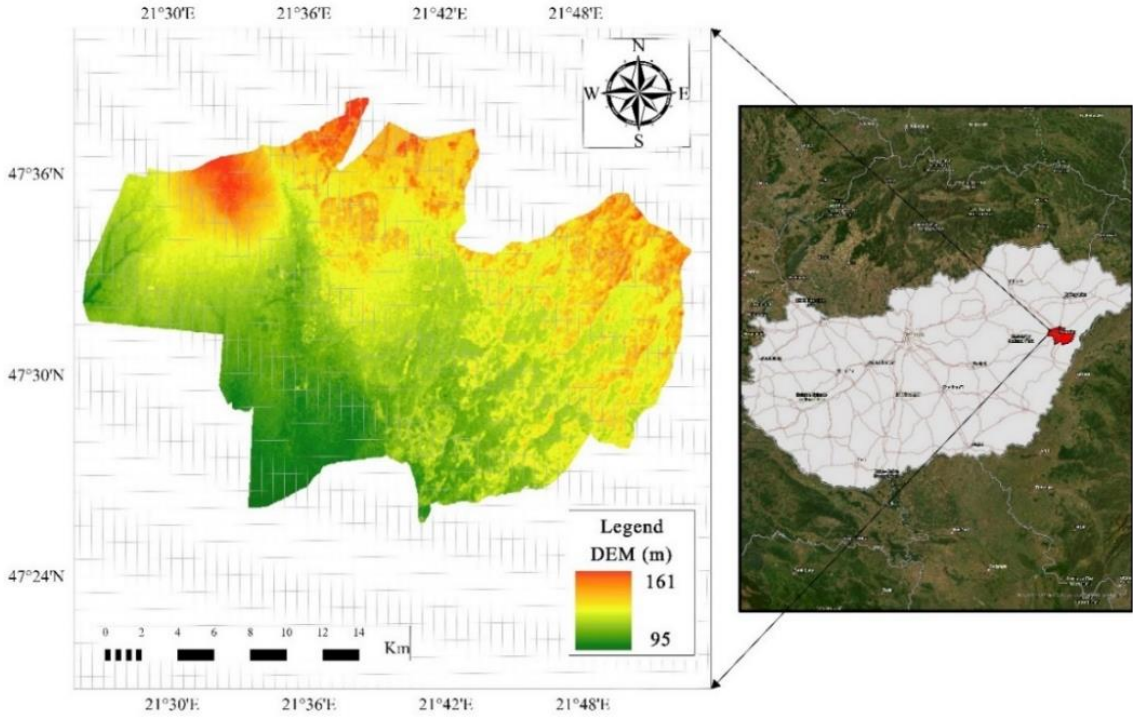

Figure 15. Location and digital elevation model of the study area (Source: Author, 2025).

According to the ASTER database (ASTER Science Team, 2013), Debrecen has an altitude of 97 m at its lowest and 161 m, at its highest. Although ASTER GDEM, SRTM, and Copernicus DEM provide similar spatial resolution and comparable vertical accuracy, ASTER GDEM was selected to maintain methodological consistency with previous studies commonly used in Central Europe and Hungary. Earlier evaluations have shown that ASTER performs reliably in low-relief environments when proper quality checks are applied, making it suitable for detailed land-surface and hydrological analyses (Józsa et al., 2014; Li et al., 2012). Furthermore, comparative assessments indicate that ASTER remains a valid option for regional-scale applications where workflow compatibility and consistency with existing datasets are required (Shen et al., 2020). For these reasons, ASTER GDEM was the most appropriate choice for the Debrecen study area. Figure 16 shows the distribution of soil texture categories based on the Hungarian agro-topographic map (AGROTOPO) (Bakacsi et al., 2014). The six main categories of soil texture are clay loam, clay, peat, sandy loam, loam, and sand. The most prevalent types are loam and sand, which are followed by clay, peat, sandy loam, and clay loam.

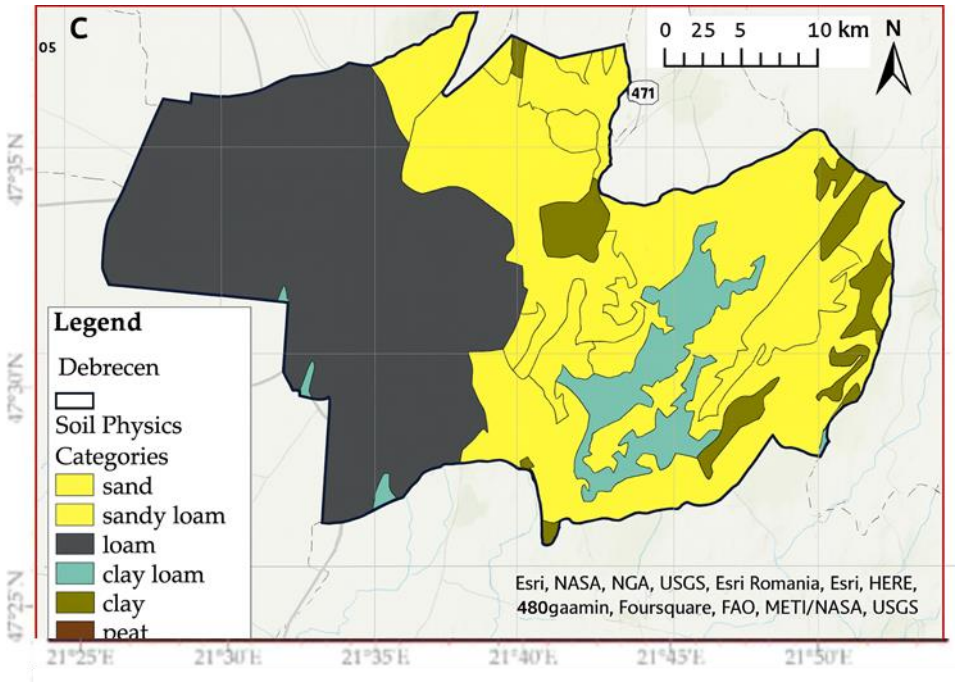

Figure 16. Agro topographic (Agrotopo) Map of the Study Area

3.1.3 Hydrographic network

Debrecen shows a duality in terms of water resources. Due to geological and geomorphological considerations, the area has a wealth of groundwater despite having insufficient surface water resources. The hydrological characterisation of Debrecen has been the subject of numerous investigations (Tamás et al., 2019; Brodmann, 2016). According to geological studies by Urbancsek (1960) and Borsy (1989), the Tisza River and its tributaries moved northward during the Pleistocene period, forming the current landscape. Descriptive and geomorphological studies, including those by Lóczy (1997) and Lóczy et al. (2009) indicate that the northward migration of watercourses has led to the formation of smaller, lower-yield streams, resulting in reduced water inflow to the region. Currently, on the city's west side, several similar ephemeral stream water resources can be found with low discharge, such as the Tócó Creek. On the east side, the Kondoros Creek (also characterized by low discharge) flows towards the Berettyó and Hortobágy rivers. The combination of low discharge and high environmental pressures leads to the poor water quality. According to Somlyai et al. (2019), the ecosystems are more susceptible to both qualitative and quantitative problems due to the decreased influx of fresh water. To address these issues, a number of systems (technical-hydrological, meteorological, aquatic and water-related terrestrial ecology) are evaluated, monitored,

and interventions are suggested to provide stakeholders and decision-makers with useful information (Hüse et al., 2016; Pregun, 2022).

The hydrographic network represents all the watercourses (creeks, lakes) (Tony and Jorge, 2022), and in the case of Debrecen, they must be used and maintained with extreme caution. Groundwater resources are also crucial, primarily for the production of energy, drinking water, and balneological purposes. It is also a great challenge to assess the environmental impacts of all members of the hydrological system of Debrecen.

Debrecen hydrographic network is a fundamental element in the shaping of local environment and in support of salient hydrological functions. It includes many surface water bodies, natural and artificial, which serve as balancing agents ecologically and in the water administration of this region.

These include seasonal and permanent streams, small creeks, and naturally formed ponds. They are influenced by local topography, precipitation, and groundwater emergence and sustain aquatic and riparian species. The artificial side, meanwhile, consists of drainage ditches and reservoirs and channels with regulated flow for conveyance, flood protection, irrigation, or the detainment of urban RO. These artificial structures usually intersect urban and agricultural areas, making their upkeep an exigent matter to stave off flooding and pollution.

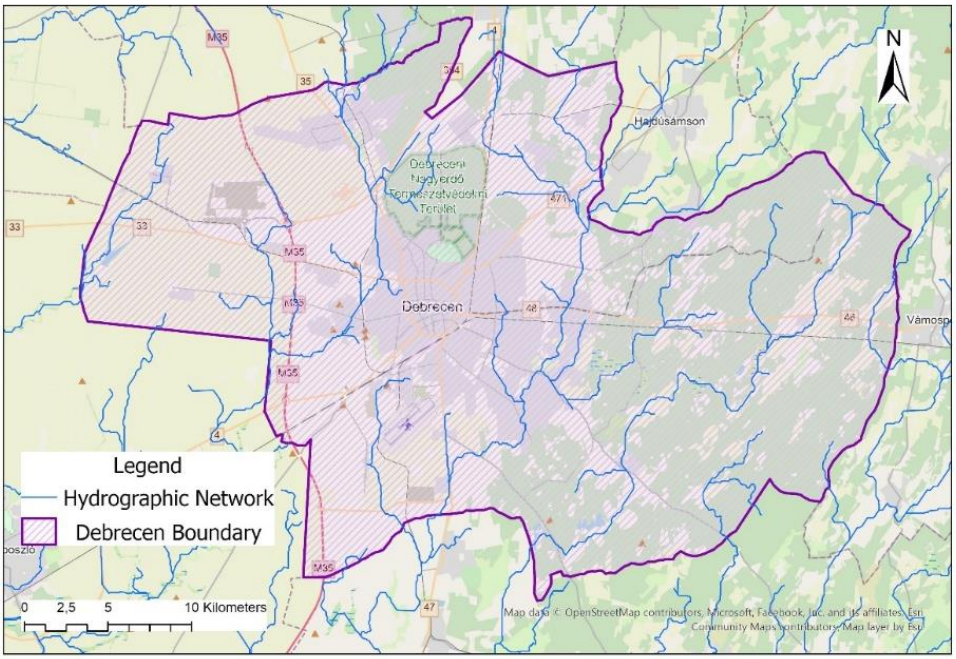

Figure 17. Study area hydrographic network (Source: Author, 2025).

The resulting map (Figure 17) shows the spatial distribution of Debrecen watercourses that have a crucial role in urban water management and local ecological processes. Due to the flat topography and increasing urbanization of the region, this water body needs constant maintenance and monitoring to prevent degradation and flooding. Groundwater resources and they are strongly interrelated with surface hydrology, thus serve as drinking water sources, for geothermal energy extraction, and balneological applications. The mapping and assessment of the hydrographic network provide the basis for implying the interconnectivity between surface and subsurface water systems.

The hydrographic layer constituted from the present study was then coupled with LC analysis and hydrological modeling modules to obtain an integrated understanding about water-related ecosystems' functions and associated environmental impacts within Debrecen.

3.2 Watershed parametrization

The time of concentration (Tc) is a fundamental hydrological parameter that governs the timing and magnitude of RO at the outlet of a watershed. It is defined as the time required for water to travel from the hydraulically most distant point in the watershed to the watershed outlet (Welle and Woodward, 1986). Accurate estimation of Tc is essential for predicting the watershed's response to rainfall events, particularly for modeling peak discharge and hydrograph shape in rainfall-runoff simulations.

The hydrological response of a watershed is influenced by multiple factors, including LC, soil characteristics, slope, and rainfall intensity. Among these, Tc acts as a key variable that integrates the watershed’s spatial and topographic characteristics, serving as an indicator of how quickly surface runoff can reach the outlet. A shorter Tc typically corresponds to steeper slopes and more impervious surfaces, leading to rapid and intense runoff, whereas a longer Tc indicates a slower hydrological response.

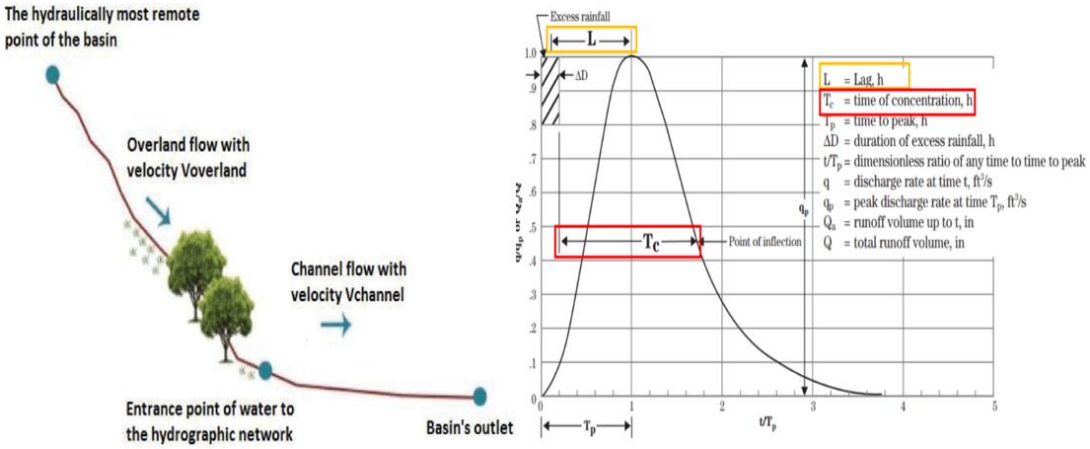

Figure 18. Visual Explanation of Time of Concentration (Tc) and Its Estimation Approach. (Source: Michailidi E.M et al 2018)

In the current study, Kirpich empirical equation (Eq 1) was employed to estimate the Tc for each delineated sub-watershed. This method is widely used due to its simplicity and reliability for small- to medium-sized rural watersheds (Edris et al., 2016). The Kirpich formula is given as:

$$Tc = 0.945 \times \left(\frac{L^{1.155}}{H^{0.385}}\right) \quad (1)$$

Where,

Tc: Concentration time (hours),

L: Maximum flow path length from the remotest point to the outlet (km)

H: Total elevation difference between the remotest point and the watershed outlet (m).

The following equation is based on overland and channel flow under natural terrain conditions and is most appropriate for ungauged or data-sparse basins. The parameters L and H were located from a high resolution DEM in a GIS based hydrologic environment.

The process was applied to each sub-watershed with Kirpich's equation to generate a spatial pattern of Tc values that capture the spatial variability in terrain and watershed shape. The values yield important information for the next hydrologic modelling steps for hydraulic structure design, flood prediction and water resources planning. The geometric shape of a watershed is an important determinant of hydrologic response, which is particularly relevant information for RO generation, flow concentration and flow lag time. A pragmatic way of estimating watershed shape is with the Compactness Coefficient (Kc), which yields an indication of how compact or elongated a catchment is.

This index is derived from the ratio of watershed perimeter (P), to the perimeter of a circle whose area is the same as the area of watershed (S). A circular watershed will have a compactness coefficient approaching 1, which means the watershed is not elongated at all, while elongated or irregular basins will have higher values. The compactness coefficient (Kc) (Eq 2) is calculated using the proposed formula from Timothée et al. (2018):

$$Kc = 0.282 \times \frac{P}{\sqrt{S}} \quad (2)$$

Where:

Kc : Compactness coefficient

P : Perimeter of the watershed (km)

S: Area of the watershed (km²)

The compactness coefficient reflects how compact the watershed is in comparison to a perfect circle. A low Kc value indicates a more circular and hydrologically efficient watershed, often associated with shorter times of concentration and quicker RO responses. Conversely, high Kc values indicate elongated or irregularly shaped watersheds, which tend to have longer flow paths and potentially delayed RO.

In this study, the compactness coefficient was computed for each delineated sub-watershed using the derived area and perimeter values obtained from the watershed shapefiles. The calculated Kc values were then used to classify the sub-watersheds into shape categories (compact, moderately elongated, and highly elongated) following the classification scheme of Timothée et al. (2018), as illustrated in Figure 19.

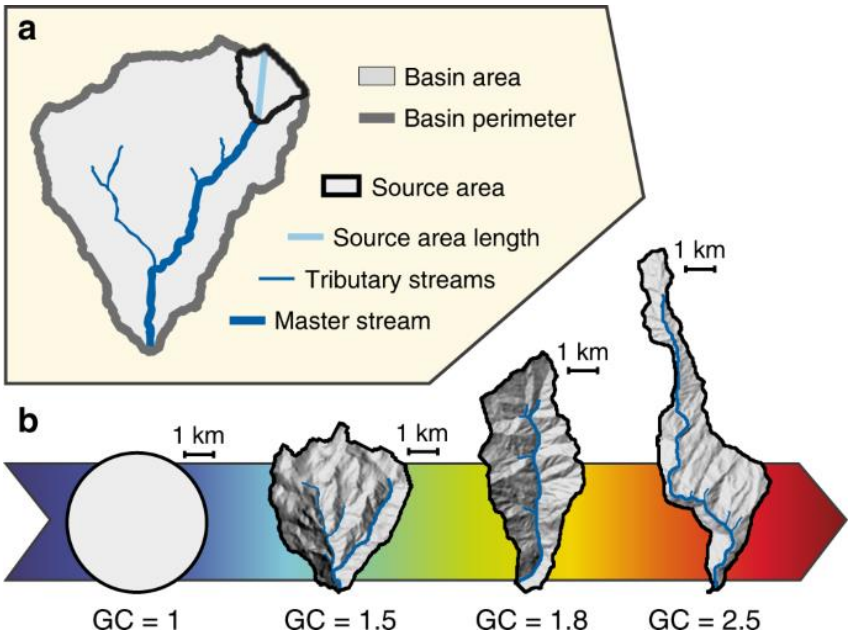

Figure 19. Watershed Geometry and Drainage Network Parameters. a) Main drainage basin features used in the study. b) Variations in basin shapes with corresponding Gravelius coefficients (GC)

The thick blue line represents the longest stream (L) in each basin. This classification supports further interpretation of runoff dynamics and flow concentration characteristics within each sub-watershed, providing valuable information for hydrological modeling and water resource planning.

3.3 Method for Rapid and quasi real time LC mapping framework

3.3.1 Design of a Replicable LC Mapping Workflow Using the MLC Method

In order to determine the city's water balance, L8 and globally accessible LC (such as Urban Atlas and CLC) RS data time series images were processed and integrated. With a high spatial resolution of 30 meters, the study used publicly available L8 data (Nwagoum et al., 2023). The selection of L8 imagery, was a foundational decision driven by the necessity for a long-term, consistent archive suitable for monitoring LC change across multiple decades. While newer sensors like S2 offer higher resolution, the decades-long record provided by the Landsat program is critical for temporal analysis and change detection (Roy et al., 2014). Using L8 established a reliable methodological baseline, ensuring that the data is highly compatible and radiometrically consistent with earlier Landsat missions. This approach maintains the continuity of the land surface record,

which is paramount for our study's objective of performing a robust, multi-temporal analysis of land cover dynamics in the region (Hermosilla et al., 2018).

The U.S. Geological Survey (USGS) website offers publicly available L8 data from 2013 to 2019 for free download (USGS, 2016).

The selected scenes corresponded to path/row 186/27 under the Worldwide Reference System (WRS), with cloud cover limited to a maximum of 35% and captured primarily between June and September to align with peak vegetation activity for optimal classification accuracy (Yan et al., 2023).

Two primary types of satellite imagery with differing spatial resolutions were analysed:

- L8 OLI, part of the USGS National Land Imaging Program, offers nine spectral bands at a 30-meter resolution across visible, near-infrared, and shortwave infrared wavelengths. Its 16-day revisit interval and long historical archive make it suitable for multi-year change detection (USGS, 2016; Nwagoum et al., 2023).
- S2 MSI, developed under the European Copernicus program, provides higher spatial resolution (10 m) and a broader 13-band spectral range. This sensor supports detailed observation of vegetation dynamics, water bodies, soil conditions, and urban features, offering complementary spatial and spectral capabilities (ESA, 2024; Acharki, 2022).

Eleven electromagnetic spectrum bands make up each L8 Collection 1 Level-1 image. Two TIRS bands 10.60 – 12.51 and nine OLI 0.45 – 1.38 μm are used by L8 (Appendix, Table 16). Along with S2 and MODIS, L8 is one of several sensors used for LC classification. S2, a high spatial resolution sensor (10 m), delivers regional coverage, whereas MODIS, a low spatial resolution sensor (500 m), offers worldwide coverage (Xu et al., 2024). Low-resolution satellite images, with their wide swath width, have a far superior synoptic perspective and temporal revisit frequency system than high-resolution sensors. However, inadequate spatial resolution and sub-pixel signal mixture have typically made it difficult to accurately detect yields, analyse and validate the signal, and rely on the information products that are obtained (Rembold et al., 2013). Furthermore, because of its increased spectral resolution, which allows for better spectral separability

across LC classes, L8 typically outperforms MODIS for LC classification. However, because MODIS has a greater temporal resolution (daily acquisitions) than L8′s 16-day repetition cycle, it is still useful for LC monitoring (Klein et al., 2012). The ability of RS data to help identify small objects will improve with increasing spatial resolution. Even though Landsat (or comparable sensors, like Satellite Pour Observation de la Terre (SPOT)) is also the main source of data, it can be challenging to get cloudless images in Hungary during the growing season in humid years because it has a 16-day interval between successive images and sufficient spatial resolution in the majority of agricultural, urban, periurban, suburban, and rural areas (Lobell, 2013). Furthermore, compared to MODIS and S2, L8 has a longer history of data collecting. For monitoring long-term LC changes, this longer time series offers useful insights (Roy et al., 2014). Layer stacking was used to pre-process the necessary data prior to categorisation. Researchers frequently use the European Environmental Agency's Urban Atlas GIS database because of its excellent quality and open access status (European Environment Agency, 2023). For 800 European Functional Urban Areas, Urban Atlas offers statistical and spatial data, including population, LC classifications, and spatial information for different LC patches (Poleman, 2018; Barranco et al., 2014). In this study, the Urban Atlas and CLC databases were utilised, particularly to distinguish between sealed and semi-sealed urban areas. Figure 20 provides a summary of the entire process, illustrating the various data processing, calibration, and validation steps used to successfully create the classified image

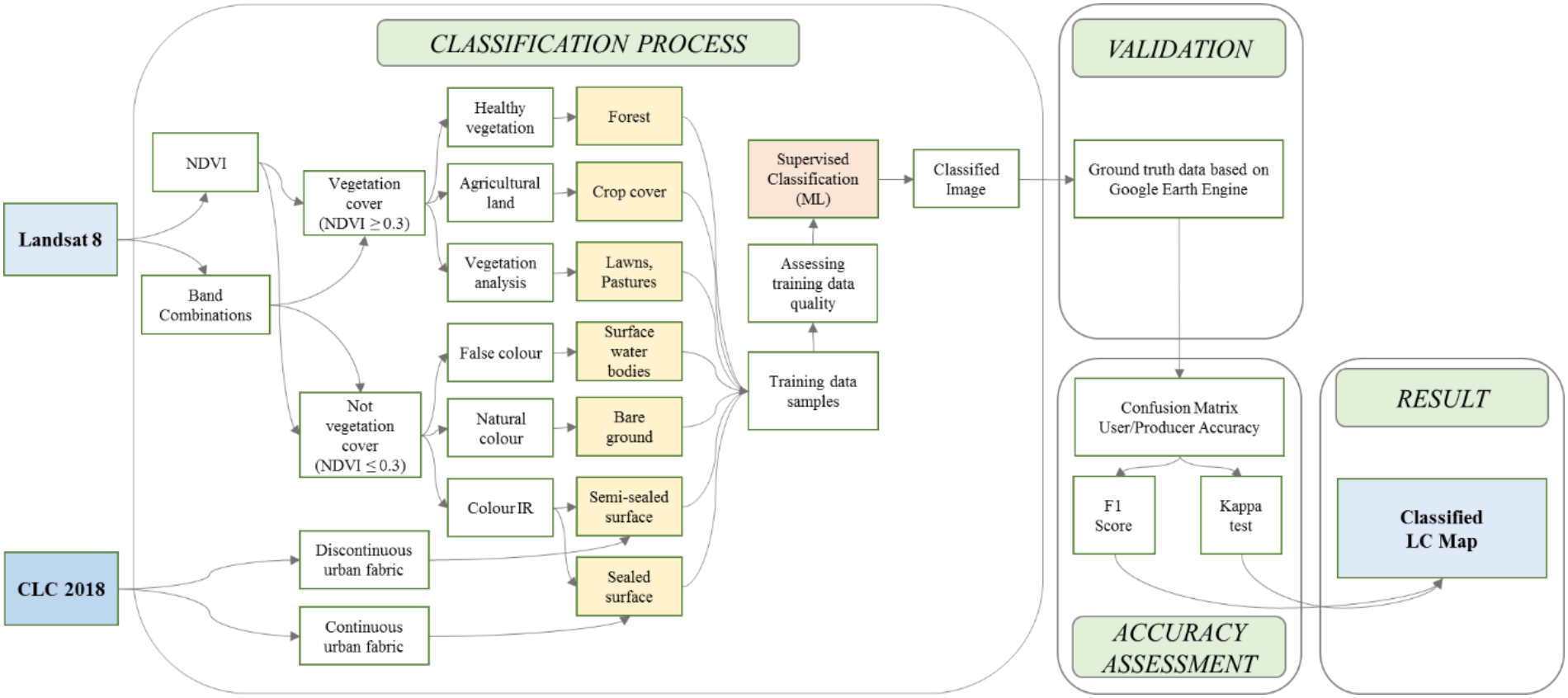

Figure 20. A schematic illustration of the image classification data processing workflow (Source: Author, 2025).

L8 satellite images were classified using MLSC (Ali et al., 2018) to produce an LC map with a spatial resolution of 30 m. The most often used supervised classification method for assessing satellite image data is the machine learning decision rule (Medina and Beatriz, 2018). For LC extraction, a number of researchers employed supervised classification (Ahmad and Quegan, 2012; Asuquo et al., 2023). A quick and usually excellent outcome is made possible by methods that offer supervised classifications (Weng and Lu, 2008). MLSC is unable to process complex images. Therefore, it is impossible to accurately classify a large number of pixels (Blaschke, 2010). The choice of starting values can introduce biases and estimate mistakes, which can have a substantial effect on MLSC performance. Although MLSC may not have the best qualities when working with tiny sample sizes, it is nonetheless frequently used for images that have low spatial resolution (Mustapha et al., 2010). On the other hand, Bolstad and Lillesand (1991) emphasised MLSC's efficiency in managing situations involving typically distributed data, its capacity to generate dependable outcomes in spite of these difficulties, and its compatibility with desktop computer systems with little memory. In their thorough analysis of LC classification techniques from 1984 to 2019, Daba and You (2022) emphasised the ML algorithm as a potent and adaptable LC classification tool. Urban planning, environmental monitoring, and the detection of LC changes over time are just a few of the applications that can benefit from its accuracy, robustness, and sensitivity to spectral variability (Daba and You, 2022). Consistent pre-classification input from the picture analyst is necessary for supervised classification techniques. Training points on the sealed and semi-sealed areas of Debrecen were gathered for the urban area using the CLC database. Selecting training locations for LC classification and creating composite images and the Normalised Difference Vegetation Index (NDVI) (Tucker, 1979) to improve spectral information for LC mapping were all part of the pre-processing of the L8 data. L8's NDVI is used to define the area covered by vegetation. In order to collect training points across different LC types in Debrecen, such as agricultural areas with crop cover, pastures, barren land, and forest parts, several Landsat composites were utilised (Qin et al., 2021). Thirty training Regions of Interest (ROI) units were chosen and altered as pixels on each assessed band combination of L8 images, and 210 training samples in total were allocated to seven LC classes as training points (Dou et al., 2024). Each of these pixels satisfies the chosen category's representativeness condition.

Building on the findings of Jamshid et al. (2013), seven composite datasets from L8 were used to select training points for various LC categories. Based on field survey in the study area, seven categories were defined (Table 1).

Table 1.LC categories and definition

Category	Definition
Sealed surfaces	Areas where buildings, roads, and other artificially covered surfaces account for more than 80% of the spatial unit (Linda and Geir, 2021).
Areas with crop cover	Relatively homogeneous agricultural fields that are easily distinguishable in Landsat imagery due to their spectral characteristics and regular geometric patterns (Matthews et al., 2022).
Grassland and pasture ground	Areas covered predominantly by grass or grass-like vegetation, typically used or suitable for livestock grazing (Schoenbaum et al., 2018).
Semi-sealed surfaces	Units where buildings, roads, and other artificial surfaces cover between 50% and 80% of the total area (Linda & Geir, 2021).
Forests	Land spanning more than 0.5 hectares with trees taller than 5 meters and a canopy cover greater than 10% (FAO, 2000).
Bare ground surfaces	Surfaces consisting of exposed soil, sand, or similar substrates not covered by vegetation, gravel, wood chips, artificial turf, or any other ground cover (Liu et al., 2022).
Surface water bodies (SWB)	Open water features such as reservoirs, ponds, lakes, or inland excess water areas (Williams et al., 2004; Monaghan et al., 2017).

This approach takes advantage of the specific sensitivity of different band combinations to distinct LC classes, as outlined in Table 2. The use of various spectral composites aided in the identification and selection of diverse training sites, which is a critical step in the classification process.

Table 2. Band combinations of L8 used for training point selection across LC categories (Jamshid et al., 2013).

Name of composite	Spectral band combination (RGB)	Role in the training site collection
Natural Colour	4 3 2	Bare ground
False Colour	7 6 4	Water/ Urban area
Colour Infrared	5 4 3	Urban area/Vegetation
Agriculture	6 5 2	Agriculture
Healthy Vegetation	5 6 2	Forest
Vegetation Analysis	6 5 4	Vegetation

The final produced LC map can be more accurate the more samples are used as training points for the classification (Zhu et al., 2016; Zhou et al., 2022). L8 data was used to generate NDVI in order to increase accuracy and decrease complexity. Using 0.3 as the plant cover threshold, NDVI was utilised for vegetation masking. Vegetation was defined as pixels with NDVI values greater than 0.3 (Lemenkova, 2018). The training points for vegetation-covered locations were gathered using the composites and this NDVI mask. Thirty training points were manually and randomly chosen for each class in this LC classification investigation. Ultimately, seven distinct LC categories were used to distribute the 210 training points that were collected. Before the selection of these training points, the data underwent the following pre-processing steps:

R–G–B	Description
7–6–4	A 7–6–4 band composition was used to differentiate SWB´s and bare land, which in the imagery showed as very dark blue and yellowish, respectively. Training points for areas covered by water (30 training samples) were then selected and designated as water bodies.
6–5–2	Crop-covered areas were distinguished from other elements by their geographic position and rectangular shape. The 6–5–2 band composition was used to identify vegetation, making it easier to distinguish between light green, which represents areas with crop cover, and dark green, which is linked with forest areas. A prominent spectral index, the NDVI, was used to highlight the variations in LC between areas covered by vegetation and those that are not. As a result, high NDVI values (0.6–0.8) were noted, which is consistent with the forest category's anticipated traits.
5–4–3	For sealed and semi-sealed areas, the colour infrared band composition (5–4–3) was used, which successfully identified metropolitan areas that look as light blue. Thus, urban areas were identified by their low NDVI values, which ranged from 0.2 to 0.5. Furthermore, the CLC 2018 data were used because Landsat 8 alone is unable to distinguish these two urban kinds from one another. Ultimately, the sealed surface category was created by combining the 30 training points that were chosen.
6–5–4 5–6–2	Two different band compositions, 6–5–4 and 5–6–2, are used in the bare ground land type classification, where bare land has a brown colour. The NDVI layers and these composites were both reclassified to reflect soil. Any pixels with a brown hue were categorised as bare terrain in terms of the composites. Pixels with values between 0 and 0.2 were classified as bare ground for the NDVI layer. The intersection of these layers produced pixels that were more likely to depict the barren earth.

3.3.2 Evaluation of Framework Adaptability and Transferability

Validation of classification

Post selection of training points, the samples were compiled and correctly identified for each LC category. The mapping and statistical assessment were performed using the Environment for Visualizing Images (ENVI v5.3) software (Bruse and Fleer, 1998). Subsequently, the spectral separability was systematically computed to analyze each training sample to verify the effectiveness and accuracy of the classification.

Separability indices, such as the Jeffries–Matusita (JM) and the Transformed Divergence (TD) distance (Padma and Sanjeevi, 2014), express values ranging from 0 to 2, where 0 signifies complete spectral overlap and 2 denotes perfect separability. These metrics are crucial for ensuring that the classes are distinguishable enough to support reliable classification results.

To support the validation process, the TD index was calculated following the formulation by Kavzoglu and Mather (2000):

$$D_{ij} = \frac{1}{2} tr\left[(\sum j - \sum i)(\sum_j^{-1} - \sum_i^{-1})\right] + \frac{1}{2} tr[(\sum_j^{-1} + \sum_i^{-1})(\mu i - \mu j)(\mu i - \mu j)^T] \quad (3)$$

The TD (Eq.4) is applied to mitigate the impact of well-separated classes, which may lead to a rise in the average divergence value and a misleading divergence measure (Kavzoglu and Mather, 2000).

$$TD_{ij} = C[1 - e^{\frac{-Dij}{8}}] \quad (4)$$

Where Σi and Σj denote the variance covariance matrices of classes I and J, μi and μj are the corresponding mean vectors, and c is a constant value that determines the range of TD values. The trace of a matrix is represented by tr, which means the sum total of the diagonal components of the matrix.

The following is a definition of the J-M distance (Eq.5) between distributions of two classes, ωi and ωj (Jia and Richards, 1999):

$$JMij = 2(1 - e^{\wedge -Bij}) \quad (5)$$

Where Bij is the Bhattacharyya distance computed as (Kailath, T, 1967) (Eq.6):

$$Bij = \frac{1}{8}((\mu i - \mu j)^T \left(\frac{\sum j + \sum i}{2}\right)(\mu i - \mu j) + \frac{1}{2}\ln\left(\frac{1}{2}\frac{|\sum j + \sum i|}{\sqrt{|\sum j|\,|\sum i|}}\right) \quad (6)$$

The mean reflectance of species I and J are denoted by μi and μj, their covariance matrices by Σi and Σj, and the determinants of Σi and Σj are represented by |Σi| and |Σj|, respectively. The symbol T indicates the transposition function, and ln refers to the natural logarithm function.

As a general rule, classes are separable if the result is greater than 1.9, fairly separable if it is between 1.7 and 1.9, and not separable if it is below 1.7 (Jensen, J.2005).

To have more accurate and up-to-date data for improved computation of water balance parameters, the resulting LC map was derived specifically for the year 2019 using L8 imagery. The classified data were then assessed using an independent validation set, with 70% of the labelled points used for training and 30% retained for testing.

Accuracy assessment of classification

To evaluate the reliability of classification outputs, this study employed widely accepted accuracy measures derived from the confusion matrix: OA, Producer's Accuracy (PA), User's Accuracy (UA), K, F1 Score, and the Quantity (Q) and Allocation (A) Disagreement metrics proposed by Pontius. Collectively, these metrics offer a robust framework for validating LC classification performance.

Classification of raster outputs was verified by comparing them with high-resolution reference data, such as Google Earth (GE) images and CLC maps (Yonaba et al., 2021). To create a validation dataset that reflects the proportion of all LC classes in the area, stratified random sampling was applied (Stehman, 2014). Sampling units were designated as 30 × 30 m pixels for that purpose, and representatives of rarer classes were oversampled to improve the representativeness and reliability of the dataset (Hermosilla et al., 2018).

In order to reduce the spatial autocorrelation effect, a total of 770 validation points were generated in such a way that there was a minimum spacing of ≥500 m between them (Su et al., 2020). It is worth noting that the Urban Atlas proved to be very helpful in discriminating between sealed and semi-sealed surfaces. Reference imagery with spatial resolutions of up to 10 m (GE) and 100 m (CLC) was employed (Liu et al., 2020).

OA along with the K constitute a standard set of evaluation tools but the limitations that they have such as insensitivity to the type of error and they are dependent on class frequency are have been extensively acknowledged (Pontius and Millones, 2011; Pontius, 2022). To address these shortcomings, the work additionally engaged among other things Quantity Disagreement and Allocation Disagreement, which are able to break down the error to a finer extent (Pontius Jr. and Millones, 2011). Quantity Disagreement represents inconsistencies in the composition of classes between the reference and the predicted maps, while Allocation Disagreement refers to the errors caused by the shift in the position of the two areas. These indicators enable a more precise understanding of the classification performance, as they are the limitations hidden in the traditional accuracy measures such as K that they point out. The following equations define the overall accuracy, kappa coefficient, and F1-score:

$$\mathrm{OA} = \frac{\mathrm{TP} + \mathrm{TN}}{\mathrm{TP} + \mathrm{TN} + \mathrm{FP} + \mathrm{FN}} \tag{7}$$

$$\mathrm{k} = \frac{\mathrm{OA} - \mathcal{P}\mathrm{e}}{1 - \mathcal{P}\mathrm{e}} \tag{8}$$

$$\text{Pe} = \left(\frac{\text{TP} + \text{FN}}{\text{TP} + \text{FN} + \text{FP} + \text{TN}} + \frac{\text{TP} + \text{FP}}{\text{TP} + \text{FN} + \text{FP} + \text{TN}}\right) * \left(\frac{\text{FP} + \text{TN}}{\text{TP} + \text{FN} + \text{FP} + \text{TN}} + \frac{\text{FN} + \text{TN}}{\text{TP} + \text{FN} + \text{FP} + \text{TN}}\right) \quad (9)$$

$$\text{F1 score} = 2 * \frac{\text{Precision} * \text{Recall}}{\text{Precision} + \text{Recall}} \quad (10)$$

$$\text{Precision} = \frac{\text{TP}}{\text{TP} + \text{FP}} \quad (11)$$

$$\text{Recall} = \frac{\text{TP}}{\text{TP} + \text{FN}} \quad (12)$$

OA (Eq. 7), K (Eq. 8), and F1-score (Eq. 9) are calculated based on the classification metrics: True Positive (TP), True Negative (TN), False Positive (FP), and False Negative (FN). These components are critical for evaluating classification model performance, as they distinguish between correctly and incorrectly classified instances. Specifically, TP refers to correctly identified positive cases, TN to correctly identified negative cases, FP to incorrectly labeled positives, and FN to incorrectly labeled negatives (Sim et al., 2024).

3.4 Application of Machine learning algorithm in LC classification

3.4.1 Data sources

This research employs multi-temporal satellite data obtained from L8 Operational Land Imager (OLI) and S2 Multispectral Instrument (MSI) for the years 2018, 2020, and 2022. These platforms were chosen for their proven spectral characteristics and effectiveness in LC classification tasks. Imagery was sourced from official repositories, specifically the USGS Earth Explorer and the Copernicus Open Access Hub.

Two types of satellite imagery with differing spatial resolutions were analysed: detailed specifications of these sensors [spectral band configurations, spatial resolutions, revisit frequencies, cloud cover thresholds (≤35%), acquisition season (June–September), and WRS path-row details (186/27)] are comprehensively described in Section 3.3.1: Design of a Replicable LC Mapping Workflow Using the MLC Method. Detailed data are presented in Appendix, Table 17, which outlines the sensor datasets and the corresponding acquisition times used in this study.

S2 provides higher spatial resolution suitable for mixed agricultural–urban mosaics, while L8 provides radiometric stability and long-term continuity. Their combined use enhances classification quality and temporal coverage (Klein et al., 2012; Acharki, 2022).

Prior to analysis, S2 and L8 imagery underwent a series of pre-processing steps to reduce atmospheric interference and enhance classification precision. The procedures included the following:

- Atmospheric Correction:
  - L8 OLI/TIRS: Surface reflectance values were derived using the Landsat Surface Reflectance Code (LaSRC) within ArcGIS Pro. This method incorporates the Quality Assessment (QA) band to effectively identify and remove cloud and shadow-affected pixels, thereby improving data quality.
  - S2 MSI: The Sen2Cor processor was employed to perform atmospheric correction, converting Level-1C data to bottom-of-atmosphere (BOA) reflectance. This step mitigates the impact of atmospheric scattering and absorption.
- Cloud and Shadow Masking:
  - L8 OLI/TIRS: The C Function of Mask (CFMask) algorithm was applied to detect and mask clouds and their shadows, refining the visibility of surface features.
  - S2 MSI: Cloud and shadow masking was carried out using the Scene Classification Layer (SCL) associated with Level-1C products, which enables the retention of only high-confidence pixels for further analysis.
- Geometric Correction:
  - L8 OLI/TIRS: Images were processed using standard geometric correction protocols to maintain spatial consistency across multiple dates.
  - S2 MSI: Ground control points and coordinate reference harmonization were used within ArcGIS Pro to ensure accurate spatial alignment with Landsat data, facilitating coherent multi-source data integration.

3.4.2 Training data and Validation

For the classification of 2018, 2020, and 2022, a similar methodology to the one described in detail for the 2019 L8 classification (see Section 3.2.1) was followed. The classification

framework was based on structured and proportionally distributed training data, prepared by carefully labelling sample points according to predefined LC categories.

The sample points were randomly split into 70% training and 30% testing subsets for each year (Aryal et al., 2023; Martinez-Sanchez et al., 2024), enabling independent validation of classification results. This framework ensured an unbiased assessment of classifier performance and generalization capacity (Amindin et al., 2024).

To support the training and spectral classification, band combinations adopted from Basheer et al. (2022) and Guizani et al. (2024) were applied to both S2 and L8 imagery. These combinations enhanced the spectral distinction among LC types and were aligned with the labelled sample points.

As outlined in Section 3.2.2, spectral separability was once again assessed using Jeffries–Matusita (JM) and Transformed Divergence (TD) indices, based on the same formulas and threshold rules previously introduced. This consistency across all years strengthened the reliability and comparability of LC maps over time.

3.4.3 Accuracy Assessment:

As discussed above, classification accuracy was evaluated with a mixture of the traditional and advanced evaluation metrics as OA, K, F1 Score, and, Pontius' Quantity and Allocation Disagreement to analyze performance. This evaluation was conducted across a number of classifiers and satellite sources (S2 and L8) for the years 2018, 2020, and 2022. The independent test datasets were interpreted by experts through visual inspection of high-resolution imagery in Google Earth using features such as color, shape, texture and context (Dermosinoglou et al., 2024). GEE was one of the primary sources of high-resolution data that contributed to the credibility of the validation (Amindin et al., 2024). In the previous section, it was mentioned that using value OA, K, and F1 Score were used, while Q and A metering (Equation 13 - 15) were even further consideration of the spatial and class-level misclassification - which in urban environments known, to be both heterogeneous and dynamic. Pontius' quantity disagreement (Q) assesses unevenness in the proportion of area assigned for each LC class. Eq. 13 provides total quantity disagreement by taking the sum differences across all J categories. Allocation disagreement (A) assesses discordance errors related to the spatial placement (or misallocation) of LC classes. Eq. 14 provides total allocated disagreement by taking the sum of class-level spatial mismatches. These metrics were introduced by Pontius and

Millones (2011) to overcome certain limitations of Cohen's Kappa, such as its reliance on the assumption that all disagreement is due to chance. Pontius' approach distinguishes between false positives and false negatives and explicitly incorporates spatial context. As defined in Eq 15, the total disagreement (D) is the sum of quantity and allocation disagreements: D = Q + A.

$$Q = \frac{1}{2}\sum_{g=1}^{J} q_g \quad (13) \quad ; \quad q_g = \left|\left(\sum_{i=1}^{J} P_{ig}\right) - \left(\sum_{j=1}^{J} P_{gj}\right)\right|$$

$$A = \frac{1}{2}\sum_{g=1}^{J} a_g \quad (14) \quad ; \quad a_g = 2\min\left[\left(\sum_{i=1}^{J} P_{ig}\right) - P_{gg}, \left(\sum_{i=1}^{J} P_{gi}\right) - P_{gg}\right]$$

$$D = Q + A \quad (15)$$

Where $\boldsymbol{q_g}$ is the quantity disagreement for an arbitrary category g, which differs from the definition of q in Olofsson et al. (2014).

Stratified random sampling was employed to develop a representative dataset for accuracy assessment. This approach ensures a proper distribution of the sample across all LC classes in proportion, leading to a more reliable evaluation of the result according to Stehman (2014).

3.5 Integrated Tool Development and Hydrological Coefficient Analysis for Improved Urban Water Balance Estimation in Debrecen

3.5.1 Description of the tool developed.

The deduction of hydrological coefficients for urban water balance estimation aimed to quantify important hydrological cycle components at both pixel and larger spatial scales for each LC category. There are many physically based distributed models to simulate flow and transport of surface and groundwater, such as the Soil and Water Assessment Tool (SWAT) (Mtibaa and Asano, 2022), the Water and Energy Transfer between Soil, Plants and Atmosphere (WetSpa) model (Safari et al., 2012) and the MIKE SHE Integrated Hydro-logical Modelling System (Sandu and Virsta, 2015). However, this

study uses a simpler approach of estimating water balance parameters by using runoff coefficients, based on regional values specific to Eastern Europe. The Turc (1961) empirical formula was used to estimate evapotranspiration because it performs reliably in data-scarce conditions and requires only temperature and precipitation, which were the consistently available variables for the study area. Temperature-based and hybrid empirical models such as Turc have been shown to provide stable ET estimates where full meteorological inputs (e.g., radiation, wind speed, humidity) are limited or unavailable (Diouf et al., 2016; Oudin et al., 2005). Comparative assessments also report that the Turc method often performs competitively against more data-intensive formulas in humid to moderately dry climates, making it a suitable and practical option for regional-scale hydrological analyses (Oudin et al., 2005; Aydin, 2021). For these reasons, Turc's formula offered an appropriate balance between accuracy and data requirements for this study. Average annual temperature and precipitation were calculated for the period of 2016-2019 to calculate the values for the evapotranspiration coefficient for each LC. Infiltration rates for each LC type were determined using the water balance equation.

To operationalize this workflow and enable spatially explicit hydrological coefficient estimation, an integrated GIS-based tool was developed specifically for this dissertation. The tool was built as a modular workflow within ArcGIS Pro, supported by Python scripting, and is designed to automatically: (i) import and process the classified land cover maps (2018, 2020, 2022); (ii) assign region-appropriate runoff coefficients for each LC class; (iii) compute evapotranspiration for every pixel using the Turc formula; (iv) estimate infiltration through the water balance equation; and (v) aggregate all hydrological components at both pixel and LC-class levels. In addition, the tool generates spatial maps of runoff, ET, and infiltration, allowing clear visualization of hydrological behavior across Debrecen. This modular workflow constitutes the original tool developed in this research, and the subsequent chapters presenting water balance maps, LC-specific hydrological coefficients, and spatial hydrological patterns are direct outputs produced through this tool

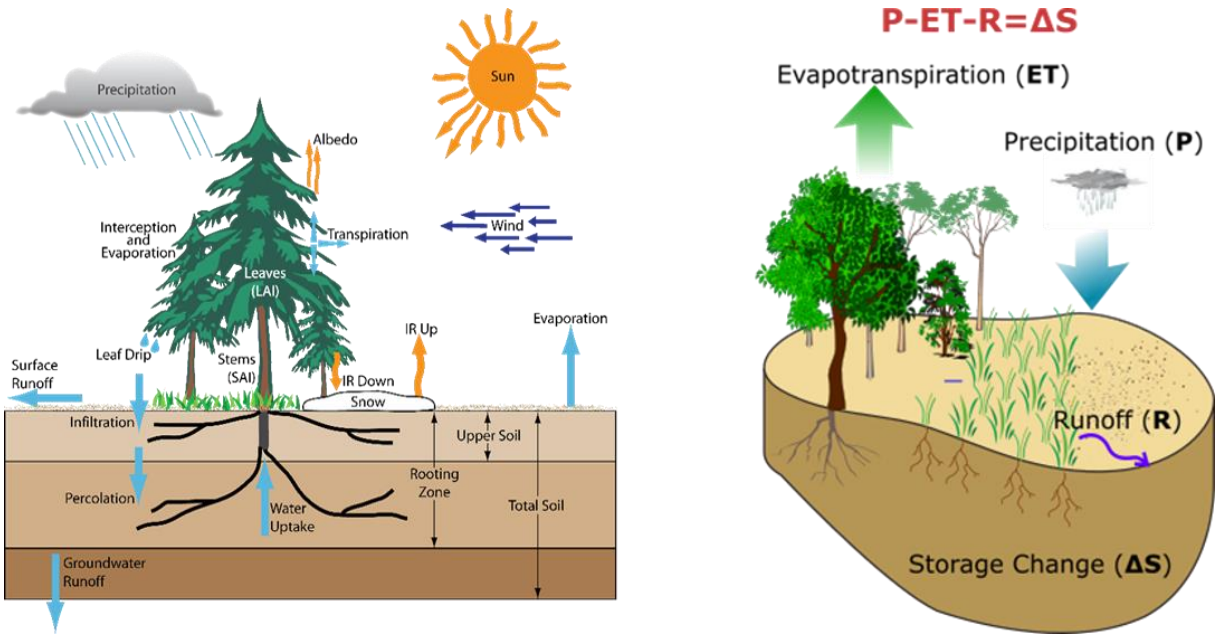

Figure 21. Energy and Water Balance Overview (Source: USGS Science for a Changing World 2019, Regional and Global Climate)

3.5.2. Calculation of hydrological coefficients.

Evapotranspiration

The basin's central precipitation value, known as the Precipitation Median Method (P_{MM}) (Eq.16), was calculated. Eq. 16 provides the calculation for the median of a set of precipitation values, which is the middle number of an ordered set of data. The median is commonly a good indication of the central or average precipitation for a given area and time period. It is a very simple method and is readily applied in a historical and real-time manner. It is a widely accepted method for dealing with such data (Soil and Water Conservation Society, 2003).

$$P_{MM} = \frac{P_{min} + P_{max}}{2} \qquad 16$$

Where,

P_{MM} Represents the mean annual precipitation in [mm/year],

P_{min} Is the minimum mean value of precipitation in [mm],

P_{max} Is the maximum mean value of precipitation in [mm].

This study utilized climatic data where the mean annual temperature was reported as a minimum (T_{min}) of 11.1 °C and a maximum (T_{max}) of 12.5 °C; the mean annual

precipitation was reported a minimum (P_{min}) of 435.9 mm and a maximum (P_{max}) of 743.9 mm. The median mean annual precipitation of the basin determined through Precipitation Median Method (P_{MM}) was 589.9 mm. Once the Turc formula was applied with P_{MM}, Tmin and Tmax, the minimum and maximum of average annual reference evapotranspiration in the basin was estimated. The average annual evapotranspiration, was determined through the Turc equation (Turc, 1961; Osorio et al., 2014; UNESCO OMM AISH, 1974) (Eq. 17).

$$E = \frac{P}{\sqrt{0.9} + \frac{P^2}{(200 + 25T_{mean} + 0.05{T_{mean}}^3)^2}} \qquad 17$$

Where,

E Represents the reference evapotranspiration in [mm/year],

P Is the annual amount of precipitation in [mm/year],

T_{mean} Is annual mean temperature in [°C].

Tallis et al. (2013) performed a comprehensive review of the literature and created a series of crop coefficient values (Kc), used in this study, which are displayed in Appendix, Table 18. To effectively use a Kc value, an understanding of the phenology and growth stages of vegetation is important. The manual which was referenced also states the coefficients for evapotranspiration can be extrapolated to other non-vegetated LC types, such as bare ground and water layers. In regard to impervious surfaces, Kc values are generally assigned a very low Kc value (e.g. 0.001) to represent a negligible addition to the drainage process. For instance, to calculate Kc values for stagnant or increasingly slow running water bodies, a Kc value of 1 is assigned according to the definition provided by Tallis et al. (2013).

In this study, ET coefficients were estimated for each LC class in Debrecen, using the dominant vegetation within the class for each LC and defining a representative crop coefficient (Kcn) for each LC category. The assignment of Kc involved the assignment of Kc values to the homogeneous classes following the classifications in Tallis et al. (2013) to allow for a mean regional Kc calculation based on the area (Appendix, Table 18).

The Kcs for the "Sealed surface" class were assigned Kc that corresponded to "urban" and "built" types; and the "Semi-sealed" class, which was assigned an average of four land types of urban, bare ground, wooded meadow, and open shrubland. Reference evapotranspiration (ET_0) was calculated at the watershed scale to develop an aggregate evapotranspiration value for all LC classes.

Evapotranspiration for each LC class (ETcn) in the Debrecen basin was subsequently modeled using Eq.18 (Kashyap and Panda, 2001).

$$ET_{cn} = K_{cn} ET_0 \qquad 18$$

Where,

ET_{cn} Maximum annual evapotranspiration for each land use class in [mm],

n Represents the number of the land use categories (n = 1, 2, 3, 4, 5, 6, 7),

K_{cn} Is the crop coefficient for the n^{th} land use categories,

ET_0 Is the mean annual reference evapotranspiration in a watershed in [mm].

Runoff

In order to assess the runoff ratio within the study area, this research implemented the methods built on data by Kenessey (1928, 1930) which has been commonly tested and used under Eastern European environmental settings, specifically in regions like Hungary, Romania, Slovakia and Ukraine. This method is tailored specifically to the land use and geomorphological aspects of the area, and relies on the cumulative assessment of a number of physical aspects of the landscape.

The watershed's runoff coefficient (or flow factor) calculation involves adding the three partial coefficients totalling α1, α2, and α3. These coefficients denote the effects of slope grade, soil and bedrock permeability and vegetation cover. Original tables developed by Kenessey provide standard values for each of these factors normalized to Hungarian conditions; therefore, they are well-suited for use in this study.

For each LC class the factors above were made part of the land use RO coefficient. Because the area was rather flat, with slopes of less than 3.5% which is very gentle terrain, the α1 values reflect that little slope would have been impacting the runoff values. To evaluate the soil permeability factor (α2), the reference soil texture data was obtained from the Hungarian agro-topographic map developed by Várallyay and Molnár (1989) at a scale of 1:100,000 and had around 3,500 soil mapping units (SMUs) with each unit

described with nine base soil parameters. The soil dataset compiled digitally by Pásztor et al. (2018) was used to classify the soil textures and permeability characteristics in each of the LC class (Fig. 1c).

Soil texture is a key factor in determining infiltration and drainage capacity. Sandy soils, which have larger pore spaces, drain quickly and have the highest permeability. Clayey soils, which have finer pores and are less permeable, hold water longer. For example, forests, lawn, and pasture are primarily located in sandy soils (81.6% and 67.7% respectively) which are defined as highly permeable by α2. All forested vegetation cover was classified as closed canopied to coincide with Kenessey's α3. Taking into consideration slope (α1), soil permeability (α2), and vegetation cover (α3) the RO coefficients of forest, and pasture/lawn areas were 11% and 28% respectively.

Areas of bare ground are largely located on loamy soils (72.25%) with moderate permeability. In terms of vegetation condition, according to Kenessey's framework, they are slightly better than marginally cultivable and worse than pasture. For this reason, I determined a runoff coefficient for bare ground of 31%. Crop-covered areas were also largely on loamy soils (48.4%) with moderate permeability (α2). Vegetation coverage is representative of a mixture of partially cultivated fields (α3) and light shrub cover; therefore, I assigned a runoff value of 22%. Because Kenessey does not identify values specifically for urban land types, especially for absolute and semi-absolute surfaces, I relied on additional literature sources (i.e. Table 4) and expert inputs to generally assign the runoff coefficients for these LC types.

Table 3. Summary of Kenessey factors and sub-factors (Kenessey 1928, 1930).

	Kenessey 1928, 1930	Mean values (%)	
Slope conditions and factors	Very strong slope (> 35 %)	α_1	26
	Strong slope (35 % – 11 %)		16
	Moderate slope (11 % – 3.5 %)		8
	Gentle slope (< 3.5 %)		3
Permeability conditions and factors	Impermeable	α_2	26
	Low permeable		16
	Permeable		8
	Very permeable		4
Sterility conditions and factors	Bare rock area	α_3	26
	Pasture		21
	Broken cultivated land and light woody shrubs		11
	Closed forest, loose rubble soil, rocky or sandy deserts		4

Table 4. Runoff coefficients for sealed and semi-sealed LC classes from various studies.

LC Categories	Runoff Coefficient (%)	Bibliographical references
Forest	11	Kenessey (1928, 1930)
Lawns and Pasture	28	
Area with Crop Cover	22	
Bare Ground	31	
Sealed Surface	82	Brown et al 1996, Malcom et al. 1997, Bourrier R 1997, Lindeburg M.1999, Musy A et al 2004, The Comet Program 2010, Seto et al 2011, Pontius et al. 2000. Town of Buckeye Public Works Department 2007.
Semi Sealed Surface	66	
SWBs	-	-

Infiltration

Infiltration is perhaps the most indefinable factor in the modelling process of the study due to its intricate foundations and the sensitive nature of soil texture. Infiltration has been impeded by manipulations and compaction of urban soils that add another layer on estimating infiltration as is. To bypass estimating infiltration directly, we used a water balance, and treated infiltration as an unknown variable, and estimated it by LC classification. The volume of infiltration per LC class was calculated by substituting the estimated variable in the water balance, and then deriving the ratio of infiltration, using Eq.19 and following the methods outlined by Batelaan and De Smedt (2001).

$$\mathrm{I} = 100 - (\mathrm{ET_{cn}} + \mathrm{R}) \qquad 19$$

Where,

I Is infiltration rate [%],

ET_{cn} Is evapotranspiration rate [%], and

I Is runoff rate [%].

We considered the runoff $C_R(n)$, infiltration $C_I(n)$ and evapotranspiration coefficient $C_{ET}(n)$ of Landuse class n (Eq. 20):

$$\begin{cases} 0 \leq \mathrm{C_R(n), C_I(n), C_{ET}(n)} \\ \mathrm{C_R(n) + C_I(n) + C_{ET}(n)}, \end{cases} \quad \forall n \qquad 20$$

Where,

$C_R(n)$ Is LC specific runoff coefficient,

$C_I(n)$ Is LC specific infiltration coefficient.

$C_{ET}(n)$ Is LC specific evapotranspiration coefficient.

Where P present the volume of total precipitation of a certain area to come up with simple, qualitative indicators, it was assumed that after an arbitrarily long period of time, this volume of water gets divided into RO water, I water, and ET water (Eq. 21-23).

$$\mathrm{R(t) = f_R(t)P} \qquad (21)$$

$$\mathrm{I(t) = f_I(t)P} \qquad (22)$$

$$\mathrm{ET(t) = f_{ET}(t)P} \qquad (23)$$

Where,

R: RO volume of the area [mm].

I: Infiltration volume of the area [mm].

ET: ET volume of the area [mm].

t: Duration of RO phase.

P: Is the volume of water falling as precipitation on area [mm].

Eq. 24 represents the proportion of precipitation that contributes to surface runoff within the study area. . However, it does not specify the subsequent fate of this runoff, which may continue flowing, infiltrate the soil, be taken up by vegetation, or evaporate. Therefore, we consider the fractions of runoff, infiltration, and evapotranspiration (f_R,f_I andf_{ET}) are simple indicators of trends in the relative importance of the three main hydrological processes runoff, infiltration, and evapotranspiration according to land use (Eq. 24).

$$\begin{cases} \mathrm{f_R(t)} = \sum_{\mathrm{n=1}}^{\mathrm{N}} \mathrm{C_R(n)a_n(t)} \\ \mathrm{f_{ET}(t)} = \sum_{\mathrm{n=1}}^{\mathrm{N}} \mathrm{C_{ET}(n)a_n(t)}, \\ \mathrm{f_I(t)} = \sum_{\mathrm{n=1}}^{\mathrm{N}} \mathrm{C_I(n)a_n(t)} \end{cases} \quad (24)$$

Where,

$C_R(n)$ Is land use specific runoff coefficient.

a_n Is land use surface.

$C_{ET}(n)$ Is land use specific evapotranspiration coefficient.

$C_I(n)$ Is land use specific infiltration coefficient.

3.6 Method to detect LC change and its impact on crop yield

3.6.1 LC Classification and Change Detection

Despite Debrecen's rapid urbanization and industrial growth (Pénzes et al., 2023), LC change detection studies focused on this region remain limited (Kovács, 2011; Szilassi, 2017). Whereas LC changes can be detected through an array of satellite data and methodologies, the process almost always turns out to be complex enough to require due methodological consideration (Haque et al., 2017; Settembre et al., 2024). LC changes

become simple to detect by comparing satellite data taken from different dates for regions-all across different countries, or instances (Boriah, 2010).

In this study, we aim to quantify the spatial extent of urban area expansion driven by industrialization between 2018 and 2022. To conduct the change detection analysis, we utilize the highest-performing LC maps generated in the previous section, based on the optimal combination of satellite imagery and classification algorithm identified through accuracy assessment. By selecting the most reliable classifications for both 2018 and 2022, we ensure maximum confidence in the analysis outcomes. This approach enables a robust comparison across years and supports the accurate identification of LC transitions. The primary focus of this analysis is on detecting and quantifying changes from non-urban to urban LC classes. The results aim to reveal the extent and spatial distribution of urban sprawl driven by industrial development in Debrecen during the study period. These findings will be presented through a combination of maps and statistical summaries highlighting both the magnitude and specific locations of urban expansion.

Trajectory analysis is a method for analyzing LC change over several periods by examining the sequence of transitions that land categories follow. This allows researchers to move beyond simple comparisons across two time periods and give a more sophisticated interpretation of temporal patterns and dynamics of LC change. This proposal employed trajectory analysis, a function within our theoretical framework, to analyze and interpret the spatiotemporal dynamics of developed land observed over a four-year period of time in Debrecen (2018 to 2022). Following the work of Bilintoh et al. (2024), we classified each pixel in our study area under LC status for each time point, and recipes for a trajectory were created based on the order in which transitions occurred and the LCD. Pixels were then classified into types of trajectories, such as Gain (Gain without Alternation), Loss (Loss without an Alternation), Stable Presence, Stable Absence, and types of Alternations. Exposure to this type of analysis provided us a way to differentiate between areas of continuous construction, temporary conversion, and transitions between multiple LC status, providing a more holistic representation of both genre and unique aspects of urban development and shrinkage. Our time-series Trajectories R package is fully functional and with documentation free to use available online at: https://github.com/bilintoh/timeseriesTrajectories. The use of trajectory analysis is also in line with the methods used by Bilintoh et al. (2024) when comparing

urban impervious surfaces, where distinct long-term and short-term Land-use changes could be identified using trajectory analysis. Inclusion of trajectory analysis in our case spatiotemporal dynamic analysis sought to contribute to a broader understanding of the complexity of urban LC dynamics.

3.6.2 Crop Yield Data and Trend Analysis

In order to evaluate the influence of urban expansion on agricultural productivity, the research collected the statistical data on crop yields from the Hungarian Central Statistical Office for Hajdú-Bihar County. The data set includes the annual numbers from 2000 to 2024 for two main crops in the county (wheat and maize) in terms of harvested area (ha), production volume (tons), and average yield (kg/ha). As specific crop yield data for Debrecen are unavailable, we used data from Hajdú-Bihar County, which encompasses Debrecen. This broader dataset offers a representative overview of agricultural trends in the region most likely affected by LC changes occurring in and around Debrecen.

To visualize the temporal trends in production, yield, and harvested area, descriptive statistics were utilized. After that, the trends in these datasets were matched against the LC change data to unravel how the urban expansion correlated with the agricultural outcomes. This hybrid of spatial and statistical analyses enables a cohesive interpretation of the landscape changes and their potential impact on agri-food systems at the regional level.

4. RESULTS

4.1 Watershed Parametrization and Morphometric Analysis

4.1.1 Delineation and Division of Sub-Watersheds

The delineation of the sub-watersheds within the Debrecen study area was established using ArcGIS software that utilized a DEM with a spatial resolution of 30 meters. Through hydrological analysis tools embedded in ArcGIS, the elevation of the terrain was studied to determine the directions of flow and the accumulation of flow, which are fundamental for drawing the outlines of the watershed and rivers.

The hydrological delineation of the watershed has allowed us to identify 9 sub-watersheds which represent the primary units of the study. Besides, these basins have a total surface area of 1,488 km². These are also the main hydrological units from which we derive the water quality monitoring network and conduct morphometric analysis, as well as develop hydrological models. The watercourse network derived from flow accumulation analysis was combined with Debrecen's administrative boundaries to highlight the relationship between the natural drainage system and the city's vegetated zones.

Figure 22 illustrates the spatial layout of the confirmed sub-watersheds, the derived hydrographic network, and the administrative boundaries of Debrecen. This layout serves as a validation of the drainage structure and demonstrates how the topography governs the division of the study area into distinct sections

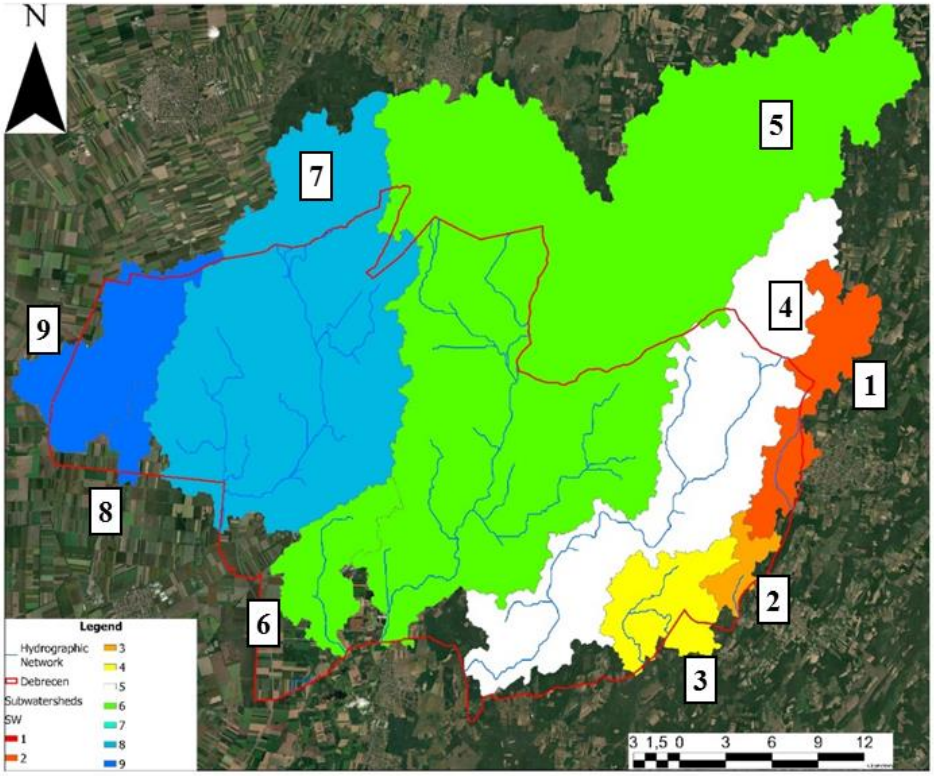

Figure 22. Sub-watersheds and Hydrographic Network of Debrecen (Source: Author, 2025).

The major physical attributes of the sub-watershed like length (L), area (A), and perimeter (P) were determined using ArcGIS's spatial analyst and zonal statistics tools (Table 5). Such parameters are vital for the study of hydrological processes, surface RO simulation, and morphometric analysis.

Table 5. Physiographic characteristics of the 9 sub-watersheds.

Id	**1**	**2**	**3**	**4**	**5**	**6**	**7**	**8**	**9**
P (km)	69.7	28.97	45.53	144.09	221.57	46.56	113.22	25.03	59.351
A (km^2)	50.34	12.85	46.57	214.56	710.34	44.30	324.19	12.238	72.83
L (km)	14.19	3.1	9.59	50.35	69.19	11.93	34.37	1.39	14.8

This sub-watershed framework sets the foundation for subsequent analysis of compactness, form, and time of concentration to better understand hydrological responses in each unit.

4.1.2 Morphometric Characterization: Gravelius Compactness Index and Basin Form

To further investigate the morphometric structure and spatial geometry of the sub-watersheds in the Debrecen, the Gravelius Compactness Index (GC) was computed for each of the 9 specifically delineated sub-basins (Table 6). This index, which is based on the area and perimeter of the basins, gives a standardized basin shape—thus enabling a comparison of how compact or elongated a watershed is compared to a perfect circle (GC = 1.0).

The necessary properties: A, P, and mainstream L, were obtained using ArcGIS spatial and hydrological analysis tools. Sub-basin 5 (SB-5) was sized as the largest unit, which contributed approximately 48% of the whole study area and had the longest main channel length of 69.19 km, signifying its deep impact on the hydrological response of the whole watershed. In contrast, SB-2 and SB-8 are the smallest sub-basins, with areas of 12.85 km^2 and 12.23 km^2, respectively.

The GC index that was calculated for all 9 sub-watersheds yielded values that were beyond 1.77, thus confirming their elongated or rectangular shapes. In other words, the sub-watersheds are nowhere near being compact or circular in shape, which are normally the conditions that would have led to faster RO concentration. Rather, the elongated nature of these basins means that RO will have to travel a longer distance in order to get to the outlet, which thus could lead to a smaller peak discharge but a longer flood response period.

Table 10 lists the compactness index and the interpreted basin form for each sub-watershed in detail. The uniform trend of stretching in all sub-basins suggests that the topography and the drainage development in the Debrecen region are strongly in favor of pulled, rectangular watershed configurations.

Table 6. GC index and Basin Form.

Sub-watershed ID	Compactness index (GC)	Basin Form	Shape
1	2.77	Elongated basin	Rectangular
2	2.27	Elongated basin	Rectangular
3	1.88	Elongated basin	Rectangular
4	2.77	Elongated basin	Rectangular
5	2.344	Elongated basin	Rectangular
6	1.9	Elongated basin	Rectangular
7	1.77	Elongated basin	Rectangular
8	2	Elongated basin	Rectangular
9	1.96	Elongated basin	Rectangular

The results indicate a clear morphometric trend across the study area, which has implications for flood management and hydrological modeling. Elongated basins, while slower to concentrate RO, are often more susceptible to extended flood durations, requiring careful planning for urban and agricultural water management strategies.

4.1.3 Estimation of Time of Concentration for Sub-Watersheds

The time of concentration (Tc) is a significant hydrological characteristic, which is used to gauge the speed at which a watershed responds to a rain event. It is a measure of the time for the most remote location in the watershed to provide water that has traveled all the way to the outlet. This factor is particularly vital for designing flood protection facilities as well as for controlling the peak discharge in urban and agricultural sectors.

In this research, the Kirpich equation was utilized to obtain the Tc for each of the 9 sub-watersheds drawn in the Debrecen area (Table 7). This empirical relation is best for small- to medium-sized basins and it takes into account both the length and the slope of the main channel. The input variables, such as basin area, mainstream length, and elevation drop (H), were derived through ArcGIS and DEM based hydrological modeling.

According to Table 7, the longest time of concentration was found in Sub-watershed 5 (SB-5), with a value of 28 h 5 min, followed by Sub-watershed 4 (SB-4) at 15 h 8 min. These large Tc values are mainly due to the fact that these basins have their areas larger

and their mainstream lengths longer, hence, the RO reaching the outlet will naturally take a longer time.

Sub-watersheds 2 and 8 (SB-2 and SB-8) however, reported the shortest concentration times of 1 h 56 min and 0 h 56 min, correspondingly. Due to their nature of being small, compact, they have short travel distances besides their steep inslopes, this helps the running water move faster.

Getting to know the variations of concentration times between the sub-watersheds over their hydrological behavior and their vulnerability to flood events provides great insights. Quick Tc value sub-basins are predicted to induce rapid flash floods, particularly under heavy rainfall, whereas, longer Tc value ones are prone to receive slow but still continuous RO, thus changing flood duration and drainage system operation.

Table 7.Time of concentration of the sub-watersheds.

Id	Area (km^2)	Perimeter (m)	H (m)	Tc
1	50.344	69.704	15.100	7 h 7 min
2	12.853	28.970	4.610	1 h 56 min
3	46.570	45.537	108.000	2 h 7 min
4	214.569	144.095	94.831	15 h 8 min
5	710.347	221.579	49.390	28 h 5 min
6	44.309	46.563	8.830	7 h 9 min
7	324.192	113.224	51.030	12 h 22 min
8	12.238	25.030	2.750	0 h 56 min
9	72.830	59.351	19.800	6 h 43 min

The differences in time of concentration reflect the hydro-morphological diversity across the Debrecen watershed and provide an essential baseline for hydrological modeling, flood prediction, and sustainable land-use planning. In future studies, these Tc values can be used to simulate flood hydrographs, assess runoff dynamics, and optimize the design of stormwater management infrastructure.

4.2 Rapid and Quasi-Real-Time LC Mapping in Urban Environments Using L8 Imagery and ML-Based MLSC for the Year 2019

4.2.1 Training data quality assessment of the mapping

Simple separability measures, such as the transformed divergence (TD), are employed to evaluate the statistical distinction between LC classes within a training dataset. These measures assess class separability in an N-dimensional spectral space, where N denotes the number of spectral bands. The pairwise separability analysis produced J-M values exceeding 1.9 and TD values reaching the maximum score of 2.0, as presented in Table 8. These high values reflect excellent spectral discrimination among classes, indicating that the training dataset effectively captures the unique spectral characteristics of each LC type.

Table 8. Spectral signature separability measures for all pairs using Jeffries-Matusita.

Class pairs		Jeffries-Matusita
Area with crop cover	Sealed surface	2
	Lawns and pasture	2
	Forest	2
	Semi-sealed surface	2
	Bare ground	2
	Surface water bodies	2
Bare ground	Semi Sealed surface	1.9
	Sealed surface	2
	Lawns and pasture	2
	Forest	2
	Surface water bodies	2
Forest	Semi Sealed surface	1.9
	Sealed surface	2
	Surface water bodies	2
	Lawns and pasture	2
Lawns and pasture	Semi-sealed surface	1.9
	Surface water bodies	2
	Sealed surface	2
Sealed surface	Semi sealed surface	1.9
	Surface water bodies	2
Semi sealed surface	Surface water bodies	2

Figure 23 illustrates the spectral signatures of various LC categories extracted from the L8 training dataset, providing insights into their reflectance behavior across different bands of the electromagnetic (EM) spectrum. In the visible portion of the spectrum, most LC classes exhibit only slight separability based on differences in reflectance intensity. Semi-sealed surfaces and crop-covered areas display the highest reflectance values in this range. Notably, forested areas and surface water bodies (SWB) show nearly identical spectral responses, including in the red wavelength, making them difficult to distinguish in the visible bands.

In the near-infrared (NIR) region, all LC categories are more distinct, with the exception of forest, bare ground, and lawns and pasture, which remain spectrally similar. Surface

water bodies are clearly differentiated in this region by their significantly lower reflectance, particularly in band 5 and the shortwave infrared (SWIR) bands. Across the SWIR bands, crop-covered areas exhibit the highest reflectance intensities, enhancing their separability from other classes.

However, certain spectral overlaps persist in the SWIR region: bare ground and semi-sealed surfaces show minimal distinction in SWIR1, while bare ground and lawns and pasture are spectrally similar in SWIR2. Among all LC categories, semi-sealed surfaces demonstrate the highest standard deviation (SD) values, ranging from 200 to 1269, indicating substantial heterogeneity and pixel mixing. In contrast, surface water bodies show the lowest SD values (12 to 23), reflecting their spectral uniformity and minimal pixel variability. This variation emphasizes the spectral complexity of urban surfaces compared to the homogeneity of water bodies.

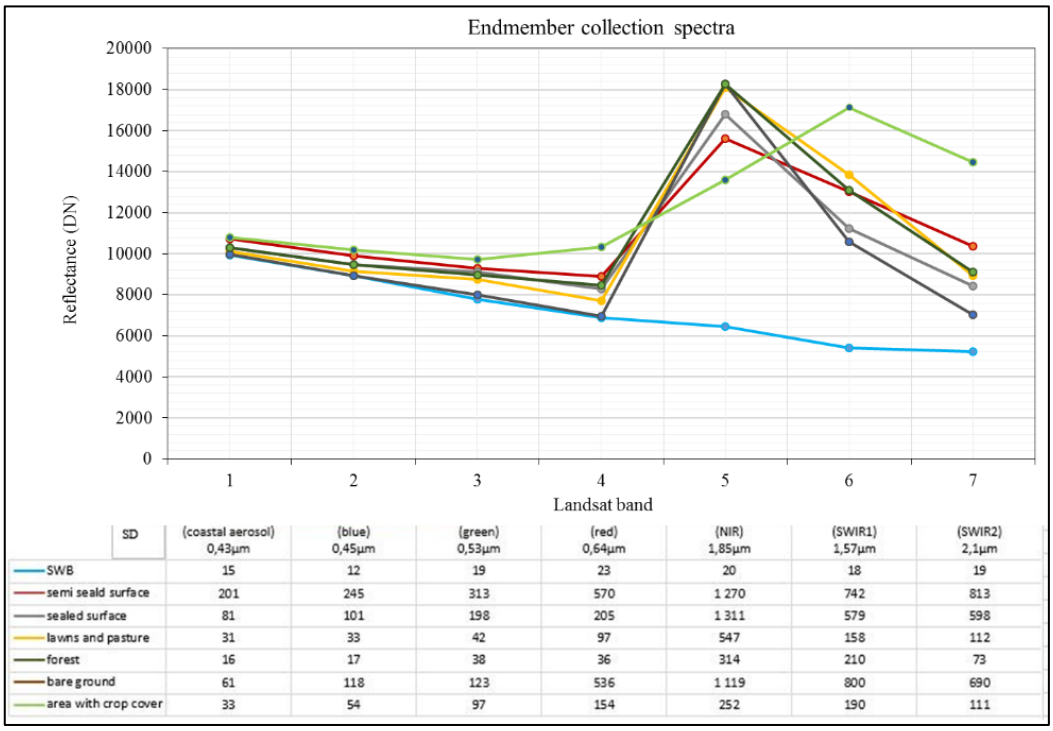

SD	(coastal aerosol) 0,43µm	(blue) 0,45µm	(green) 0,53µm	(red) 0,64µm	(NIR) 1,85µm	(SWIR1) 1,57µm	(SWIR2) 2,1µm
SWB	15	12	19	23	20	18	19
semi seald surface	201	245	313	570	1 270	742	813
sealed surface	81	101	198	205	1 311	579	598
lawns and pasture	31	33	42	97	547	158	112
forest	16	17	38	36	314	210	73
bare ground	61	118	123	536	1 119	800	690
area with crop cover	33	54	97	154	252	190	111

Figure 23. Plot of spectral reflectance for L8 bands 1, 2, 3, 4, 5, 6 and 7 with standard deviation (SD) values (Source: Author, 2025)

4.2.2 Validation and LC mapping in Debrecen

To assess the final LC map's robustness, first, the accuracy of classification was assessed. The OA reached 81.2% and the Kappa was above 0.78, meaning that around 81.2% of the 770 reference samples (110 per LCclass) were correctly classified and

18.8% were misclassified. According to Sajjad et al. (2022), Kappa statistics between 0.50 and 0.75 display acceptable model performance, indicating that the classification results are robust and reflective of reality.

Further assessment of classification performance at the class level was conducted using the F1-score metric (per class), as recommended by Talha et al. (2023). The highest and most balanced F1-scores were observed for forests (0.97), semi-sealed areas (0.94), and surface water bodies (0.90), reflecting strong model accuracy for these categories. In contrast, LC classes such as crop-covered areas, lawns, and pastures displayed lower and more imbalanced F1-scores, suggesting the presence of spectral confusion or signal mixing during classification. Specifically, the F1-scores for crop cover and for lawns and pastures were 0.647 and 0.668, respectively (Table 9).

Table 9. Accuracy assessment: K error matrix resulting from classifying test pixels.

LC category	Users' accuracy [%]	Producers' accuracy [%]	F1 score
Surface water body	83.3	100	0.908
Lawns and pasture	64	70	0.668
Forest	94.4	100	0.971
Semi sealed surface	88.8	100	0.940
Area with crop cover	63	66.6	0.647
Bare Ground	83.3	63.6	0.721
Sealed surface	88.8	72.7	0.799

In addition to classification errors, there are other uncertainties regarding the OA of LC classifications such as the quality of the training or validation samples used, interpretation errors, positional errors in images resulting from image registration process. Typically when assessing accuracy we assume the discrepancies between the classified outputs and reference data can be fully attributed to classification error. There are many other factors that can create uncertainty for examples, the geographic and radiometric resolution of any RS data is finite, the atmospheric condition during scene capture can add uncertainty, limitations with the sensor can lead to uncertainty, positional error from geometric rectification and image registration procedures can lead to positional inaccuracies, and any processes used for atmospheric or topographic correction may add radiometric errors (Lu et al., 2008). The actual LC map and associated hydrological parameters for the year

2019 are shown as an example. The LC distribution from Figure 24 highlights some significant spatial variability in the LC within the study areas.

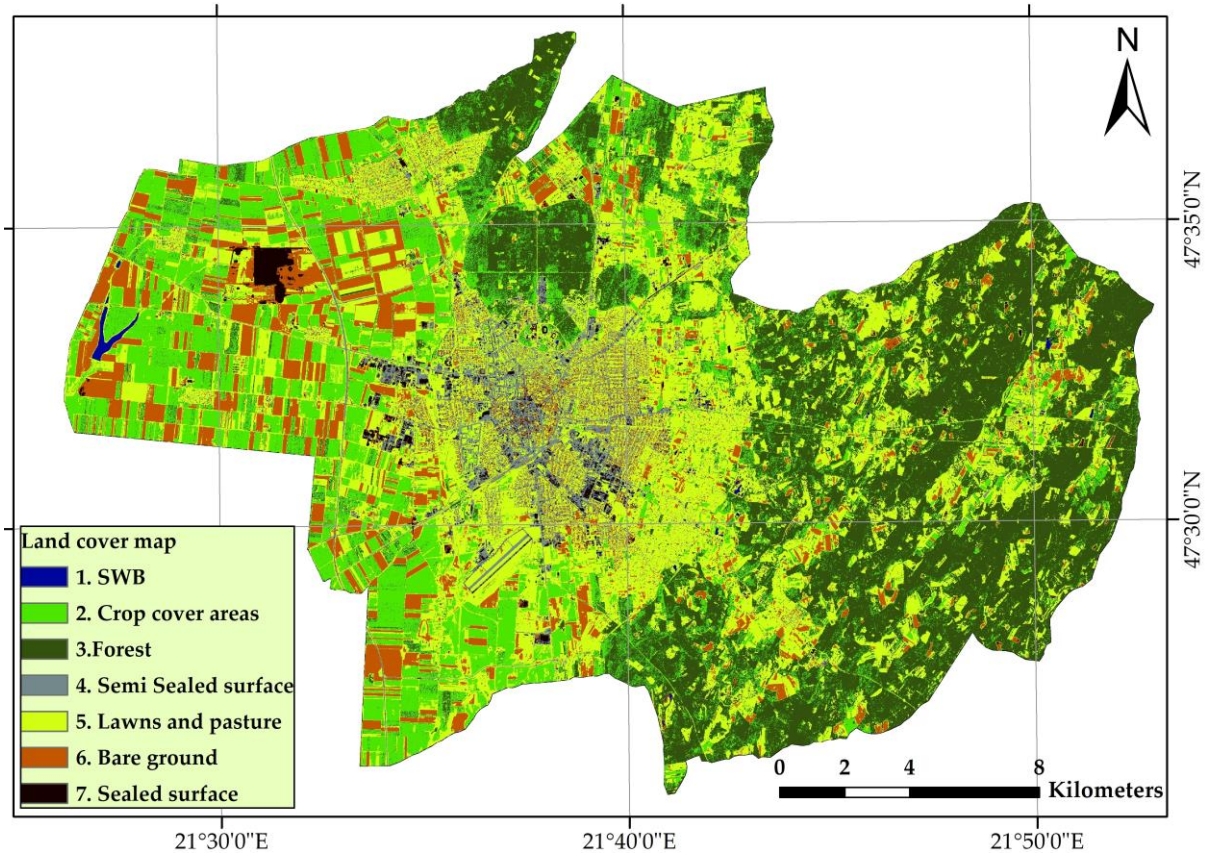

Figure 24. LC map for Debrecen based on L8 data (19/06/2019) (Source: Author, 2025).

Forests are predominantly found in the northern and eastern parts of the watershed, while crop-covered areas make up the largest share of LC. Urban development is mainly concentrated in the central region of the basin. Based on statistical analysis, crop-covered areas are the dominant LC class, occupying 32.78% of the total area—equivalent to 15,120.22 hectares. It is worth noting that both crop-covered and bare ground areas are utilized for agricultural production. Forests account for a significant portion of the landscape as well, covering 30.26% (13,958.05 hectares). Sealed surfaces, mainly located in the basin's central area, represent 1.5% of the region, or 692.46 hectares. Lawns and pastures extend across 9,415.21 hectares, comprising 20.41% of the total area. Bare ground, covering 10.18% or 4,698 hectares, also plays a role in the region's agricultural use (Table 10).

According to Iváncsics and Kovács (2021), between 2000 and 2006, the area of sealed surface in Debrecen grew by 285.9 hectares which was a result of increased population, economic development and expansion of the services sector and

infrastructure. Urban sprawl had a serious impact on agricultural land in the city (Tarawally et al., 2019). The dominant crops grown in the study area are corn and wheat, and the fields are usually left relatively bare after harvest. This means that the bare ground and crop cover types are constantly changing within the yearly cycles, and also vary each year due to crop rotation. Conversely, forest type is much more stable and experienced very little change throughout the year, except for seasonal changes that cause leaves to drop at different times throughout the year.

Table 10. Area and percentage of different LC categories in Debrecen basin.

LC category	Area [ha]	Proportion [%]
Surface water body	82.65	0.17
Lawns and pasture	9415.21	20.41
Forest	13958.05	30.26
Semi sealed surface	2149.53	4.66
Area with crop cover	15120.22	32.78
Bare Ground	4698.1	10.18
Sealed surface	692.46	1.5
Total	46116.25	100

4.3 Accuracy Enhancement of LC Classification Using Multi-Sensor RS and Machine Learning

4.3.1 Training data and Validation

Both the L8 (2018, 2020, and 2022) and S2 (2018, 2020, and 2022) datasets' excellent quality and efficacy were validated by the spectral separability study utilising the J-M and T-D indices. Every pair of LC classes displayed excellent spectral separability, with T-D and J-M values much above the 1.9 criterion. This demonstrates how the training data was able to capture the distinct spectral features of the various LC classes, leading to an accurate and trustworthy classification:

- All class pairs reached J-M index values higher than 1.9, meaning sufficient separability for a correct classification.
- The index of T-D showed a constant score of 2, representing total separability for the training data.

The results of the separability analysis show that there is clear separation between the spectral signatures of all pairs of LC class pairs. J-M index and TD indices showed a great outcomes (>1.9). The results indicate that the training dataset captured unique spectral properties for each LC class. The values of >1.9 for separability show that the training samples were of sufficient quality and suitability for suitable classification.

4.3.2 Machine learning based LC classification

The classification performance of the LC types is compared in Table 11. Three classification methods were trailed (SVM, MLC, RF) using satellite images from two sources, L8 and S2 captured in 2018, 2020, and 2022. Performance was evaluated with many metrics such as F1 score for the LC types, OA, K, and Pontius accuracy metrics.

Table 11. Accuracy assessment for all combinations of satellite imagery and ML classifiers.

satellite	classifiers	years	F1 score per LC types						OA%	K	Q %	A %	D %
			forest	developed	crop covered areas	grassland	surface water bodies	bare ground					
Landsat 8	SVM	2018	0.86	0.72	0.74	0.72	0.31	0.87	80	0.74	4.91	12.58	17.5
		2020	0. 96	0.74	0.63	0.88	0.66	0.7	83	0.78	11.8	5.9	17.7
		2022	0.92	0.75	0.75	0.83	1	0.82	85	0.8	7.05	8.33	15.3
	MLC	2018	0.83	0.6	0.78	0.8	0.53	0.78	78	0.72	7.8	10	17.8
		2020	0.95	0.44	0.52	0.67	0.9	0.72	71	0.63	4.48	15.22	19.7
		2022	0.96	0.8	0.7	0.79	0.66	0.75	83	0.77	3.9	10.6	14.5
	RF	2018	0.82	0.77	0.73	0.76	0.5	0.86	77	0.7	7.14	10.61	17.8
		2020	0.93	0.72	0.52	0.84	1	0.69	80	0.73	6.7	10.9	17.6
		2022	0.95	0.78	0.61	0.72	0.61	0.88	81	0.75	11.9	6.4	18.3
Sentinel 2	SVM	2018	0.87	0.88	0.86	0.89	0.57	0.86	85	0.81	3.69	9.43	13.1
		2020	0.98	0.77	0.88	0.92	0.66	0.75	90	0.87	5.6	7	12.6
		2022	0.94	0.75	0.87	0.9	0.73	0.93	89	0.85	4.2	11.1	15.3
	MLC	2018	0.93	0.45	0.66	0.78	0.85	0.9	80	0.75	5.5	14.5	20
		2020	0.95	0.79	0.93	0.87	0.66	0.75	85	0.8	4.33	9	13.3
		2022	0.92	0.67	0.73	0.81	0.73	0.8	83	0.79	8	13.3	21.3
	RF	2018	0.88	0.73	0.8	0.79	0.5	0.78	78	0.72	15	8.18	23.1
		2020	0.94	0.8	0.64	0.77	0.8	0.76	82	0.73	2.67	15.3	17.9
		2022	0.9	0.72	0.67	0.75	0.66	0.74	80	0.74	8	24	32

Overall, the results show the combination of S2 imagery and the SVM classifier achieved an OA greater than most other classifier-satellite pair combinations. For instance, with the SVM and S2 data in 2020 alone, the OA was 90% with a Kappa coefficient of 0.87. This combination also supported classifying some LC types better than the others, such as forest (F1 score = 0.98), developed (F1 score = 0.77), and grass (F1 score = 0.92) in the same year.

A primary goal of this analysis was to determine the best combination for urban area detection. Each evaluation indicates that the SVM and S2 combination outperformed any of the classification methods in regard to all performance indices. The F1 score for developed areas was high at 0.88 in 2018 with this combination and was substantially higher than any other classifier–image combinations. Overall, results indicate that SVM adequately captures the complex spatial and spectral signature of urban environments, along with the high spectral and spatial resolution of S2 providing the most relevant input for accurate urban classifications.

While this study confirmed that the SVM-S2 method provided the highest classification accuracy for mapping Debrecen's urban environment, it should be noted that the most suitable approach may differ depending on the goals of the research and the specific region (Cortes & Vapnik, 1995; Mountrakis et al., 2011).

In general, the findings emphasize the promise of combining SVM with S2 data for urban LC mapping. The findings have significance for urban planning, agricultural land management, and environmental monitoring. Figure 25 depicts the mean F1 scores that were produced for each LC category during the study, and the figure shows that the SVM–S2 combination performed better in their F1 scores for most classes.

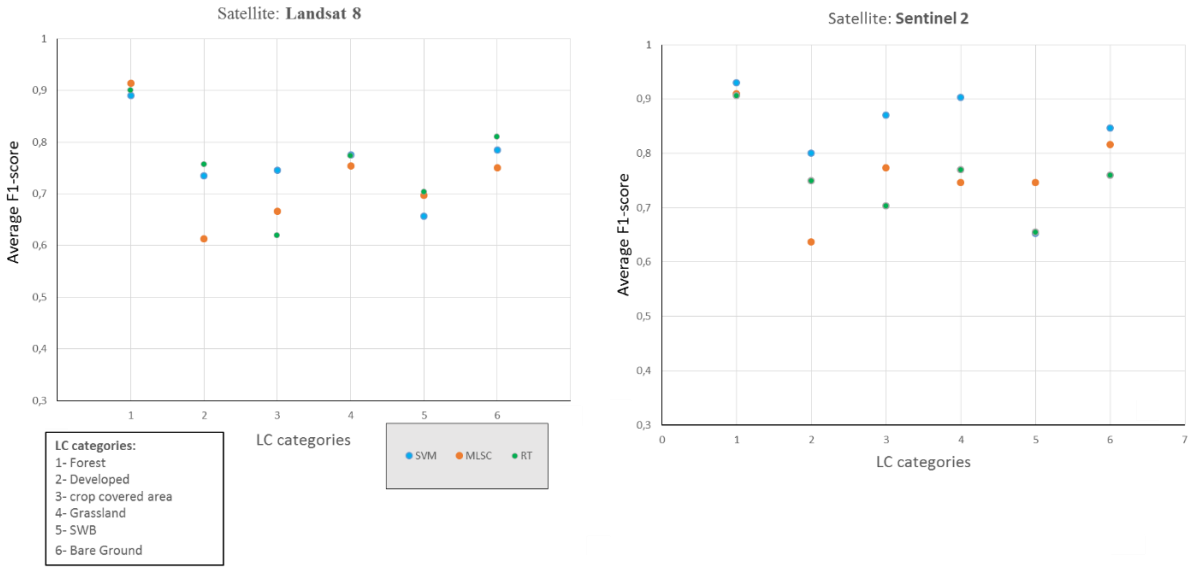

Figure 25. Average F1-score distribution per categories (Source: Author, 2025)

The summary of the classifiers' performance, shown in figure 25, shows clearly distinguishable patterns in the six LC classes F1-scores. Importantly, the combination of S2 imagery and the SVM classifier always yielded the best accuracy. For example, the average F1-score for the forest classification provided its highest F1-score of about 0.93 using S2+SVM, better than the other combinations. Similarly, crop-covered areas provided their average F1-score of about 0.85 with S2+SVM compared to using L8. For developed areas, an important LC class in urban studies, S2+SVM provided the average F1-score of about 0.80, which was the greatest depth of all classifier-sensor combinations for that class.

These results highlight the considerable ability of S2 data to capture complex LC patterns due to its high spatial and spectral resolution. To highlight the advantage in spatial resolution in the use of S2, it should be noted that the forest classification with L8+SVM returned an F1-score of 0.87, and S2+SVM returned an F1-score of 0.93. A comparable pattern was present for grassland, where S2+SVM returned an F1-score of 0.90, versus 0.77 with L8.

The SVM classifier achieved the most stable and accurate performance across LC types in the Debrecen study area. F1-scores usually remain above 0.85 for some classes, with particularly high scores for the forest (0.93) and bare ground (0.846) classes. The strength of the SVM classification process is especially realized when coupled with S2 data because SVM can define complex boundary delineations in mapping LC types (Pal & Mather, 2003; Zhao et al., 2023). Conversely, the MLC and RF classifiers exhibited the

most variability in classification results and F1 scores. The MLC classifier did not perform well and often failed downgrade classifications, particularly for developed and crop-covered areas, with the MLC F1-score of 0.636 for developed areas, compared to 0.80 with SVM (using S2). While RF performed moderately well, it tended to perform better than MLC with developed areas (F1 = 0.75) and grassland (F1 = 0.78) using S2 data, but significantly underperformed for crop-covered classifications (F1 = 0.703 vs. 0.87 with SVM).

Overall, combining S2 imagery with SVM always provided the highest and most robust classification performance across all evaluated LC types. This highlights the advantage of utilizing high-resolution satellite imagery as well as the use of robust machine learning algorithms for LC mapping.

Along with F1-scores, this study also used disagreement measures—Quantity Disagreement Q %), Allocation Disagreement (A %), and Total Disagreement (D %)—to analyze classification performance. Disagreement measures effectively describe sources of classification error by differentiating errors associated with incorrect proportion of classes and spatial misallocations.

According to the results, S2+SVM achieved the highest level of accuracy and the lowest disagreement values. In 2020, S2+SVM produced the lowest D% of all classifiers and sensor pairings, with a D% of only 12.6% – L8+SVM had 17.7 D% and no other classifier-sensor pairing produced lower total disagreement values. This reinforces the benefits of using S2 data, where classification errors are minimized due to superior spatial and spectral characteristics.

In terms of Q%, S2+SVM produced relatively low Q% values, with 5.6% in 2020 and 4.2% in 2022 being some of the lowest values from 2020-2022. In 2022, the MLC produce Q% 8% for S2, and the L8+SVM produced an 11.8% Q% for the 2020 D% calculation. This highlights SVM's excellent capability to accurately estimate class proportion when the spatial and spectral resolution of the data is high.

In this fashion, A %'s further bolster the strength of S2+SVM in spatially accurate classification. In 2020, S2+SVM's A% was 7%, compared to L8+SVM's (8.33%) and was also considerably better than MLC with S2's (13.3% in 2022). This indicates S2+"SVM were capable of spatially aligning LC classes to their actual geographic location, more accurately than MLC, as is intuitively perceived.

To conclude, all three of Q%, A%, and D% suggest SVM, particularly when used with S2, produces the best proportionate and accurate classification. Consistently producing

low total disagreement (D% = 12.6 in 2020 and 13.1 in 2022) puts SVM firmly on the map as robust for mapping both urban and natural LC classes in Debrecen.

4.3.3 Classification results

LC Classification of L8 Imagery in ArcGIS Pro

Using L8 imagery, the LC classification accuracy for 2018, 2020, and 2022 shows significant variations among classes and classifiers, as shown in Figure 26.

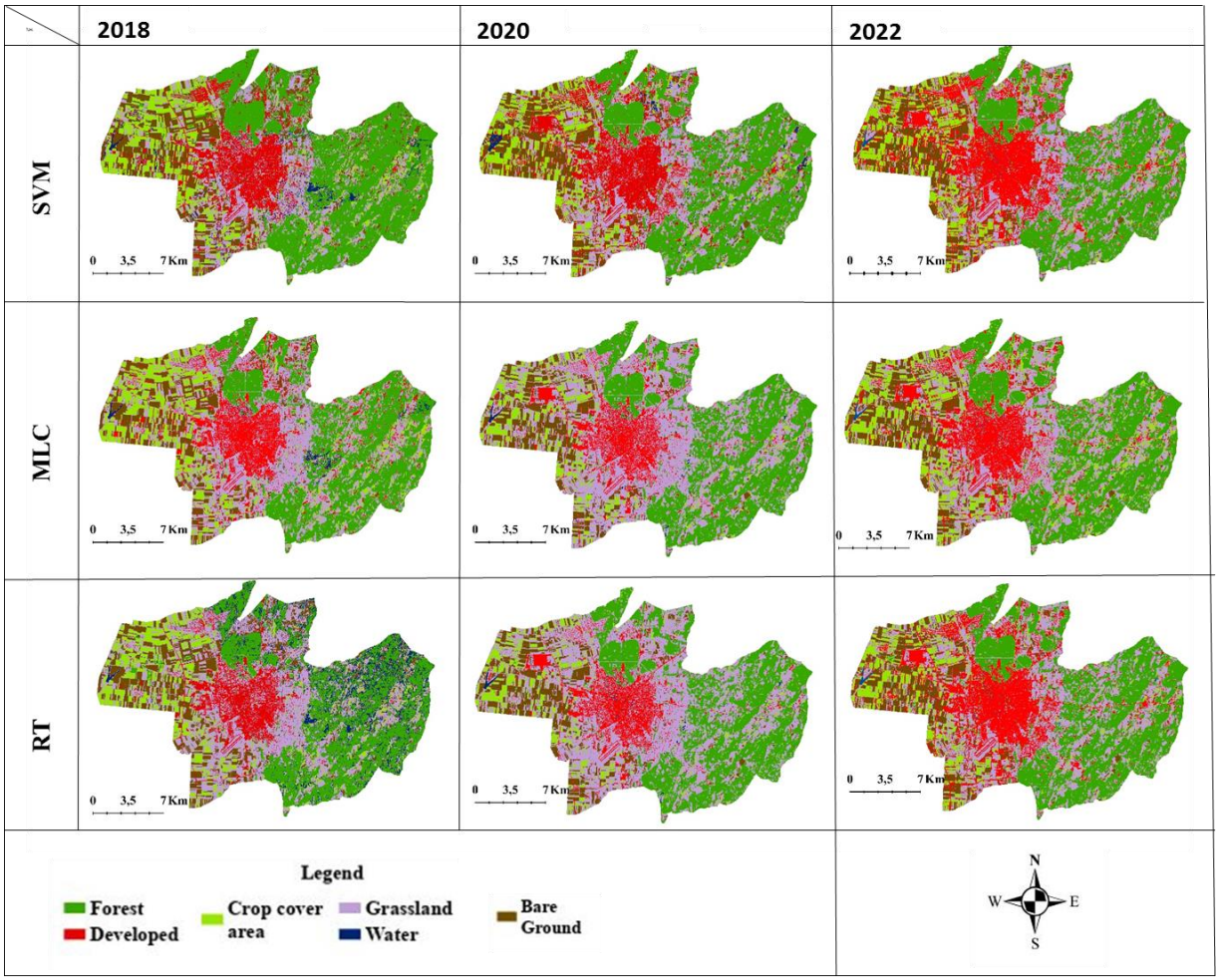

Figure 26. LC classification maps of L8 images using SVM, MLC, and RF classifiers for the years 2018 to 2020 and 2022 in ArcGIS Pro (Source: Author, 2025).

The RF classifier had major limitations in the 2018 year and did not distinguish forested areas from grassland or surface water bodies. In 2020, RF identified areas of crop cover as bare land or grassland. Likewise, the MLC classifier confused areas of developed land with current bare land and grassland in 2020. Grassland was expectedly misclassified as forest and as crop covered areas in years 2018 and 2022. The SVM classifier consistently had higher OA and F1 scores than both RF and MLC across all L8 images and years.

Even though SVM was better, it sometimes misidentified grasslands and even urban areas in 2020.

A regular classification error seen in both MLC and RF algorithms is the misclassification of vegetation as grassland, particularly in 2018 and 2020, usually due to spectral similarity among the LC types. The comparison of maps of LC comparison developed using L8 with multiple classifiers for 2018, 2020 and 2022 evidenced significant differences in the performance of the classifiers. Visual checks in individual years showed very clear differences between classifiers and noted LC changes across years. These findings highlight the importance of selecting classifiers that match the assumptions of the study area and the LC types. Considerations such as these are important for increasing the consistency and reliability of RS-derived land cover mapping.

LC Classification of S2 Imagery in ArcGIS Pro

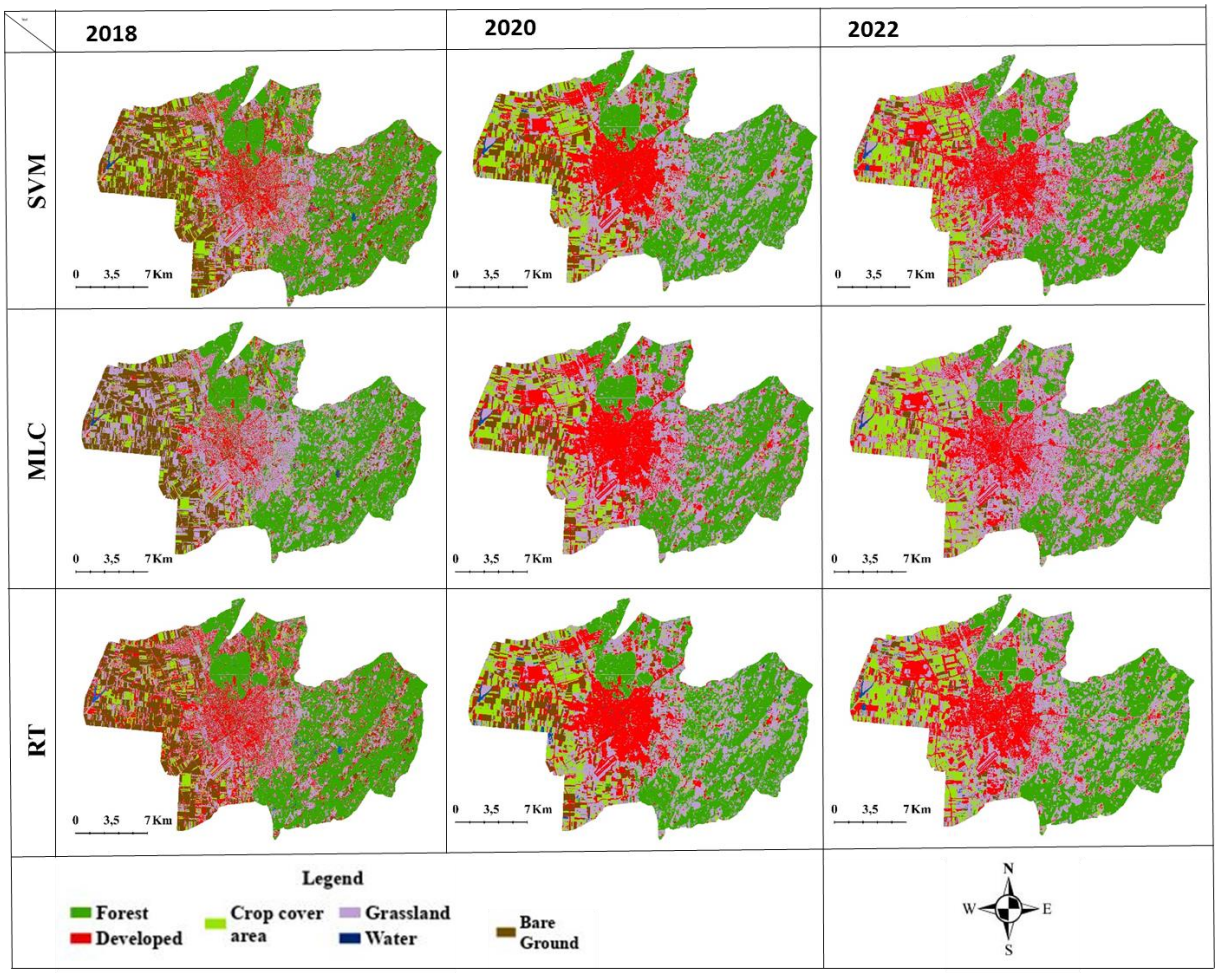

Figure 27. S2 maps of image classification produced with ArcGIS Pro by SVM, MLC, and RF classifiers for the time interval 2018–2020 and 2022 (Source: Author, 2025).

This section describes the performance of the three ML algorithms for classifying LC with S2 imagery. The research compared urban growth of LC from 2018 to 2022, and assessed some advantages and disadvantages of each classifier for single LC classes. The SVM consistently provided the best results across all classifiers, obtaining higher OA and F1 scores than MLC and RF. For example, in 2020, the SVM classifier obtained F1 scores of 0.98 for forest, 0.77 for developed, 0.88 for crop covers, 0.92 for grasslands, 0.66 for surface water, and 0.75 for bare ground. The F1 scores overall show that SVM had a better capacity to separate various LC types, and perform well relative to MLC and RF, when the landscapes were complex and contained urban and vegetative areas.

Overall SVM performed better than all other classifiers, but each ML method had its own advantages and disadvantages depending on the specific LC type. The MLC algorithm

was regularly challenged by developed areas, consistently misclassifying developed areas as grassland or bare ground. The RF classifier performed comparatively well for forest, developed, and bare ground classes, but was limited in correctly identifying areas as crop-covered or grassland. Although each of the classifiers had its unique struggles, it was worthwhile to notice that there was an increase in built-up areas from 2018 to 2022 based on change detection analyses of LC maps derived by all three classifiers (Figure 27).

The SVM classifier, being superior in identifying developed areas, gave the best performing representation for urban expansion. The incorporation of S2 imagery contributed to the OA of the LC classification. High spatial and spectral resolution, along with frequent revisit time, made S2 very useful in capturing subtle changes in LCs, especially within the urban areas. The availability of multi-years S2 imagery enabled accurate monitoring of the development of urban areas and proper assessment of the performance of classifiers over time.

4.4 Hydrological Modeling Integration with LC Dynamics for Urban Water Balance Analysis

Factors such as LC impacting hydrological variables, for instance, ET, RO, and I, are examined in the Debrecen basin to magnify certain aspects of the patterns generated. The area is predominantly flat in terms of topography, and the LC classification considers images taken at summer (July) in the narrower sense when maximum biomass and vitality of plants are usually observed. However, it should be noted that plant cover can undergo changes in different seasons throughout the year. The methodology of hydrological indicator calculation and validation is similarly flexible and can be applied to any other area in physical or temporal terms. ET, RO, and I were measured as percentage values of the total volume of average annual precipitation in the study. The values corresponding to the parameters measured for each LC type of the basin are summarized in table 12.

Table 12. Watershed Hydrological Responses to LC categories

LC class	ET Ratio			I Ratio
	Min [%]	Max [%]	Average [%]	Average [%]
SWB	83.40	88.59	85.99	-
Grassland	57.90	61.40	59.65	12.35
Forest	69.54	73.82	71.68	17.32
Semi sealed surface	18.00	19.19	18.59	15.40
Area with crop cover	54.45	57.80	56.12	21.87
Bare ground	6.95	7.38	7.165	61.83
Sealed surface	6.95	7.30	7.127	10.87

ET ratios for SWB were highest between 83.4% and 88.59%. The elevated ET rate can largely be attributed to the direct radiation of solar energy onto water surfaces. I was not computed for SWB as I from watercourses results largely from RO from catchments and not precipitation directly. Hence, the RO for SWB was calculated from the remaining precipitation after ET, which ranges from 11.41% to 16.6%, averaging 14%.

For forested areas, the model indicates that the evapotranspiration usually ranges between 69.54% and 73.82%. On the contrary, high runoff ratios exist for sealed, semi-sealed, and bare ground surfaces due to the absence of vegetation, which reduces the water-retaining capability and increases surface RO. In contrast, LC such as forests, crop covered areas, and grassland tend to have lower levels of RO, thus attesting to the value of vegetation in reducing losses of surface water via RO. Concrete, sealed surfaces are characterized by a high RO coefficient of 82%, whereas the ET coefficient decreases impressively to 7.13%. Semi-sealed surfaces display a RO coefficient of 66%, while the ET rate is 18.59%.

SWB and forests had the highest mean annual ET values among LC categories (85.99% and 71.68%, respectively) and sealed surfaces (7.13%) and bare ground (7.16%) had the lowest values. Sealed (82% RO of total annual precipitation) and semi-sealed (66% RO) LC provided the highest mean annual RO values. Crop covered areas provided 22% RO. Forests and bare ground only contributed 11% and 31% runoff, respectively. These data certainly represent the impact of urban LC where storm water RO is heightened due to reduced vegetative cover and increased impervious LC.

The overwhelming role of ET and surface RO compared to groundwater recharge in the basin emphasizes the need to improve the conditions of the environment to optimize I to augment groundwater recharge. This need shows the viability of using excessive RO to design artificial recharge systems. I rates recorded in forests, grassland, and crop covered areas, were 17.32%, 12.35%, and 21.88%, respectively. In contrast, sealed surfaces had a low infiltration value of only 10.87%. This proves the importance of vegetation in developing soil infiltration processes.

4.5 Spatiotemporal Analysis of LC Change and Urban Growth in Debrecen (2018–2022)

4.5.1 LC Dynamics and Transformation Patterns

Figure 28 shows the changes in Debrecen City's LC categories from 2018 to 2022.

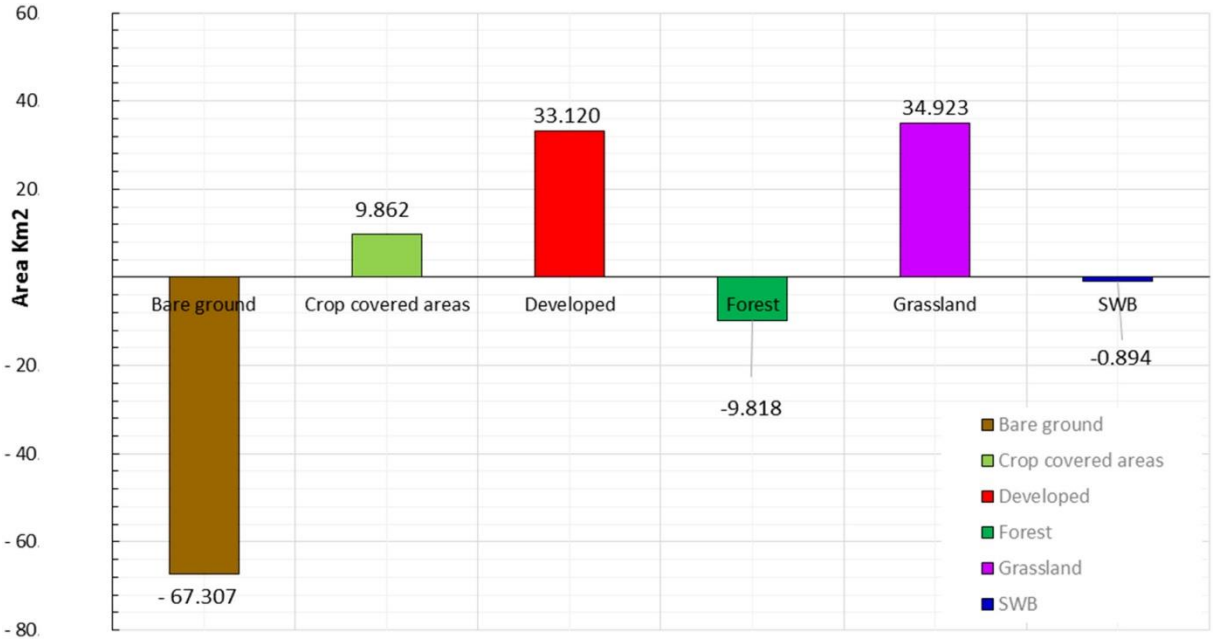

Figure 28. Assessment of Debrecen City's LC changes from 2018 to 2022 (Source: Author, 2025).

Between 2018 and 2022, Debrecen underwent noteworthy shifts in basically all types of LCs. One of the conspicuous changes was the loss of an SWB of about 0.89 km², which corresponds with precipitation trends in the region. 2018 was a relatively wet year with rainfall above the Central European average. This scenario changed quite drastically with the onset of an exceptional drought that was prolonged and a high-intensity one at that,

marked with temperature anomalies and persistent precipitation deficits, stretching over the period from 2018 to 2020. By 2022, the drought engulfed even larger proportions with the occurrence of one of the driest summers ever recorded and widespread soil moisture deficits being categorized under A-level drought classes (Aalbers et al., 2023; Copernicus Climate Services, 2023).

Referring to Debrecen, its forest area witnessed a drastic reduction by around 9.8 km². This can be viewed as the result of the combined effects of prolonged drought episodes and urban expansion. Elevated temperatures and long dry spells resulted in a heavy strain on the vegetation that led to diminishing forest cover. On the other end, urbanization stood as a culprit in transforming these natural habitats into infrastructure and industrial development. Similar observations are registered across Central Europe, where the build-up of more frequent and intense droughts-altered through an induced change in atmospheric circulation due to climate variability-has put ecosystems under pressure, subsequently initiating severe land-use change (Gombos et al., 2023).

The barren land in the area experienced a 67 km² decline while grassland grew by 34 km² and cropland extended by 9.8 km². The land transitions probably show a mix of farming development with tree-planting programs which environmental factors together with socioeconomic regulations affect (STRATEGY 24, 2023). The rapid expansion of developed areas took place through an increase of 33 km² which demonstrates fast urban development together with infrastructure construction. These modifications demonstrate the intricate relationship between climate-related environmental stress and human land-use changes which currently transform the Debrecen landscape.

The environmental conditions of Debrecen show signs of growing human-induced pressure because of urban expansion together with decreasing forested and aquatic regions. The ability to detect patterns along with their comprehension forms the foundation for successful urban planning activities and sustainable resource allocation and land management practices. The research delivers detailed findings about how urban development evolves through three core processes which include both the survival and transformation and reclassification of developed zones. The annual change of developed LC category appears in Figure 29 which breaks down the changes into three main parts including quantity gain and exchange and alternation. The analysis of these components

enables the identification of core processes that drive urban growth along with LC changes across the research territory.

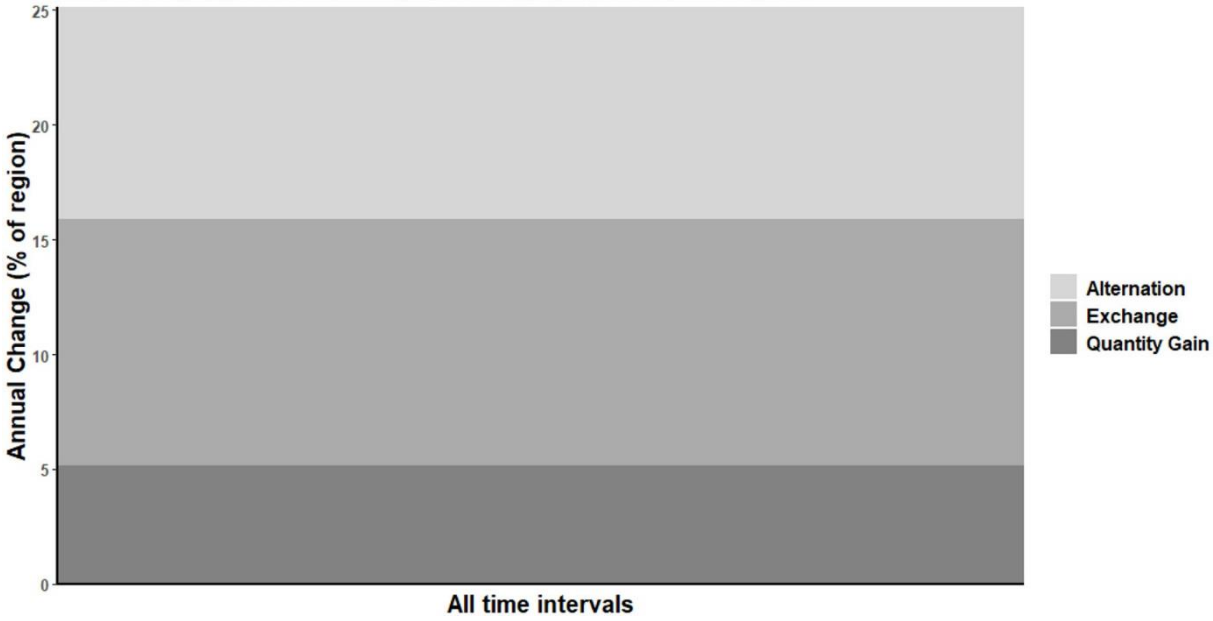

Figure 29. Three components of change during the temporal extent expressed as the annual percentage of the unified size (Source: Author, 2025).

The amount of area converted to urban through quantity gain accounts for about 5 % of the study area because land moved permanently into developed status. The exchange component covers nearly 10 %, reflecting bidirectional shifts between developed and non-developed classes, indicating that certain areas remain in a state of flux rather than following a consistent urbanization trend. The alternation component, which exceeds 10 %, identifies locations that experienced developed land reclassification during different time intervals, demonstrating substantial land use competition and temporal instability. The research results parallel Bilintoh et al. (2024) who explain land-use alternation as an indicator of temporary urban development's together with ongoing construction activities and RS dataset classification problems. A more detailed classification of these transitions is presented in the Developed Area Trajectories for Two Time Intervals (Figure 30).

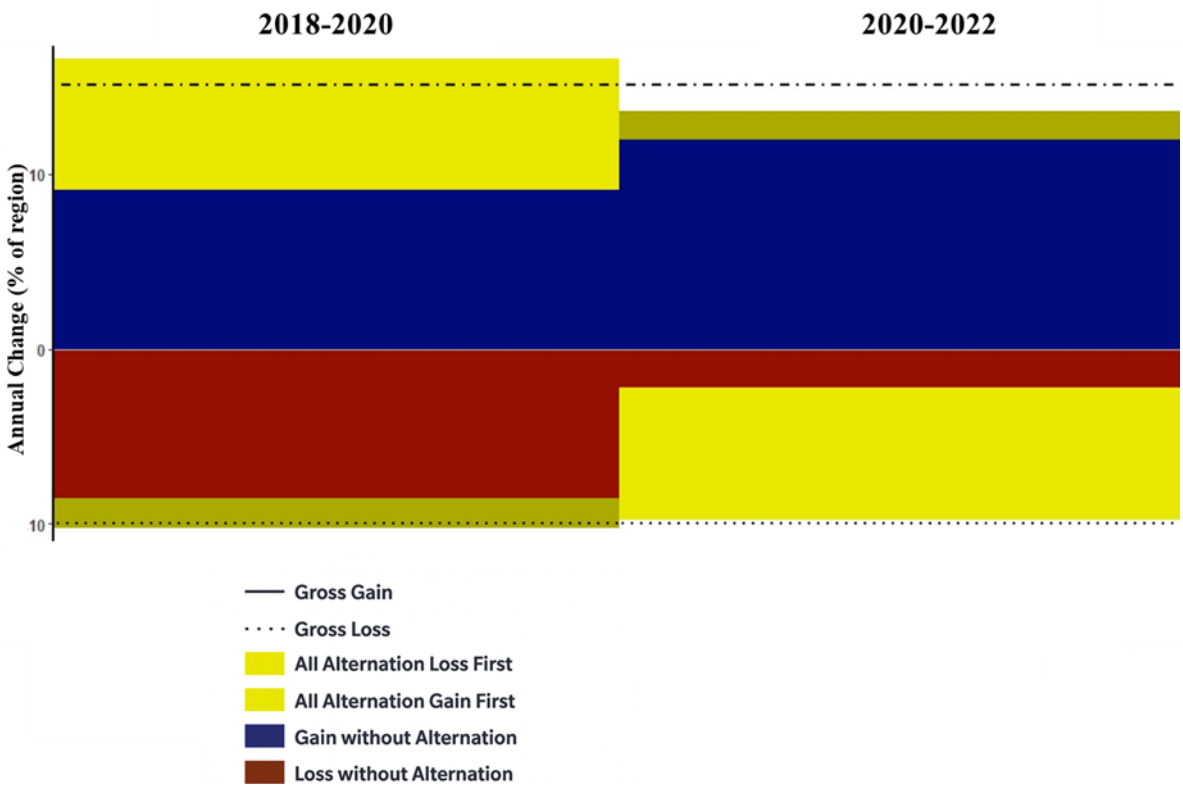

Figure 30. Annual Gain and Loss for developed area category during two time interval (Source: Author, 2025).

The plot identifies three categories of LC changes through Loss without Alternation and Gain without Alternation and Alternation. More than 10 % of the region includes Gain without Alternation which represents areas that became developed land and stayed stable to show permanent urban expansion. The Loss without Alternation category encompasses almost 5 % of the area and signifies uses where developed land has been permanently lost thus indicating zoning changes and redevelopment or land-use conversion. The alternation categories including "Alternation Gain First" and "Alternation Loss First" together impact more than 5 % of the study area to demonstrate land use classification instability. The findings by Bilintoh et al. (2024) receive validation through these results which demonstrate that trajectory-based urban land assessments play a vital role in identifying transient changes from permanent urban development. The combination of these findings highlights the essential role of trajectory analysis in land change detection methods since traditional classification-based approaches might misinterpret alternating land-use patterns. Our study demonstrates substantial alternation which validates the need for a multi-component framework to properly evaluate urban development patterns and

achieve better comprehension of long-term urbanization processes along with land-use competition and built environment stability in fast-growing cities such as Debrecen.

4.5.2 Mapping Urban Expansion and Development Trajectories

The evaluation of figure. 31, figure. 32 proves that Debrecen experienced distinct LC modifications from 2018 to 2022 because of urban growth together with industrial development. Grasslands experienced the biggest transformation since 28.89 km² of land became developed land. Bare ground (16.96 km²) and crop-covered areas (12.21 km²) came next. Since 2019 the growth of new companies and industrial zones in the city brought a rapid increase in industrial expansion to Debrecen.

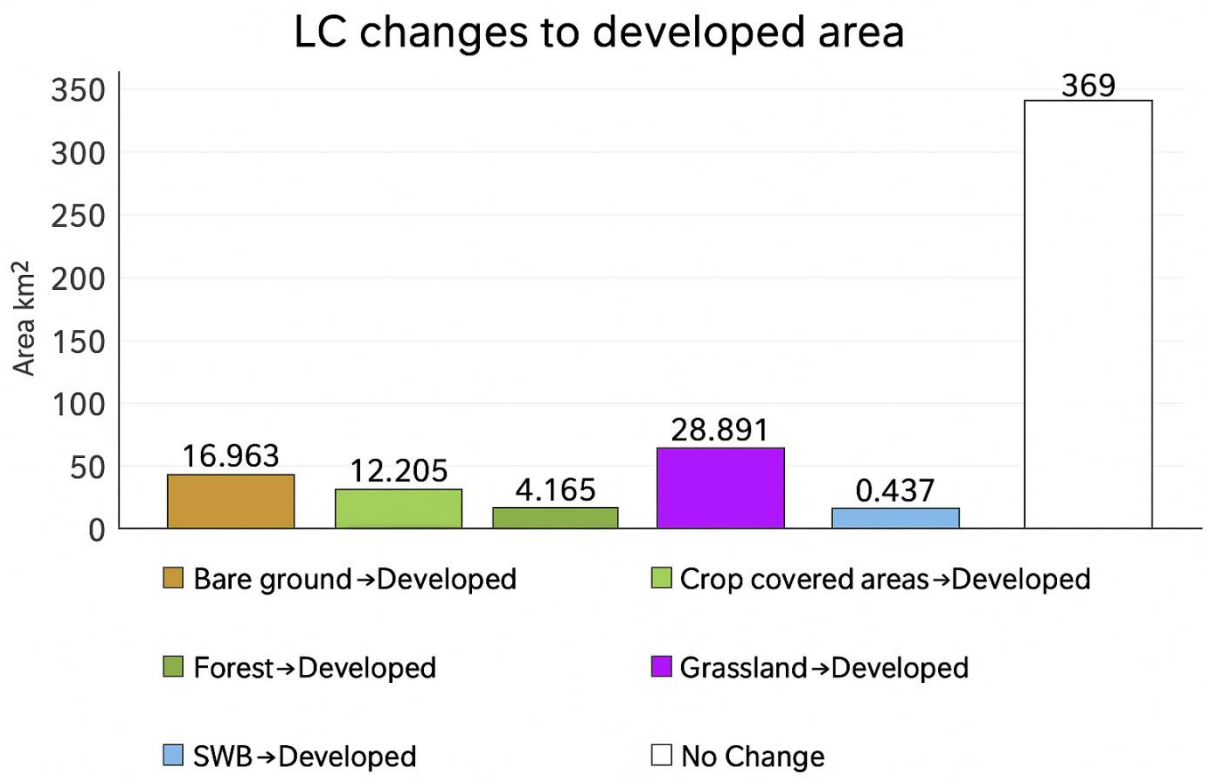

Figure 31. Debrecen Urban Sprawl mapping based on LC changes between 2018 and 2022 (Source: Author, 2025).

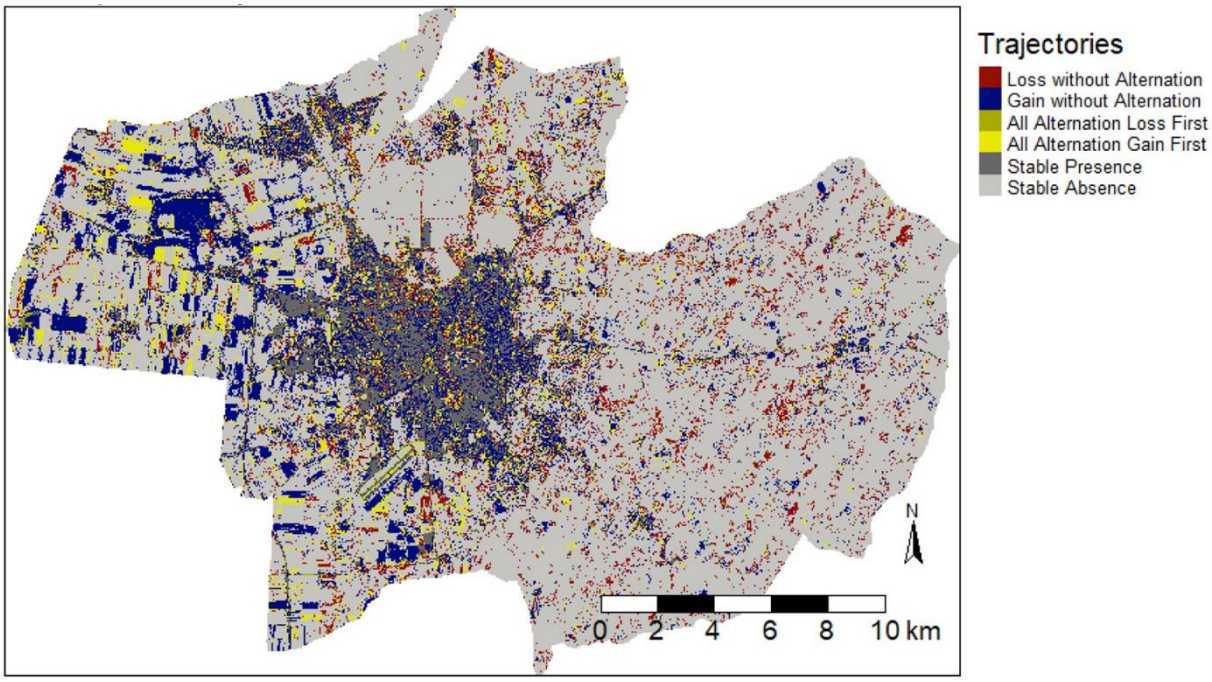

Figure 32. Developed area Trajectories for two time intervals (2018–2022) (Source: Author, 2025).

The transformation of grasslands and agricultural areas demonstrates these regions on urban peripheries became prime development targets since they offered easy access combined with lower market worth compared to forested areas. The process of industrialization probably served as the main driver for these conversions because new factories demanded extensive flat territories to establish their infrastructure. The small amount of forest area (4.17 km²) and surface water bodies (0.44 km²) that underwent conversion indicates either environmental protection measures exist or these regions don't meet industrial or urban development requirements. New factory construction might result in small-scale deforestation because of infrastructure needs.

The "No Change" category, accounting for 369 km², reflects that a substantial portion of Debrecen's land remained untouched. Although industrial investments have triggered faster urban spread since 2019, a large amount of land remains protected or has yet to be chosen for development. The analysis of developed regions between 2018–2020 and 2020–2022 appears in Figure 32 to demonstrate the spatial and temporal urban transformation patterns. The classification system identifies stable, expanding, contracting, and fluctuating developed areas which helps separate permanent urban zones from land changes that occur over time.

The results indicate that: The urban center consists mostly of developed areas in gray because these areas remain permanently established. Urban expansion takes place primarily in suburban areas and along transportation corridors because infrastructure development drives this growth. Temporary urban areas (yellow and brown) appear mostly on the city's edges because redevelopment and land use changes cause these fluctuations. Certain regions display land-use contraction (red) because they experience land reclassification or shifts in land use patterns. The study shows urban development patterns through which outer areas experience constant changes although the core area stays stable. A trajectory-based evaluation offers a deeper understanding of urban transformations which helps urban planners develop strategies for sustainable growth control and land-use stability management.

In addition to the observed land-use transitions, the substantial conversion of arable land and grassland into built-up areas between 2018 and 2022 raises important considerations regarding underlying soil resources. While the present study focused primarily on mapping and quantifying L transformations, these shifts are likely to have influenced local soil quality and soil functional capacity. To address this aspect more comprehensively, future research should incorporate detailed soil information to evaluate how urban expansion may have affected soil structure, fertility, and long-term agricultural potential. High-resolution datasets such as the AGROTOPO soil database or the Géczy soil maps would provide an appropriate foundation for assessing spatial variations in soil properties and for identifying areas most vulnerable to degradation. Integrating these soil-quality indicators into future LC change analyses would offer a deeper understanding of the environmental consequences of urban growth in Debrecen.

4.5.3 Identification and Analysis of Urban Change Hotspots

The spatial map (Figure 33) shows that, mostly due to industrial growth beyond 2019, the majority of Debrecen's development is focused around already-existing metropolitan areas.

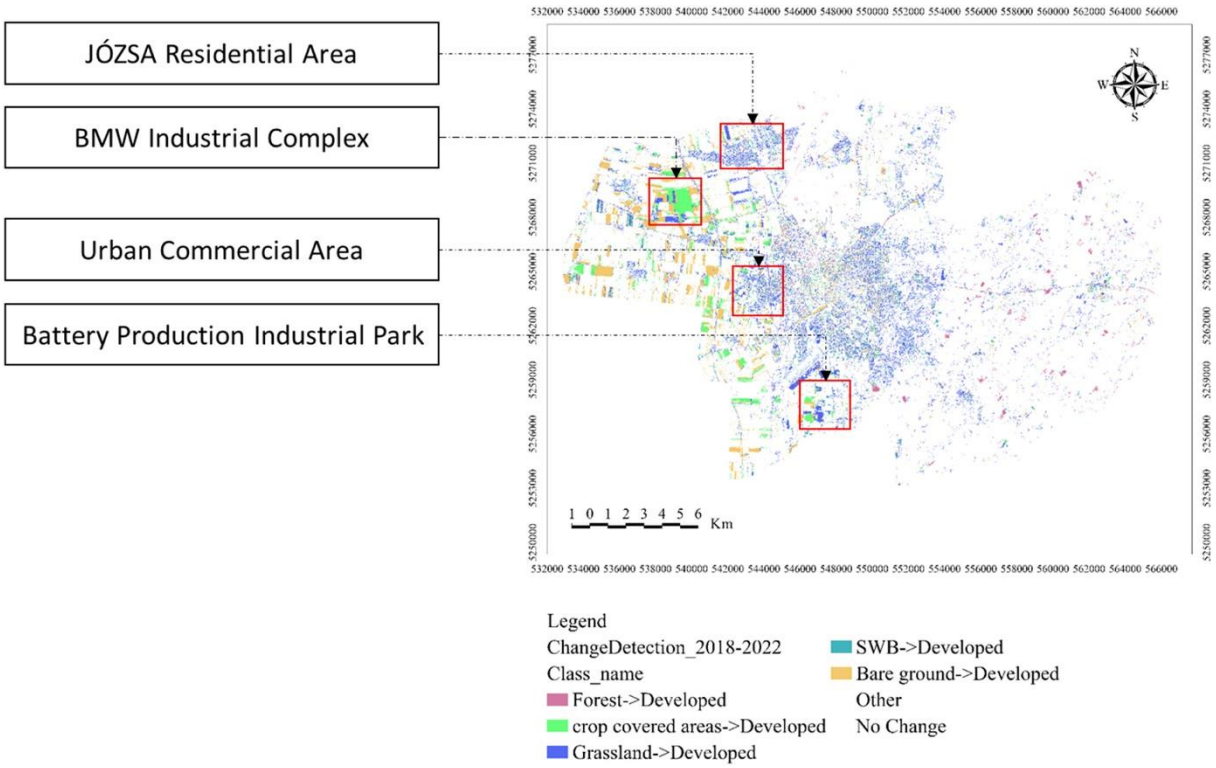

Figure 33. Visualizing Urban Sprawl: LC Dynamics in Debrecen (Source: Author, 2025).

The primary effect of expansion has been the spread of urban areas across grasslands and agricultural lands. The small alterations in forested regions and water bodies indicate some environmental protection but further expansion creates potential future dangers. The growing city of Debrecen needs sustainable urban planning to prevent natural habitat destruction while protecting its environment and resource supply from increasing environmental damage and resource strain. The comparison between 2018 and 2022 LC changes in four different areas appears in Figure 34 after applying optimal satellite imagery classification methods. The combination of classified imagery with Google Earth high-resolution aerial photographs in the figure provides a detailed assessment of urban development intensity changes.

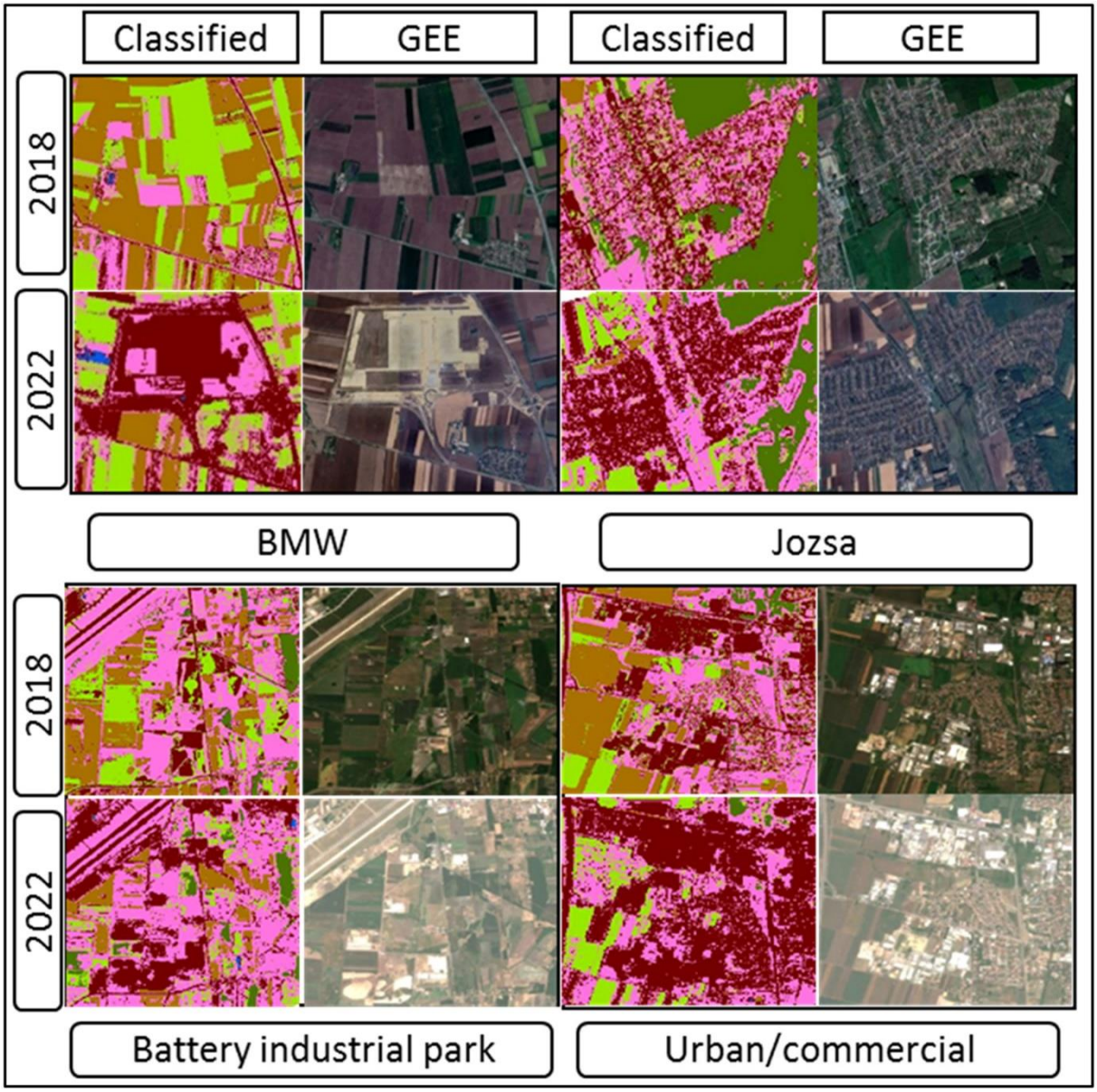

Figure 34. Four sample areas represent the change in urban development intensity between 2018 and 2022 (Source: Author, 2025).

The selected study areas represent a diverse spectrum of LC types to capture the multifaceted nature of urbanization. These include:

- BMW Industrial Complex: Established in 2019, this site showcases rapid industrial expansion, enabling the quantification of land transformation from green fields to industrial areas.
- JÓZSA Residential Area: This residential development provides insights into suburban growth patterns and the conversion of agricultural or green spaces into residential neighbourhoods.

- Battery Production Industrial Park: This site is essential for evaluating the impact of emerging industrial sectors on land use, particularly focusing on the transformation of previously undeveloped or agricultural land.
- Urban Commercial Area: This area illustrates the changes in commercial LC, including the development of retail spaces, offices, and entertainment facilities.

The research work establishes an enhanced foundation for upcoming urban water balance analyses in Debrecen through its evaluation of machine learning classifier combinations with satellite images to produce accurate LC maps that deliver precise class data which improves their usage in hydrological modeling. More precise infiltration, evapotranspiration, and runoff calculations will be possible with the integration of the revised LC data into the current hydrological frameworks developed in our earlier study (Guizani et al., 2024). High-resolution LC maps using our previous methods will be used to set up the integrated framework, allowing for pixel-based hydrological parameter calculations at the Debrecen scale. Additionally, in order to gain a better understanding of the dynamics of urban growth, LC change analysis will be conducted during the study period using the best-performing categorisation algorithms. By combining these findings with our earlier research, we can create a modern, precise urban water balance assessment tool that will aid in well-informed choices and sustainable urban design.

For the year 2019, we performed LC classification through the MLC technique that resulted in an OA of 81.2 % and a kappa statistic of 0.78. The F1 scores for classes of LC in specific areas were 0.70 for settlements, 0.72 for barren land, 0.66 for grass, and 0.60 for agricultural crops. Alternatively, this part illustrates a better classification efficiency throughout the period of the study (2018–2022) by leveraging Sentinel-2 satellite images and SVM as a classifier. The mean OA over the 3 years of investigation was of 88.0±2.3 %, whilst the mean kappa index was 0.84±0.03, indicating increased reliability and precision. Out of the F1 score tests, the highest numbers were attributed to the grassland class (0.90), while the bare ground, developed areas, and crop-covered classes had 0.85, 0.80, and 0.85, respectively. This improvement demonstrates how the use of Sentinel-2 together with SVM increases accuracy on classification tasks.

The better classification results give a more confident picture of LC trends in Debrecen. Such improved LC maps are going to serve at better integrating hydrological models, which were created in our previous study, therefore lending themselves to more precise

and meaningful simulations of water resources management in the Debrecen urban area. The increased accuracy and strength of the findings reinforce the potential for employing RS techniques and sophisticated classification algorithms in LC explorations to more effectively back up hydrological and urban planning efforts.

Future work should assess a broader range of classification algorithms and remote sensing data sources across more diverse geographical contexts. Building on the combination of L8 and S2 used in this study, future analyses could incorporate Landsat 9 to extend the temporal record with a sensor that maintains near-identical radiometric characteristics to L8, thereby improving temporal continuity and enhancing long-term monitoring capabilities. Expanding the use of S2's high temporal and spatial resolution would further allow evaluation of how multisensor fusion influences classification accuracy, particularly in landscapes with fine-scale heterogeneity. Additional platforms (such as Sentinel-1 SAR, PlanetScope, or commercial very-high-resolution optical sensors) may strengthen LC detection by contributing complementary spectral and structural information (Sim et al., 2024; Klein et al., 2012; Acharki, 2022).

Building on the results and methodological framework presented in this study, future research should also focus on integrating multi-source datasets that combine satellite imagery with ground-based observations and socio-economic indicators. Coupling these data streams with more advanced analytical approaches (such as deep learning, time-series modelling, and spatial–temporal fusion) would enhance the ability to capture, interpret, and model the dynamic mechanisms driving LC change and urban vitality. Such methodological expansion will support the development of more sustainable, adaptive, and data-informed planning and environmental management strategies

4.5.4 Impact of Urban Expansion on Agricultural Land Dynamics and Crop Yield Loss in Debrecen (2018–2022)

The LC classification results during the period from 2018 to 2022 reveal significant spatial changes in the landscape of Debrecen, marked with a strong urbanism. The major increments were in developed areas (+33 km²) and grasslands (+34 km²), while losses were much higher for bare ground (-67 km²) and forest (-9.8 km²). Crop-covered areas increased slightly, by +9.8 km², probably due to the conversion of some bare and grassland areas into cultivated fields.

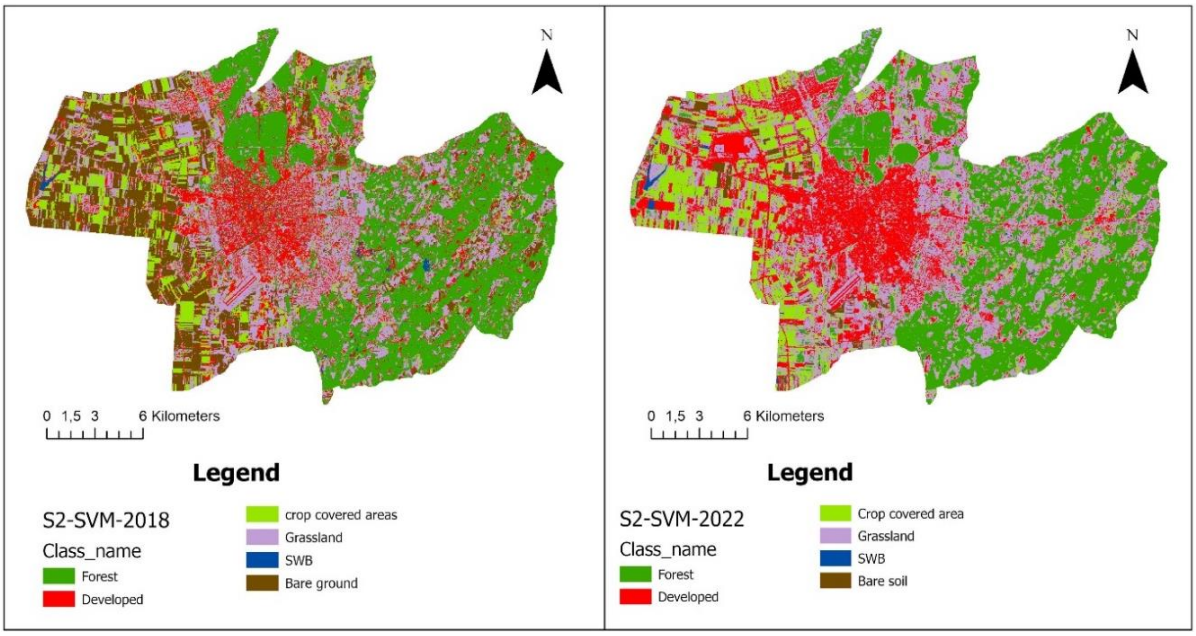

Figure 35. LC Maps of Debrecen in 2018 and 2022 (classified using SVM algorithm) (Source: Author, 2025)

This expansion of developed land correlates with population growth and industrialization, especially after 2019, when several manufacturing and service sector facilities were established. While some cropland areas remained stable or even increased slightly within Debrecen, the county-wide trend reveals a more substantial and consistent decline in agricultural LC. Wheat and maize, two staples of regional food production, have shown variable trends. Wheat harvested area fell from over 58,459 ha in 2018 to 48,334 ha in 2021, and maize dropped from 95,585 ha in 2018 to only 54,698 ha in 2022, marking a significant decline. Interestingly, yield data reveal a degree of resilience in some years, likely driven by favorable weather conditions or more intensive cultivation practices. However, in 2022, both wheat and maize yields experienced a marked decline. This drop occurred despite relatively stable agricultural land area and coincided with a notably dry year in Debrecen. The sharp reduction in output highlights the vulnerability of crop production to climatic variability and underscores the increasing instability of yields in the face of extreme weather events.

Table 13. Wheat and Maize Yield and Production Statistics (2018–2024) for Hajdú Bihar

Year	Wheat area (ha)	Wheat prod. (t)	Wheat yield (kg/ha)	Maize area (ha)	Maize prod (t)	Maize yield (kg/ha)
2018	58,459	310,903	5,320	95,585	865,206	9,050
2019	59,764	324,931	5,440	103,018	902,596	8,760
2020	51,929	287,548	5,540	92,638	933,657	10,080
2021	48,334	327,959	6,790	102,850	697,585	6,780
2022	59,088	205,810	3,480	54,698	137,785	2,520
2023	67,529	408,488	6,050	69,610	573,315	8,240
2024	59,683	368,836	6,180	82,820	562,473	6,790

Urban expansion poses a significant threat to agricultural productivity, particularly in regions experiencing rapid land conversion from crop-covered or bare ground to developed areas. Based on Figure 35, the total area converted to urban land use between 2018 and 2022 in Debrecen was 29.168 km², including 16.963 km² previously categorized as bare ground and 12.205 km² as crop-covered area. To quantify the potential agricultural loss due to this transformation, an estimation of forgone crop yields was conducted under three hypothetical scenarios, assuming the entire 29.168 km² (or 2,916.8 hectares) of newly developed land would have been used for maize, wheat, or sunflower cultivation. The average yield data (kg/ha) from the Hungarian Central Statistical Office for the period 2018–2022 were used:

Maize = 7.438 kg/ha

Wheat= 5.314 kg/ha

Sunflower= 2.852 kg/ha

Using these averages, the estimated annual yield losses are as follows (Table 14):

Table 14. Annual yield losses; Maize, Wheat and Sunflower

Scenario	Average yield (kg/ha)	Lost area (ha)	Total yield loss (tonnes)
Maize	7.438	2.916	21.687
Wheat	5.314	2.916	15.512
Sunflower	2.852	2.916	8.326

These scenario-based estimations reveal the considerable impact of urban sprawl on local agricultural productivity. If the land had remained dedicated to maize production, for example, the Debrecen area could have continued yielding over 21.600 tonnes of maize annually. This magnitude of yield loss underscores the trade-offs between urban development and food security, especially in regions like Hajdú-Bihar County, which are traditionally reliant on intensive agricultural land use. Moreover, these figures highlight the importance of sustainable urban planning that considers the long-term implications of land conversion on crop output, local food systems, and regional economic stability.

The analysis of wheat and maize yields between 2018 and 2022 must be interpreted with caution. The Hungarian Central Statistical Office yield data employed in this study are based on harvested area, which does not always reflect the true extent of sown or cultivated land. This limitation was particularly evident in 2022, when severe drought conditions in the Hajdúság region led many farmers to abandon maize harvesting altogether. As a result, the recorded harvested area sharply declined, artificially amplifying the apparent drop in production and creating the misleading impression that cropping extent had contracted substantially. Therefore, yield reductions during this period cannot be attributed solely to the conversion of agricultural land to urban or industrial land uses, but must be understood in conjunction with climatic extremes and data-reporting constraints.

This subsection also presents a scenario-based assessment, illustrating what potential agricultural output could have been achieved if the land converted to built-up and industrial areas had instead remained available for cultivation. For example, estimating the hypothetical production of maize or sunflower on these formerly suitable agricultural areas provides insight into the scale of potential crop loss associated with urban

expansion. To strengthen such assessments in future studies, the integration of historical cropping-pattern maps and sown-area records is recommended. These data sources would enable a more accurate reconstruction of past cultivation patterns and allow for a more reliable evaluation of how urbanisation interacts with environmental pressures to affect agricultural productivity.

Although arable land is steadily decreasing, the importance of urban farming is rapidly emerging as a vital solution for sustainable food production. Globally, examples provide a broad spectrum of possible methods which urban farming can take and the successes of its applications. When the food crisis came to Cuba in the 1990s, "organopónicos" supported by the state initiated urban farming practices, which now meet more than 60% of Havana's vegetable demand (Altieri et al., 1999). The rise of urban agriculture in Detroit, USA, focuses on establishing urban agriculture as part of recovering an economy while reusing land. The city and region undertook projects to convert dismantled buildings, lots now rendered as vacant, and abandoned homes into community gardens. Shanghai is developing peri-urban farming into its urban growth scenario, whereby producing agricultural crops and controlling urban growth need not be mutually exclusive (Colasanti et al., 2012). Municipal officers in Johannesburg promote urban gardening as part of an overall program to govern social development, economic and physical development, and poverty relief efforts. The "Parisculteurs" project in Paris seeks to develop biodiversity by covering roofs and walls with growing things and food production locations (Rogerson, 2010). Multiple examples illustrate how urban farming can adapt to create climate, conditions, and cultural exchange.

The variety of urban farming types reflects the adaptations to space constraints and socioeconomic circumstances. Often referred to as a home or backyard garden, these gardens blossom in developing countries, where a family grows vegetables and herbs for their own consumption, for instance, in Kampala and Accra (Zezza and Tasciotti, 2010). Community gardens, managed by their members, have in recent decades grown to become important social and food networks in New York and Toronto (Lovell, 2010). In space-constrained and highly industrialized cities, rooftop farms and vertical farming systems have emerged as innovative solutions. For instance, Brooklyn Grange in New York and Lufa Farms in Montreal have successfully utilized the rooftops that otherwise would have gone to waste (Thomaier et al., 2015). In addition, soil-less growing systems such as hydroponics and aquaponics are increasingly being adopted in cities such as

Singapore and Tokyo, where land is scarce but high-tech solutions allow for highly efficient food production (dos Santos, 2016). Finally, peri-urban farming, which arises at the edge of urbanization, is very important in the African and Asian context as a primary source of fresh vegetables and dairy for the urban population (Drechsel and Dongus, 2010). A summary of soilless crop production systems using alternative water sources, highlighting their viability and performance presents in Table 19.

Table 19: Summary of Soilless Crop Production Using Different Water Sources

Crop/System	Water Source	Key Finding	Reference
Lettuce (vertical hydroponics)	Harvested rainwater (indoor RWH)	Rainwater harvesting in indoor vertical hydroponics met ~35–90% of lettuce water needs, depending on system design.	Jurga (2021)
Tomato (greenhouse hydroponics)	Rainwater collected from roof	Seasonal rainfall sufficed for tomato irrigation across diverse climates using hydroponic greenhouses.	Rajalakshmi, M (2022)
Leafy veggies (hydroponics)	Reclaimed rainwater (urban RWH)	Urban rooftop RWH systems supplied sufficient volume (~75–100% efficiency) for small-scale hydroponic greens.	Sucozhañay, A (2024)
Lettuce/Chinese cabbage (DWC)	Primary & secondary municipal wastewater	Butterhead lettuce grew to maturity; yields lower but viable with secondary treatment.	Chow et al (2001)
Aquaponic (lettuce + fish)	Recirculating aquaculture effluent	Aquaculture effluent provides nutrients and water reuse; low water loss (~2–3% daily).	Graber & Junge (2009)
Hydroponic & aquaponic review	Greywater from bioretention + aquaculture	Combined treatment supports spinach, lettuce growth in hydroponics; bioretention helps reduce contamination.	Widiyanti et al (2022)

In indoor vertical hydroponics, Jurga (2021) found that harvested rainwater could meet 35–90% of lettuce water requirements, depending on the system's storage and efficiency. Similarly, Rajalakshmi (2022) demonstrated that roof-collected rainwater was sufficient

for tomato irrigation in greenhouse hydroponics across various climates, proving the potential of rainwater harvesting (RWH) for controlled environment agriculture. Urban applications also showed promise. Sucozhañay (2024) reported that rooftop RWH systems provided 75–100% of the needed water for leafy vegetables in small-scale hydroponic setups, indicating high efficiency for urban farming. In more unconventional approaches, Chow et al. (2001) used primary and secondary treated municipal wastewater in deep-water culture (DWC) systems to successfully grow lettuce and Chinese cabbage, although yields were slightly reduced. Moreover, integrated systems such as aquaponics (lettuce with fish) were found to be effective. Graber & Junge (2009) showed that recirculating aquaculture effluent supplied both nutrients and water, with minimal daily loss (~2–3%). Lastly, Widiyanti et al. (2022) reviewed systems using greywater from bioretention and aquaculture, which successfully supported the growth of spinach and lettuce while reducing contamination risks. These findings confirm that multiple water sources—including rainwater, wastewater, and aquaculture effluent—can effectively support soilless crop production with proper treatment and system design.

5. CONCLUSIONS AND RECOMMENDATIONS

This dissertation has demonstrated the feasibility and effectiveness of integrating remote RS data with advanced ML algorithms for rapid, accurate LC classification, change detection, and hydrological assessment within urban and peri-urban environments. The methodological framework applied in the Debrecen region represents a comprehensive approach that synergizes spectral data analysis, supervised classification, and LC–based hydrological modeling to address the complex challenges arising from urbanization and its cascading impacts on agriculture and water resources.

The developed quasi-real-time LC classification framework using L8 OLI imagery and MLC produced strong results, with an OA of 81.2% and a K of 0.78, validated against 770 ground-truth points. The high spectral separability indices (J-M > 1.9; TD = 2.0) confirm the effectiveness of the selected spectral bands in distinguishing between major LC types. The framework performed well in identifying forested areas (F1 = 0.97), semi-sealed urban surfaces (F1 = 0.94), and SWB (F1 = 0.90), indicating its robustness in detecting permanent and well-defined LC features. However, it was less effective in classifying crop-covered areas (F1 = 0.647) and grasslands (F1 = 0.668), due to spectral confusion and seasonal variability. These results demonstrate that while the framework is reliable for mapping stable LC categories, its accuracy decreases when dealing with dynamic vegetation types, highlighting the need for finer spatial and spectral resolution imagery to improve classification precision for such classes.

The second phase of the study confirmed that the combination of S2 imagery and the SVM classifier offers the most effective and accurate framework for LC classification. This pairing consistently delivered the highest OA (up to 90% in 2020), strong K values (up to 0.87), and the lowest total disagreement rates (12.6% in 2020 and 13.1% in 2022). It achieved excellent F1-scores for forests (0.98), grasslands (0.92), and crop-covered areas (0.88), making it the most recommended approach for monitoring vegetated and dynamic LC types. Developed urban areas were also well captured (F1 = 0.77), while SWB showed moderate results (F1 = 0.66–0.73). In comparison, Landsat 8 + SVM showed acceptable performance for forests and urban areas (F1 = 0.96 and 0.75 in 2022) but was less effective for bare ground and surface water bodies, reflecting limitations in spatial resolution. MLC consistently underperformed in developed areas (F1 as low as 0.44–0.45), and its variable results across years and satellites make it the least reliable

option for heterogeneous classes. RF yielded fair results in forests and urban classes but was weaker in identifying crops and water bodies, especially with S2 in 2022. Therefore, we recommend the S2 + SVM combination as the most robust solution for detailed and reliable classification of forests, grasslands, and agricultural areas, while discouraging the use of MLC and RF for complex urban or water-dominated landscapes where accuracy is critical.

The third component of this research introduced a pixel-level water balance model tailored to Debrecen, integrating LC–derived crop coefficients with the Kenessey RO estimation method to calculate ET, I, and RO. By combining empirically derived hydrological parameters with the classified LC maps, the model enabled detailed, spatially explicit (pixel-based) calculations of water balance components. These pixel-level outputs allow us to examine the hydrological parameter (ET, I, and RO) for any specific location, neighbourhood, or district within the study area.

The strength of this modeling framework lies in its adaptability and scalability. By modifying input layers (such as updated LC maps or different meteorological datasets) the same pixel-based approach can be applied to other urban areas with similar climatic and physiographic conditions. This makes it a valuable, transferable tool for water resource management, enabling hydrological analysis not just for entire cities, but for individual watersheds or even sub-districts undergoing dynamic land use change.

A multi-temporal LC analysis between 2018 and 2022 revealed a rapid urban expansion of approximately 33 km² in Debrecen, largely at the expense of agricultural and undeveloped lands. Specifically, 12.21 km² of cropland and 16.96 km² of bare land were converted into developed areas. Key urban growth hotspots such as the BMW Industrial Complex and the Józsa residential district reflect concentrated pressures from industrial and residential developments. This spatial transformation underscores the urgent need to implement stronger municipal-level land use monitoring. Urban growth boundaries, targeted zoning restrictions, and infrastructure planning must be reinforced (especially in areas undergoing rapid change) to protect land that holds ecological or agricultural value.

This land conversion has already contributed to notable pressures on the agricultural sector in Hajdú-Bihar County; however, the interpretation of crop production trends between 2018 and 2022 requires caution. During this period, wheat cultivation areas decreased from 58,459 ha to 48,334 ha, and maize areas from 95,585 ha to 54,698 ha.

Wheat yields fell from 5,320 to 3,480 kg/ha, and maize yields declined sharply from 9,050 to 2,520 kg/ha. Importantly, the Hungarian Central Statistical Office data used here refer to harvested rather than sown area. This distinction became critical in 2022, when extreme drought conditions in the Hajdúság region led many farmers to abandon maize harvesting entirely. The resulting reduction in harvested area artificially amplified the apparent drop in yields, creating the misleading impression that cropping extent declined more than it actually did. Therefore, the observed reductions in crop output cannot be attributed solely to land-use change, but rather reflect the combined influence of climatic extremes and dataset limitations.

Despite these uncertainties, the conversion of approximately 2,916.8 hectares of cropland still represents a significant loss of agricultural potential. To illustrate this, a scenario-based assessment was conducted to estimate the potential production that could have been achieved had these areas remained under cultivation. Under this hypothetical scenario, the region could have produced approximately 21,693 tons of maize, 15,500 tons of wheat, and 8,320 tons of sunflower annually—demonstrating the scale of foregone agricultural output directly linked to urban expansion, independent of climate-induced yield variability.

These findings underscore the need to protect high-yield agricultural zones in future land-use planning by applying agro-ecological zoning, offering sustainable land-use incentives, and establishing systematic monitoring to prevent further encroachment. To strengthen future analyses, the integration of historical cropping-pattern maps and sown-area records is recommended, as these data would enable a more accurate reconstruction of cultivated areas prior to urban development. Overall, while climate extremes remain a major driver of annual yield fluctuations, unmanaged urbanisation poses a growing structural threat to regional agricultural capacity and long-term food security. Integrating land-cover classification with robust productivity and climatic datasets will support more adaptive and informed planning that balances urban growth with environmental sustainability.

While this dissertation provides a comprehensive assessment of LC dynamics, urban expansion, and their implications for hydrological responses, several opportunities remain to advance this field of research. Future studies should explore dynamic changes in urban vitality by integrating real-time, multisource datasets, such as mobile phone

activity data, traffic density information, social media geotags, and IoT-based environmental sensors. Combining these rapidly acquired datasets with satellite-derived land cover information would allow researchers to monitor urban processes with significantly higher temporal granularity.

Moreover, incorporating advanced deep learning techniques (including convolutional neural networks (CNNs), graph neural networks (GNNs), and transformer-based architectures) could further improve the precision of land function classification and strengthen the understanding of the evolving relationship between land cover patterns and indicators of urban vitality. These methods have the potential to outperform traditional machine learning algorithms by capturing spatial heterogeneity, complex texture information, and non-linear interactions across multiple scales.

Overall, this dissertation contributes a comprehensive and interdisciplinary framework that combines RS, ML, hydrological modeling, and innovative urban agriculture to deepen understanding of the interconnected challenges of land transformation, water resource dynamics, and food production in rapidly urbanizing environments. The findings underscore the urgency of adopting integrated land and water management policies that leverage advanced monitoring technologies to support evidence-based urban planning. Protecting remaining agricultural lands through sustainable zoning, promoting green infrastructure to mitigate hydrological disruptions, and supporting circular water use and urban agriculture are essential to fostering resilient, sustainable urban development.

By bridging technology and practical solutions, this research offers a pathway to balance urban growth with ecological and food security goals. The demonstrated methodology and insights provide valuable tools for policymakers, planners, and communities striving to create adaptive, resilient cities where economic development and environmental stewardship coexist harmoniously. The adoption of such integrated approaches will be crucial in ensuring the sustainability of urban ecosystems and the well-being of future generations.

6. NEW SCIENTIFIC RESULT

1. I developed a rapid, quasi-real-time LC classification framework for Debrecen using L8 OLI imagery and MLC. The framework resulted an OA of 81.2% and a Kappa coefficient of 0.78, and the best performed with the highest F1-scores class-levels for forest (0.97), semi-sealed areas (0.94), and surface water (0.90) in LC classification., while crop cover and grassland classes showed lower F1-scores (0.647 and 0.668), likely due to spectral mixing.

2. I integrated multi-sensor RS data with ML algorithms to classify urban LC. S2 imagery combined with the SVM classifier yielded the highest and most consistent performance (OA: $88 \pm 2.1\%$; Kappa coefficient: 0.84 ± 0.03), particularly for forest (F1-score: 0.93 ± 0.05), developed areas (F1-score: 0.80 ± 0.07), and grassland (F1-score: 0.90 ± 0.02). This combination also achieved the lowest total disagreement values (12.6% in 2020 and 13.1% in 2022), highlighting its reliability for accurate urban LC mapping.

3. I developed an LC-based hydrological framework for Debrecen to estimate ET, I, and RO at the pixel level with spatial resolution 10 m. By linking classified LC types with reference Kc and applying the Kenessey method for RO estimation, the model captured spatial water balance patterns across the city. Results showed highest ET in SWB (86%) and forests (72%), while sealed surfaces had the lowest (~7%). Infiltration was highest in crop-covered areas (22%) and lowest in sealed zones, where RO reached 82%. This adaptable and replicable approach supports high-resolution hydrological modeling in urban environments, offering a practical tool for climate-resilient water management.

4. Between 2018 and 2022, Debrecen's urban area expanded by 33 km², mainly replacing cropland (12.21 km²) and bare ground (16.96 km²). Grasslands increased by 34 km², while bare ground and forest areas declined by 67 km² and 9.8 km², respectively, reflecting the impacts of urbanization and climatic factors. Urban growth was concentrated in suburban zones and industrial hubs, notably the BMW Complex and JÓZSA area. This land transformation coincided with sharp agricultural declines in Hajdú-Bihar County, where wheat and maize areas dropped by 17% and 43%, and yields fell by 34% and 72%, respectively. The conversion of 2,916.8 ha of cropland led to estimated annual losses of ~21,693 t maize, 15,500 t wheat, and 8,320 t sunflower. These findings highlight the

trade-offs between urban expansion and agricultural productivity in rapidly developing regions.

7. PRACTICAL RESULTS

1. The developed LC classification framework using L8 and MLC enables rapid generation of LC maps for urban areas. It supports near-real-time monitoring of vegetation and land transformations with minimal input. The method is adaptable for other cities by adjusting training data and thresholds, making it ideal for planners and GIS specialists needing fast urban mapping tools.
2. The integration of S2 imagery with SVM classifier provides highly accurate LC classification results for urban areas, especially in differentiating developed, agricultural, and forested zones. This supports municipalities in tracking urban growth and land use changes, allowing timely decision-making for zoning, infrastructure planning, and environmental assessments.
3. The LC-based hydrological model offers a pixel-level estimation of ET, I, and RO, using RS and LC-specific Kc values. It enables urban water managers and hydrologists to simulate water balance under changing land use conditions. The method is easily transferable to other urban regions with similar topography and climate.
4. LC change analysis from 2018–2022 revealed urban expansion patterns in Debrecen and their impacts on agriculture. These spatial insights can guide regional authorities in urban planning to minimize cropland loss. The results can support agricultural policies to compensate for or adapt to productivity decline in peri-urban zones.

8. SUMMARY

Urban growth and land transformation are among the most pressing environmental and planning challenges of the 21st century, particularly in Central and Eastern Europe where economic development is driving significant LC changes. This PhD research addresses the need for timely and accurate mapping of LC dynamics, as well as their hydrological and agricultural implications, by integrating RS, ML, and hydrological modeling techniques.

The research is built around four core objectives. First, it aims to develop a rapid, transferable, and cost-effective LC classification framework using medium-resolution satellite imagery and the MLC algorithm. Second, it evaluates and compares the performance of multiple ML classifiers (SVM, MLC, and RF) when applied to L8 and S2 imagery from 2018, 2020, and 2022. Third, it introduces a pixel-based urban hydrological model to estimate key water balance components (ET, I, and RO) based on classified LC maps and biophysical parameters. Lastly, the research investigates the impact of urban expansion on cropland extent and productivity, quantifying yield loss for key crops

The first phase of the study focused on generating a rapid LC map of Debrecen using 2019 L8 imagery. The MLC method was employed following essential pre-processing steps including radiometric correction, NDVI-based masking, and training sample selection. Spectral separability among classes was quantitatively assessed using JM and TD indices to ensure reliable class discrimination. The MLC approach achieved an OA of 81.2% and a Kappa coefficient of 0.78. High F1-scores were recorded for stable classes such as forest (0.97), semi-sealed areas (0.94), and surface water (0.91), while lower accuracy for crops (0.65) and grasslands (0.67) underscored the method's limitations in distinguishing spectrally similar vegetation types. Despite these constraints, MLC proved effective for rapid urban LC assessments, especially in data-scarce or resource-limited contexts.

In the second phase, a multi-temporal and multi-sensor classification was performed for 2018, 2020, and 2022 using S2 and L8 imagery. For each year, cloud-free composite images were generated using the median reflectance of selected bands during peak vegetation periods (May–September), ensuring consistent seasonal representation. All imagery underwent atmospheric correction and spatial co-registration before being used

for classification. S2 images classified with the SVM algorithm outperformed all other combinations, achieving overall accuracies of up to 90% and Kappa values exceeding 0.85. The SVM classifier demonstrated strong reliability in complex urban environments, particularly in distinguishing developed areas, croplands, and grasslands. RF and MLC methods showed acceptable performance but were less accurate in delineating fragmented or seasonally variable classes. The results suggest that S2 data combined with SVM offer a robust and scalable approach for urban LC monitoring across fine spatial and temporal scales.

To assess the implications of LC changes on urban hydrology, a pixel-based model was developed integrating LC types, crop coefficients, and RO coefficients following the Kenessey method. The model quantified ET, I, and RO across Debrecen's territory. Forests and SWB exhibited the highest evapotranspiration (up to 86%), while croplands showed moderate infiltration rates (around 22%). In contrast, built-up areas exhibited low infiltration and high RO, underscoring the increased risk of urban flooding. These spatially explicit hydrological parameters provide essential input for water resource management and urban planning.

Between 2018 and 2022, Debrecen experienced significant LC change, notably the conversion of 33 km² of cropland and bare land into industrial, residential, and commercial areas. Major transformation zones included the BMW factory area and the northern suburbs such as Józsa. This urban expansion resulted in measurable impacts on agricultural production. Comparing land use changes with statistical crop yield data for maize and wheat revealed that urbanization led to the loss of over 10,000 hectares of cropland, with average yield reductions of 1,840 kg/ha for wheat and 6,530 kg/ha for maize. In total, this corresponds to an annual loss of approximately 21,693 tons of maize and 15,500 tons of wheat. These findings highlight the vulnerability of peri-urban agriculture to unplanned development and support the need for zoning policies and green belt preservation.

In conclusion, this PhD thesis provides an integrated, multi-disciplinary approach to analyzing and managing land and water resources in urban environments. The combination of RS, ML, hydrological modeling, and practical innovation in urban agriculture offers a replicable framework for other cities facing similar challenges. The study not only contributes to scientific understanding of LC dynamics and their

hydrological and agricultural impacts but also proposes tangible solutions for sustainable urban development. Through detailed mapping, modeling, and innovation, the research promotes data-driven decision-making for land use planning, water management, and urban resilience in the context of accelerating urbanization and climate change.

9. CERTIFICATED PUBLICATIONS

UNIVERSITY AND NATIONAL LIBRARY
UNIVERSITY OF DEBRECEN
H-4002 Egyetem tér 1, Debrecen
Phone: +3652/410-443, email: publikaciok@lib.unideb.hu

Registry number: DEENK/456/2025.PL
Subject: PhD Publication List

Candidate: Douraied Guizani
Doctoral School: Doctoral School of Nutrition and Food Sciences
MTMT ID: 10079642

List of publications related to the dissertation

Foreign language scientific articles in Hungarian journals (3)

1. **Guizani, D.**, Bódi, E., Tamás, J., Nagy, A.: An advanced classification method for urban land cover classification.
   Acta agrar. Debr. 2024 (1), 51-57, 2024. ISSN: 2416-1640.
   DOI: http://dx.doi.org/10.34101/actaagrar/1/13652
2. **Guizani, D.**, Bódi, E., Tamás, J., Nagy, A.: Land cover modelling with Sentinel 2 in water balance calculations of urban sites.
   J. Cent. Eu. Green Innov. 11 (3), 70-83, 2023. EISSN: 2064-3004.
3. **Guizani, D.**, Bódi, E., Tamás, J., Nagy, A.: Characterisation of basic water balance parameters of Debrecen.
   Agrártud. közl. 1, 35-40, 2022. ISSN: 1587-1282.
   DOI: http://dx.doi.org/10.34101/actaagrar/1/10427

Foreign language scientific articles in international journals (2)

4. **Guizani, D.**, Tamás, J., Pásztor, D., Nagy, A.: Refining land cover classification and change detection for urban water management using comparative machine learning approach.
   Environmental Challenges. 19, 1-19, 2025. ISSN: 2667-0100.
   DOI: http://dx.doi.org/10.1016/j.envc.2025.101118
5. **Guizani, D.**, Bódi, E., Tamás, J., Nagy, A.: Enhancing water balance assessment in urban areas through high-resolution land cover mapping: Case study of Debrecen, Hungary.
   Environmental Challenges. 15, 1-17, 2024. ISSN: 2667-0100.
   DOI: http://dx.doi.org/10.1016/j.envc.2024.100906

Foreign language conference proceedings (1)

6. **Guizani, D.**, Bódi, E., Tamás, J., Nagy, A.: Enhancing the Urban Atlas Features with the Water Balance Estimates Using the Landsat 8 Imagery.
   IOP Conf. Ser.: Earth Environ. Sci. 1189 (1), 1-15, 2023. ISSN: 1755-1307.
   DOI: http://dx.doi.org/10.1088/1755-1315/1189/1/012027

UNIVERSITY AND NATIONAL LIBRARY
UNIVERSITY OF DEBRECEN
H-4002 Egyetem tér 1, Debrecen
Phone: +3652/410-443, email: publikaciok@lib.unideb.hu

Foreign language abstracts (2)

7. **Guizani, D.**, Tamás, J., Nagy, A.: Sustainable urban development in Debrecen: addressing water scarcity, agricultural decline, and industrial expansion through community-based hydroponic solutions.
   In: Abstract Book of the 8th International Scientific Conference on Water, Magyar Agrár-és Élettudományi Egyetem, Gödöllő, 35, 2025. ISBN: 9789636231156(pdf)
8. **Guizani, D.**, Bódi, E., Tamás, J., Nagy, A.: Identification of water balance properties of urban atlas using Landsat 8 data.
   In: Book of abstract XXII Conference of PhD Students and Young Scientists : Interdisciplinary topics in mining and geology. Szerk.: Jan Blachowski, Wrocaw University of Science and Technology Publishing House, Wrocaw, 41-42, 2022. ISBN: 9788374932202

The Candidate's publication data submitted to the Tudóstér have been validated by DEENK on the basis of the Journal Citation Report (Impact Factor) database.

28 July, 2025

DEBRECENI EGYETEM Egyetemi és Nemzeti Könyvtár

DEBRECENI EGYETEM
EGYETEMI ÉS NEMZETI KÖNYVTÁR
H-4002 Debrecen, Egyetem tér 1, Pf.: 400
Tel.: 52/410-443, e-mail: publikaciok@lib.unideb.hu

Nyilvántartási szám: DEENK/456/2025.PL
Tárgy: PhD Publikációs Lista

Jelölt: Guizani, Douraied
Doktori Iskola: Táplálkozás- és Élelmiszertudományi Doktori Iskola. Élelmiszertudományi doktori program
MTMT azonosító: 10079642

A PhD értekezés alapjául szolgáló közlemények

Idegen nyelvű tudományos közlemények hazai folyóiratban (3)

1. **Guizani, D.**, Bódi, E., Tamás, J., Nagy, A.: An advanced classification method for urban land cover classification.
   Acta agrar. Debr. 2024 (1), 51-57, 2024. ISSN: 2416-1640.
   DOI: http://dx.doi.org/10.34101/actaagrar/1/13652
2. **Guizani, D.**, Bódi, E., Tamás, J., Nagy, A.: Land cover modelling with Sentinel 2 in water balance calculations of urban sites.
   J. Cent. Eu. Green Innov. 11 (3), 70-83, 2023. EISSN: 2064-3004.
3. **Guizani, D.**, Bódi, E., Tamás, J., Nagy, A.: Characterisation of basic water balance parameters of Debrecen.
   Agrártud. közl. 1, 35-40, 2022. ISSN: 1587-1282.
   DOI: http://dx.doi.org/10.34101/actaagrar/1/10427

Idegen nyelvű tudományos közlemények külföldi folyóiratban (2)

4. **Guizani, D.**, Tamás, J., Pásztor, D., Nagy, A.: Refining land cover classification and change detection for urban water management using comparative machine learning approach.
   Environmental Challenges. 19, 1-19, 2025. ISSN: 2667-0100.
   DOI: http://dx.doi.org/10.1016/j.envc.2025.101118
5. **Guizani, D.**, Bódi, E., Tamás, J., Nagy, A.: Enhancing water balance assessment in urban areas through high-resolution land cover mapping: Case study of Debrecen, Hungary.
   Environmental Challenges. 15, 1-17, 2024. ISSN: 2667-0100.
   DOI: http://dx.doi.org/10.1016/j.envc.2024.100906

Idegen nyelvű konferencia közlemények (1)

6. **Guizani, D.**, Bódi, E., Tamás, J., Nagy, A.: Enhancing the Urban Atlas Features with the Water Balance Estimates Using the Landsat 8 Imagery.
   IOP Conf. Ser.: Earth Environ. Sci. 1189 (1), 1-15, 2023. ISSN: 1755-1307.
   DOI: http://dx.doi.org/10.1088/1755-1315/1189/1/012027

DEBRECENI EGYETEM
EGYETEMI ÉS NEMZETI KÖNYVTÁR
H-4002 Debrecen, Egyetem tér 1, Pf.: 400
Tel.: 52/410-443, e-mail: publikaciok@lib.unideb.hu

Idegen nyelvű absztrakt kiadványok (2)

7. **Guizani, D.**, Tamás, J., Nagy, A.: Sustainable urban development in Debrecen: addressing water scarcity, agricultural decline, and industrial expansion through community-based hydroponic solutions.
   In: Abstract Book of the 8th International Scientific Conference on Water, Magyar Agrár-és Élettudományi Egyetem, Gödöllő, 35, 2025. ISBN: 9789636231156(pdf)
8. **Guizani, D.**, Bódi, E., Tamás, J., Nagy, A.: Identification of water balance properties of urban atlas using Landsat 8 data.
   In: Book of abstract XXII Conference of PhD Students and Young Scientists : Interdisciplinary topics in mining and geology. Szerk.: Jan Blachowski, Wrocaw University of Science and Technology Publishing House, Wrocaw, 41-42, 2022. ISBN: 9788374932202

A DEENK a Jelölt által a Tudóstérbe feltöltött adatok bibliográfiai és tudománymetriai ellenőrzését a tudományos adatbázisok és a Journal Citation Reports Impact Factor lista alapján elvégezte.

Debrecen, 2025.07.28.

DEBRECENI EGYETEM * Egyetemi és Nemzeti Könyvtár *

10. REFERENCES

1. Ali, M. Z., Qazi, W., & Aslam, N. (2018). A comparative study of ALOS-2 PALSAR and Landsat-8 imagery for land cover classification using maximum likelihood classifier. *Egyptian Journal of Remote Sensing and Space Sciences, 21*, S29–S35. https://doi.org/10.1016/j.ejrs.2018.03.003
2. Aalbers, E. E., van Meijgaard, E., Lenderink, G., de Vries, H., & van den Hurk, B. J. J. M. (2023). The 2018 west-central European drought projected in a warmer climate: How much drier can it get? *Natural Hazards and Earth System Sciences, 23*, 1921–1946. https://doi.org/10.5194/nhess-23-1921-2023
3. Al Kafy, A., Bakshi, A., Saha, M., Al Faisal, A., Almulhim, A. I., Rahman, Z. A., & Mohammad, P. (2023). Assessment and prediction of index-based agricultural drought vulnerability using machine learning algorithms. *Science of the Total Environment, 867*, Article 161394. https://doi.org/10.1016/j.scitotenv.2023.161394
4. Acharki, S. (2022). PlanetScope contributions compared to Sentinel-2, and Landsat-8 for LULC mapping. *Remote Sensing Applications: Society and Environment, 27*, 100774. https://doi.org/10.1016/j.rsase.2022.100774
5. Adugna, T., Xu, W., & Fan, J. (2022). Comparison of Random Forest and Support Vector Machine classifiers for regional land cover mapping using coarse resolution FY-3C images. *Remote Sensing, 14*(3), 574. https://doi.org/10.3390/rs14030574
6. Asghar, A., Iqbal, J., Amin, A., & Ribbe, L. (2019). Integrated hydrological modeling for assessment of water demand and supply under socio-economic and IPCC climate change scenarios using WEAP in Central Indus Basin. *Journal of Water Supply: Research and Technology–Aqua, 68*(2), 136–148. https://doi.org/10.2166/aqua.2019.106
7. Altieri, M. A., Companioni, N., Cañizares, K., Murphy, C., Rosset, P., Bourque, M., & Nicholls, C. I. (1999). The greening of the 'barrios': Urban agriculture for food security in Cuba. *Agriculture and Human Values, 16*(2), 131–140. https://doi.org/10.1023/A:1007545304561
8. Ahmad, A., & Quegan, S. (2012). Analysis of maximum likelihood classification on multispectral. *Applied Mathematical Sciences, 6*(129), 6425–6436. https://www.researchgate.net/publication/279541271

9. Amindin, A., Siamian, N., Kariminejad, N., Clague, J. J., & Pourghasemi, H. R. (2024). An integrated GEE and machine learning framework for detecting ecological stability under land use/land cover changes. Global Ecology and Conservation, 53, e03010. https://doi.org/10.1016/j.gecco.2024.e03010
10. Aryal, J., Sitaula, C., & Frery, A. C. (2023). Land use and land cover (LULC) performance modeling using machine learning algorithms: A case study of the city of Melbourne. Scientific Reports, 13(1), 13510. https://doi.org/10.1038/s41598-023-40564-0
11. Aydin Y. (2021). Assessing of evapotranspiration models using limited climatic data in Southeast Anatolian Project Region of Turkey. PeerJ 9:e11571 https://doi.org/10.7717/peerj.11571
12. Asuquo, E. M., Ebere, N. R., & Chinenye, O. U. (2023). Modeling and mapping the spatial temporal changes in land use and land cover in Lagos: A dynamics for building a sustainable urban city. *Advances in Space Research*, *72*(3), 694–710. https://doi.org/10.1016/j.asr.2022.07.042
13. Boriah, S. (2010). *Time series change detection: Algorithms for land cover change* (Doctoral dissertation, University of Minnesota). Retrieved from https://hdl.handle.net/11299/90706
14. Bilintoh, E., Ali, M., & Smith, D. (2024). Analyzing the losses and gains of a land category: Insights from the total operating characteristic. *Land*, *13*(8), 1177. https://doi.org/10.3390/land13081177
15. Batelaan, O., & De Smedt, F. (2001). WetSpass: A flexible, GIS-based, distributed recharge methodology for regional groundwater modelling. *IAHS–AISH Publication*, *269*, 11–18. Retrieved from https://www.researchgate.net/publication/251732752_WetSpass_A_flexible_GIS_based_distributed_recharge_methodology_for_regional_groundwater_modelling
16. Botero-Acosta, A., Chu, M. L., Wu, C. L., McIsaac, G. F., & Knouft, J. H. (2025). Model-based estimation of the isolated impacts of urban expansion on projected streamflow values under varied climate scenarios. Computers, Environment and Urban Systems, 118, 102259. https://doi.org/10.1016/j.compenvurbsys.2025.102259
17. Brown, S. A., Stein, S. M., & Warner, J. C. (1996). *Urban drainage design manual* (3rd ed.). Hydraulic Engineering Circular 22, FHWA-SA-96-078.

Washington, DC: Federal Highway Administration. Retrieved from https://rosap.ntl.bts.gov/view/dot/54350/dot_54350_DS1.pdf

18. Barranco, R., Silva, F. B. E., Herrera, M. M., & Lavalle, C. (2014). Integrating the MOLAND and the Urban Atlas geo-databases to analyze urban growth in European cities. *Journal of Map & Geography Libraries, 10*(3), 305–328. https://doi.org/10.1080/15420353.2014.952485
19. Blaschke, T. (2010). Object based image analysis for remote sensing. *ISPRS Journal of Photogrammetry and Remote Sensing, 65*(1), 2–16. https://doi.org/10.1016/j.isprsjprs.2009.06.004
20. Bolstad, P. V., & Lillesand, T. M. (1991). Rapid maximum likelihood classification. *Photogrammetric Engineering and Remote Sensing, 57*, 67–74.
21. Bruse, M., & Fleer, H. (1998). Simulating surface–plant–air interactions inside urban environments with a three-dimensional numerical model. *Environmental Modelling & Software, 13*(3–4), 373–384. https://doi.org/10.1016/S1364-8152(98)00042-5
22. Borsy, Z. (1989). Az Alföld hordalékkúpjainak negyedidőszaki fejlődéstörténete. *Földrajzi Értesítő, 38*, 211–224. https://www.scopus.com/inward/record.url?eid=2-s2.0-0024936307&partnerID=10&rel=R3.0.0
23. Barbosa, G. L., Gadelha, F. D. A., Kublik, N., Proctor, A., Reichelm, L., Weissinger, E., Wohlleb, G. M., & Halden, R. U. (2015). Comparison of land, water, and energy requirements of lettuce grown using hydroponic vs. conventional agricultural methods. *International Journal of Environmental Research and Public Health, 12*(6), 6879–6891. https://doi.org/10.3390/ijerph120606879
24. Bashir, B. Morphometric Parameters and Geospatial Analysis for Flash Flood Susceptibility Assessment: A Case Study of Jeddah City along the Red Sea Coast, Saudi Arabia. *Water* 2023, *15*, 870. https://doi.org/10.3390/w15050870
25. Benzougagh, B., Meshram, S.G., Dridri, A. *et al.* Identification of critical watershed at risk of soil erosion using morphometric and geographic information system analysis. *Appl Water Sci* 12, 8 (2022). https://doi.org/10.1007/s13201-021-01532-z

26. Bañares, E. N., Mehboob, M. S., Khan, A. R., & Cacal, J. C. (2024). Projecting hydrological response to climate change and urbanization using WEAP model: A case study for the main watersheds of Bicol River Basin, Philippines. Journal of Hydrology: Regional Studies, *54*, Article 101846. https://doi.org/10.1016/j.ejrh.2024.101846
27. B.R. Deilmai, B.B. Ahmad, H. Zabihi Comparison of two classification methods (MLC and SVM) to extract land use and land cover in Johor Malaysia IOP Conf. Ser.: Earth Environ. Sci., 20 (2014), 10.1088/1755-1315/20/1/012052
28. B. Norovsuren, B. Tseveen,V. Batomunkuev, T. Renchin, E. Natsagdorj, A. Yangiv, Z. Mart Land cover classification using maximum likelihood method (2000 and 2019) at Khandgait Valley in Mongolia IOP Conference Series: Earth and Environmental Science, 381 (2019), Article 012054, 10.1088/1755-1315/381/1/012054
29. L. Breiman Random forests Mach. Learn., 45 (1) (2001), pp. 5-32, 10.1023/A:1010933404324
30. Belgiu, M., & Drăguţ, L. (2016). Random forest in remote sensing: A review of applications and future directions. *ISPRS Journal of Photogrammetry and Remote Sensing*, *114*, 24–31. https://doi.org/10.1016/j.isprsjprs.2016.01.011
31. Basheer, S., Wang, X., Farooque, A. A., Nawaz, R. A., Liu, K., Adekanmbi, T., & Liu, S. (2022). Comparison of land use land cover classifiers using different satellite imagery and machine learning techniques. *Remote Sensing*, *14*(19), 4978. https://doi.org/10.3390/rs14194978
32. Brazel, A. J., et al. (2000). Time-trend analysis of Phoenix Sky Harbor nighttime temperatures: summer winter differences. *Decision Center for a Desert City*. https://sustainability-innovation.asu.edu/dcdc/2014/07/?utm_source=chatgpt.com
33. Bueno-Suárez, C., & Coq-Huelva, D. (2020). Sustaining what is unsustainable: A review of urban sprawl and urban socio-environmental policies in North America and Western Europe. *Sustainability*, *12*(11), 4445. https://doi.org/10.3390/su12114445
34. Banjara, M., Bhusal, A., Ghimire, A. B., & Kalra, A. (2024). Impact of land use and land cover change on hydrological processes in urban watersheds: Analysis and forecasting for flood risk management. *Geosciences*, *14*(2), 40. https://doi.org/10.3390/geosciences14020040

35. Chemak, F., Nouir, I., Bellali, H., & Chahed, M. K. (2022). Irrigation practices, prevalence of leishmaniasis and sustainable development: Evidence from the Sidi Bouzid region in central Tunisia. *Scientific African, 15*, e01094. https://doi.org/10.1016/j.sciaf.2022.e01094
36. Caldwell, P. V., Sun, G., McNulty, S. G., Cohen, E. C., & Myers, M. J. A. (2012). Impacts of impervious cover, water withdrawals, and climate change on river flows in the conterminous U.S. *Hydrology and Earth System Sciences, 16*, 2839–2857. https://doi.org/10.5194/hessd-9-4263-2012
37. Choi, Y.-Y., Suh, M.-S., & Park, K.-H. (2014). Assessment of surface urban heat islands over three megacities in East Asia using land surface temperature data retrieved from COMS. *Remote Sensing, 6*(6), 5852–5867. https://doi.org/10.3390/rs6065852
38. Chow, K. K., Wang, J. Y., & Tay, J. H. (2001). Hydroponic cultivation of leafy vegetables in primary and secondary municipal wastewater. *Acta Horticulturae*, 554, 139–146. https://doi.org/10.17660/ActaHortic.2001.554.14
39. Colasanti, K. J. A., Hamm, M. W., & Litjens, C. M. (2012). The city as an "agricultural powerhouse"? Perspectives on expanding urban agriculture from Detroit, Michigan. *Urban Geography, 33*(3), 348–369. https://doi.org/10.2747/0272-3638.33.3.348
40. Corrigan, S. (2023, November 22). *How to build resilient cities with green infrastructure*. CityGreen. https://citygreen.com/green-infrastructure-in-urban-planning
41. City of Raleigh. (2024). *Stormwater Design Manual: Chapter Three – Hydrology*. Retrieved from: https://cityofraleigh0drupal.blob.core.usgovcloudapi.net/drupal-prod/COR16/Stormwater%20Design%20Manual.pdf?utm_source=chatgpt.com
42. Cortes, C., & Vapnik, V. (1995). Support-vector networks. *Machine Learning, 20*, 273–297. https://doi.org/10.1023/A:1022627411411
43. Diouf, O. C., Weihermüller, L., Ba, K., Faye, S. C., & Faye, S. (2016). Estimation of Turc reference evapotranspiration with limited data against the Penman-Monteith formula in Senegal. *Journal of Agriculture and Environment for International Development (JAEID), 110*(1). https://doi.org/10.12895/jaeid.20161.417
44. Campisano, A., Butler, D., Ward, S., Burns, M. J., Friedler, E., DeBusk, K., ... & Han, M. (2017). Urban rainwater harvesting systems: Research, implementation

and future perspectives. *Water Research*, *115*, 195–209. https://doi.org/10.1016/j.watres.2017.02.056

45. Dermosinoglou, A., & Petropoulos, G. P. (2024). Exploring long term impervious surface areas (ISA) dynamics using Landsat imagery, machine learning and GEE: The case of Attica, Greece. Remote Sensing Applications: Society and Environment, 36, 101338. https://doi.org/10.1016/j.rsase.2024.101338
46. Daba, M. H., & You, S. (2022). Quantitatively assessing the future land-use/land-cover changes and their driving factors in the upper stream of the Awash River based on the CA–Markov model and their implications for water resources management. *Sustainability*, *14*(3), Article 1538. https://doi.org/10.3390/su14031538
47. Dou, P., Huang, C., Han, W., Hou, J., Zhang, Y., & Gu, J. (2024). Remote sensing image classification using an ensemble framework without multiple classifiers. *ISPRS Journal of Photogrammetry and Remote Sensing*, *208*, 190–209. https://doi.org/10.1016/j.isprsjprs.2023.12.012
48. Dubbeling, M., de Zeeuw, H., & van Veenhuizen, R. (2010). Cities, poverty and food: Multi-stakeholder policy and planning in urban agriculture. In Mougeot, L. J. A. (Ed.), *Agropolis: The social, political and environmental dimensions of urban agriculture* (pp. 1–30). Earthscan.
49. Drechsel, P., & Dongus, S. (2010). Dynamics and sustainability of urban agriculture: Examples from sub-Saharan Africa. *Sustainability Science*, *5*(1), 69–78. https://doi.org/10.1007/s11625-009-0097-x
50. dos Santos, M. J. P. L. (2016). Smart cities and urban areas—Aquaponics as innovative urban agriculture. *Urban Forestry & Urban Greening*, *20*, 402–406. https://doi.org/10.1016/j.ufug.2016.10.004
51. Environmental Protection Agency. (2020). *Different shades of green: Green infrastructure research at the U.S. Environmental Protection Agency*. EPA. chrome-extension://efaidnbmnnnibpcajpcglclefindmkaj/https://www.epa.gov/sites/default/files/2016-10/documents/green_infrastructure_brochure_final.pdf
52. Elmqvist, T., Fragkias, M., Goodness, J., Güneralp, B., Marcotullio, P. J., McDonald, R. I., & Wilkinson, C. (Eds.). (2013). *Urbanization, biodiversity and ecosystem services: Challenges and opportunities*. Springer. https://doi.org/10.1007/978-94-007-7088-1

53. Edris,T.S.–Majid,H.–Arash,M.(2016): Estimating time of concentration in large watersheds: Article in Paddy and Water Environment June 2016
54. European Space Agency. (2024). *Sentinel-2 user guide*. https://sentinel.esa.int/web/sentinel/user-guides/sentinel-2-msi/overview
55. Fletcher, T. D., Shuster, W., Hunt, W. F., Ashley, R., Butler, D., Arthur, S., & Mikkelsen, P. S. (2015). SUDS, LID, BMPs and more–The evolution and application of terminology surrounding urban drainage. *Urban Water Journal*, *12*(7), 525–542. https://doi.org/10.1080/1573062X.2014.916314
56. FAO. (2020). *the state of the world's land and water resources for food and agriculture – Systems at breaking point*. Food and Agriculture Organization of the United Nations. https://doi.org/10.4060/cb1447en
57. FAO. (2014). *growing greener cities in Latin America and the Caribbean: An FAO report on urban and peri-urban agriculture in the region*. Food and Agriculture Organization of the United Nations. https://www.fao.org/3/i3696e/i3696e.pdf
58. Frank, M., & Benon, B. (2016). The centrality of water resources to the realization of Sustainable Development Goals (SDG): A review of potentials and constraints on the African continent. *International Soil and Water Conservation Research*, *4*(3), 215–223. https://doi.org/10.1016/j.iswcr.2016.05.004
59. Gombos, B., Nagy, Z., Hajdu, A., & Nagy, J. (2023). Climate change in the Debrecen area in the last 50 years and its impact on maize production. *Időjárás / Quarterly Journal of the Hungarian Meteorological Service*, *127*(4), 485–504. https://doi.org/10.28974/idojaras.2023.4.5
60. Guizani, D., Bódi, E. B., Tamás, J., & Nagy, A. (2024). Enhancing water balance assessment in urban areas through high-resolution land cover mapping: Case study of Debrecen, Hungary. Environmental Challenges, 15, 100906. https://doi.org/10.1016/j.envc.2024.100906
61. Guizani, D., Budayné Bódi, E., Tamás, J., & Nagy, A. (2022). Characterisation of basic water balance parameters of Debrecen. *Acta Agraria Debreceniensis*, *1*, 35–40. https://doi.org/10.34101/actaagrar/1/10427
62. Grimmond, C. S. B., Blackett, M., Best, M. J., Barlow, J., Baik, J. J., Belcher, S. E., & Voogt, J. A. (2010). The international urban energy balance models comparison project: First results from phase 1. *Journal of Applied Meteorology and Climatology*, *49*(6), 1268–1292. https://doi.org/10.1175/2010JAMC2354.1

63. Guduru, J. U., & Mohammed, A. S. (2024). *Hydrological modeling using HEC-HMS model, case of Tikur Wuha River Basin, Rift Valley River Basin, Ethiopia*. *Environmental Challenges, 17,* Article 101017. https://doi.org/10.1016/j.envc.2024.101017
64. Gassman, P.W., et al. (2007) The Soil and Water Assessment Tool: Historical Development, Applications, and Future Research Directions. Transactions of the ASABE, 50, 1211-1250. http://dx.doi.org/10.13031/2013.23637
65. Graber, A., & Junge, R. (2009). Aquaponic systems: Nutrient recycling from fish wastewater by vegetable production. *Desalination*, 246(1–3), 147–156. https://doi.org/10.1016/j.desal.2008.03.068
66. Gaffin, S., Rosenzweig, C., Parshall, L., Hillel, D., Eichenbaum-Pikser, J., Greenbaum, A., Blake, R., Beattie, D., & Berghage, R. (2006). Quantifying evaporative cooling from green roofs and comparison to other land surfaces. *Report*, Columbia University Center for Climate Systems Research. https://scholar.google.com/scholar_lookup?title=Quantifying%20Evaporative%20Cooling%20from%20Green%20Roofs%20and%20Comparison%20to%20Other%20Land%20Surfaces&publication_year=2006&author=S.%20Gaffin
67. Haque, M. I., & Basak, R. (2017). Land cover change detection using GIS and remote sensing techniques: A spatio-temporal study on Tanguar Haor, Sunamganj, Bangladesh. *Egyptian Journal of Remote Sensing and Space Science*, *20*(2), 251–263. https://doi.org/10.1016/j.ejrs.2016.12.003
68. Hermosilla, T., Wulder, M. A., White, J. C., Coops, N. C., & Hobart, G. W. (2018). Disturbance-informed annual land cover classification maps of Canada's forested ecosystems for a 29-year Landsat time series. *Canadian Journal of Remote Sensing*, *44*(1), 67–87. https://doi.org/10.1080/07038992.2018.1437719
69. Hüse, B., Szabó, S., Deák, B., & Tóthmérész, B. (2016). Mapping an ecological network of green habitat patches and their role in maintaining urban biodiversity in and around Debrecen city (Eastern Hungary). *Land Use Policy*, *57*, 574–581. https://doi.org/10.1016/j.landusepol.2016.06.026
70. Hamilton, A. J., Burry, K., Mok, H. F., Barker, S. F., Grove, J. R., & Williamson, V. G. (2014). Give peas a chance? Urban agriculture in developing countries. *A review*. *Agronomy for Sustainable Development*, *34*(1), 45–73. https://doi.org/10.1007/s13593-013-0155-8

71. Hung, C. L. J. L., James, A., & Carbone, G. J. (2018). Impacts of urbanization on stormflow magnitudes in small catchments in the Sand Hills of South Carolina, USA. *Anthropocene, 23*, 17–28. https://doi.org/10.1016/j.ancene.2018.08.001
72. Heath, R. C. (1983). *Basic ground-water hydrology* (U.S. Geological Survey Water-Supply Paper 2220). U.S. Government Printing Office. https://doi.org/10.3133/wsp2220
73. Iváncsics, V., & Kovács, K. F. (2021). Analyses of new artificial surfaces in the catchment area of 12 Hungarian middle-sized towns between 1990 and 2018. *Land Use Policy, 109*, 105644. https://doi.org/10.1016/j.landusepol.2021.105644
74. Jimenez, D. A., Jimenez, C. A., Menapace, A., de Andrade Pinto, E. J., Brentan, B., & Avila-Diaz, A. (2025). Changes in the frequencies of occurrence of maximum daily precipitation for the metropolitan region of Belo Horizonte – Brazil. *Urban Climate, 61*, 102461. https://doi.org/10.1016/j.uclim.2025.102461
75. Jurga, A., Pacak, A., Pandelidis, D., & Kaźmierczak, B. (2021). A long-term analysis of the possibility of water recovery for hydroponic lettuce irrigation in an indoor vertical farm. Part 2: Rainwater harvesting. *Applied Sciences*, 11(1), 310. https://doi.org/10.3390/app11010310
76. Jensen, J. R. (2005). *Introductory digital image processing: A remote sensing perspective* (4th ed., pp. 136–142). In Keith, C. C. (Ed.), *Prentice Hall Series in Geographic Information Science*. Saddle River, NJ, USA: Prentice Hall. https://doi.org/10.1080/10106048709354084
77. Jensen, J. R. (2000). *Introductory digital image processing: A remote sensing perspective* (3rd ed.). Prentice Hall Inc. Available at: https://scholar.google.com/scholar_lookup?title=Introductory%20Digital%20Image%20processing%3A%20a%20Remote%20Sensing%20perspective&publication_year=2000&author=J.R.%20Jensen
78. Johnson, R. D., & Kasischke, E. S. (1998). Change vector analysis: A technique for the multispectral monitoring of land cover and condition. *International Journal of Remote Sensing, 19*(3), 411–426. https://doi.org/10.1080/014311698216062
79. Jamshid, T., Nasser, L., & Mina, F. (2013). Satellite image classification methods and Landsat 5TM bands. *Department of Computer Engineering, EMU University, North Cyprus, Famagusta.* https://doi.org/10.48550/arXiv.1308.1801

80. Jensen, J. R. (2005). *Introductory digital image processing: A remote sensing perspective* (4th ed.). Prentice Hall.
81. Józsa, E., Fábián, S. Á., & Kovács, M. (2014). An evaluation of EU-DEM in comparison with ASTER GDEM, SRTM and contour-based DEMs over the Eastern Mecsek Mountains. Hungarian Geographical Bulletin, 63(4), 401–423. https://doi.org/10.15201/hungeobull.63.4.3
82. Jia, X., & Richards, J. (1999). Segmented principal components transformation for efficient hyperspectral remote-sensing image display and classification. *IEEE Transactions on Geoscience and Remote Sensing*, *37*, 25–27. https://doi.org/10.1109/36.739109
83. Kovács, F. (2011). Az alföldi területhasználat és változásainak értékelése. In J. Rakonczai (Ed.), *Környezeti Változások és az Alföld* (Nagyalföld Alapítvány Kötetei, Vol. 7, pp. 159–166). Békéscsaba: Nagyalföld Alapítvány. Retrieved from https://scholar.google.com/scholar_lookup?title=Az%20alf%C3%B6ldi%20ter%C3%BClethaszn%C3%A1lat%20%C3%A9s%20v%C3%A1ltoz%C3%A1sainak%20%C3%A9rt%C3%A9kel%C3%A9se&publication_year=2011&author=F.%20Kov%C3%A1cs
84. Kashyap, P. S., & Panda, R. K. (2001). Evaluation of evapotranspiration estimation methods and development of crop-coefficients for potato crop in a sub-humid region. *Agricultural Water Management*, *50*(1), 9–25. https://doi.org/10.1016/S0378-3774(01)00102-0
85. Kenessey, B. (1928). *The Lake Balaton* [A Balaton]. p. 43. Retrieved from https://scholar.google.com/scholar_lookup?title=The%20lake%20balaton&publication_year=1928&author=B.%20Kenessey
86. Kenessey, B., 1930. Lefolyási tényezők és retenciók. Hidrológiai tanulmány [Flow factors and retention. Hydrological study]. *Vízügyi Közlemények*, 12(1), 55–76. (In Hungarian). Available from: https://adtplus.arcanum.hu/en/collection/VizugyiKozlemenyek/
87. Kailath, T. (1967). The divergence and Bhattacharyya distance measures in signal selection. *IEEE Transactions on Communication Technology*, *15*, 52–60. https://doi.org/10.1109/TCOM.1967.1089532
88. Kovács, Z., Farkas, J., Egedy, T., Kondor, A., Szabó, B., Lennert, J., Baka, D., & Kohán, B. (2019). Urban sprawl and land conversion in post-socialist cities: The

case of metropolitan Budapest. *Cities, 92*, 71–81. https://doi.org/10.1016/j.cities.2019.03.018

89. Klein, I., Gessner, U., & Kuenzer, C. (2012). Regional land cover mapping and change detection in Central Asia using MODIS time-series. *Applied Geography, 35*(1–2), 219–234. https://doi.org/10.1016/j.apgeog.2012.06.016
90. Kou, L.; Li, X.; Lin, J.; Kang, J. Simulation of Urban Water Resources in Xiamen Based on a WEAP Model. *Water* 2018, *10*, 732. https://doi.org/10.3390/w10060732
91. Kintu, M., Shitenga, A., & Shitenga, M. (2019). A literature review of impacts of urbanization on water resource management: A case study in South Africa. *International Journal of Scientific and Research Publications, 9*(6). https://doi.org/10.29322/IJSRP.9.06.2019.p9051
92. Lauer, A., Pausata, F. S. R., Leroyer, S., & Argueso, D. (2023). Effect of urban heat island mitigation strategies on precipitation and temperature in Montreal, Canada: Case studies. *PLOS Climate, 2*(6), e0000196. https://doi.org/10.1371/journal.pclm.0000196
93. Lóczy, D., Éva, K., & Schweitzer, F. (2009). Local flood hazards assessed from channel morphometry along the Tisza River in Hungary. *Geomorphology, 113*(3–4), 200–209. https://doi.org/10.1016/j.geomorph.2009.03.013
94. Liu, H., Huang, B., Zhan, Q., Gao, S., Li, R., & Fan, Z. (2021). The influence of urban form on surface urban heat island and its planning implications: Evidence from 1288 urban clusters in China. *Sustainable Cities and Society, 71*, 102987. https://doi.org/10.1016/j.scs.2021.102987
95. Lee, Y. Y., Din, M. F. M., Ponraj, M., Noor, Z. Z., Iwao, K., & Chelliapan, S. (2017). Overview of urban heat island (UHI) phenomenon towards human thermal comfort. *Environmental Engineering and Management Journal, 16*(9), 2097–2105. https://scholar.google.com/scholar_lookup?title=Overview%20of%20urban%20heat%20island%20%20phenomenon%20towards%20human%20thermal%20comfort&publication_year=2017&author=Y.Y.%20Lee
96. Liao, K. H., et al. (2017). Green infrastructure: A new frontier for sustainable urban stormwater management. *ScienceDirect Topics*. https://www.sciencedirect.com/topics/earth-and-planetary-sciences/green-infrastructure

97. Li, P., Shi, C., Li, Z., Müller, J.-P., Drummond, J., Li, X., & Liu, J. (2012). Evaluation of ASTER GDEM ver2 using GPS measurements and SRTM v4.1 in China. ISPRS Annals of the Photogrammetry, Remote Sensing and Spatial Information Sciences, I-4, 181–186. https://doi.org/10.5194/isprsannals-I-4-181-2012

98. Lu, D., Batistella, M., Moran, E., & de Moraes, M. (2008). A comparative study of Landsat TM and SPOT HRG images for vegetation classification in the Brazilian Amazon. *Photogrammetric Engineering & Remote Sensing*, *74*(3), 311–321. https://doi.org/10.14358/PERS.74.3.311

99. Lindeburg, M. R. (1999). *Civil engineering reference manual for the PE exam* (7th ed.). Belmont, CA: Professional Publications Inc. https://scholar.google.com/scholar_lookup?title=Civil%20Engineering%20Reference%20Manual%20for%20the%20Pe%20Exam&publication_year=1999&author=M.R.%20Lindeburg

100. Liu, A., Wu, Q., & Cheng, X. (2020). Using the Google Earth Engine to estimate a 10 m resolution monthly inventory of soil fugitive dust emissions in Beijing, China. *Science of the Total Environment*, *735*, 139174. https://doi.org/10.1016/j.scitotenv.2020.139174

101. Lemenkova, P. (2018). Detection of vegetation coverage in urban agglomeration of Brussels by NDVI indicator using eCognition software and remote sensing measurements. https://doi.org/10.6084/m9.figshare

102. Lobell, D. B. (2013). The use of satellite data for crop yield gap analysis. *Field Crops Research*, *143*, 56–64. https://doi.org/10.1016/j.fcr.2012.08.008

103. Lóczy, D. (1997). Human impact on rivers in Hungary as reflected in changes of channel planform. *Zeitschrift für Geomorphologie, 110*, 219–231. https://www.scopus.com/pages/publications/0031425351?inward

104. Shen, J., Han, W. L., Zhang, L. B., & Ge, J. (2020). Analysis and comparison of SRTM3 DEM and ASTER GDEM v2. ISPRS Archives – Photogrammetry, Remote Sensing and Spatial Information Sciences, 42(3/W10), 529–536. https://doi.org/10.5194/isprs-archives-XLII-3-W10-529-2020

105. Lóczy, D., Éva, K., & Schweitzer, F. (2009). Local flood hazards assessed from channel morphometry along the Tisza River in Hungary. *Geomorphology, 113*(3–4), 200–209. https://doi.org/10.1016/j.geomorph.2009.03.013

106. Lovell, S. T. (2010). Multifunctional urban agriculture for sustainable land use planning in the United States. *Sustainability*, *2*(8), 2499–2522. https://doi.org/10.3390/su2082499

107. Michelle, T. H. V., Edward, R. J., Martina, F., Wietse, H. P. F., Naota, H., Yoshihide, W., & John, R. Y. (2021). Global water scarcity including surface water quality and expansions of clean water technologies. *Environmental Research Letters*, *16*, Article 024020. https://doi.org/10.1088/1748-9326/abbfc3

108. Ma, X., Xu, J., Luo, Y., Aggarwal, S. P., & Li, J. (2009). Response of hydrological processes to land-cover and climate changes in Kejie watershed, south-west China. *Hydrological Processes*, *23*(8), 1179–1191. https://doi.org/10.1002/hyp.7233

109. Manandhar, B., Cui, S., Wang, L., & Shrestha, S. (2023). Urban flood hazard assessment and management practices in South Asia: A review. *Land*, *12*(3), Article 627. https://doi.org/10.3390/land12030627

110. Molnár, E., & Kozma, G. (2018). A debreceni gazdaságfejlesztés zászlóshajói: A városban működő ipari parkok jellegzetességei [Flagships of economic development of Debrecen: Characteristics of industrial parks in the city]. *Tér és Társadalom, 33*(3), 49–71. https://doi.org/10.17649/TET.33.3.3188

111. Manandhar, B., Cui, S., Wang, L., & Shrestha, S. (2023). Urban flood hazard assessment and management practices in South Asia: A review. *Land*, *12*(3), 627. https://doi.org/10.3390/land12030627

112. Mudereri, B. T., Ayisi, K. K., & Ramudzuli, M. R. (2023). A systematic review on advancements in remote sensing for assessing and monitoring land use and land cover changes impacts on surface water resources in semi-arid tropical environments. *Remote Sensing*, *15*(16), 3926. https://doi.org/10.3390/rs15163926

113. Mengistu, T. D., Chung, I., Kim, M., Chang, S. W., & Lee, J. E. (2022). Impacts and implications of land use land cover dynamics on groundwater recharge and surface runoff in East African watershed. *Water*, *14*(13), 2068. https://doi.org/10.3390/w14132068

114. M. Pal: Random forest classifier for remote sensing classification Int. J. Remote Sens., 26 (1) (2005), pp. 217-222, 10.1080/01431160412331269698

115. Mougeot, L. J. A. (2000). Urban agriculture: Definition, presence, potentials and risks. In N. Bakker, M. Dubbeling, S. Guendel, U. Sabel-Koschella, & H. de Zeeuw (Eds.), Growing cities, growing food: Urban agriculture on the

policy agenda (pp. 1–42). Deutsche Stiftung für Internationale Entwicklung (DSE).

116. McClintock, N., et al. (2018). Urban agriculture and sustainability transitions. Journal of Agriculture, Food Systems, and Community Development.

117. Medina, J. A. V., & Beatriz, E. A. A. (2018). Comparison of maximum likelihood, support vector machines, and random forest techniques in satellite images classification. *Tecnura*, *23*(59), 13–26. https://doi.org/10.14483/22487638.14826

118. Mustapha, M. R., Lim, H. S., & Mat Jafri, M. Z. (2010). Comparison of neural network and maximum likelihood approaches in image classification. *Journal of Applied Sciences*, *10*(22), 2847–2854. https://doi.org/10.3923/jas.2010.2847.2854

119. Mtibaa, S., & Asano, S. (2022). Hydrological evaluation of radar and satellite gauge-merged precipitation datasets using the SWAT model: Case of the Terauchi catchment in Japan. *Journal of Hydrology: Regional Studies*, *42*, 101134. https://doi.org/10.1016/j.ejrh.2022.101134

120. Malcom, H. R. (1997). *Elements of storm water design* (Tech. Rep. 85). Raleigh, NC: North Carolina State University, Industrial Extension Service. Retrieved from https://www.deq.nc.gov/water-quality/surface-water-protection/spu/spu-bmp-manual-documents/bmpman-appendix-b-20070629-dwq-spu/download

121. Mountrakis, G., Im, J., & Ogole, C. (2011). Support vector machines in remote sensing: A review. *ISPRS Journal of Photogrammetry and Remote Sensing*, *66*(3), 247–259. https://doi.org/10.1016/j.isprsjprs.2010.11.001

122. Musy, A., & Higy, C. (2004). *Hydrologie: Une science de la nature* (p. 314). Lausanne, Switzerland: Presses Polytechniques et Universitaires Romandes. https://scholar.google.com/scholar_lookup?title=Hydrologie%2C%20Une%20Science%20De%20La%20Nature&publication_year=2004&author=A.%20Musy&author=C.%20Higy

123. Mehta, O., Kansal, M. L., & Bisht, D. S. (2022). A comparative study of the time of concentration methods for designing urban drainage infrastructure. *AQUA - Water Infrastructure, Ecosystems and Society*, *71*(10), 1197–1218. https://doi.org/10.2166/aqua.2022.107

124. Martinez-Sanchez, L., See, L., Yordanov, M., Verhegghen, A., Elvekjaer, N., Muraro, D., d'Andrimont, R., & van der Velde, M. (2024). Automatic classification of land cover from LUCAS in-situ landscape photos using semantic segmentation and a Random Forest model. *Environmental Modelling & Software, 172*, Article 105931. https://doi.org/10.1016/j.envsoft.2023.105931

125. Nwagoum, C. S. K., Yemefack, M., Tedou, F. B. S., & Oben, F. T. (2023). Sentinel-2 and Landsat-8 potentials for high-resolution mapping of the shifting agricultural landscape mosaic systems of southern Cameroon. *International Journal of Applied Earth Observation and Geoinformation, 124*, Article 103545. https://doi.org/10.1016/j.jag.2023.103545

126. Osorio, J., Jeong, J., Bieger, K., & Arnold, J. (2014). Influence of potential evapotranspiration on the water balance of sugarcane fields in Maui, Hawaii. *Journal of Water Resource and Protection, 6*(9). https://doi.org/10.4236/jwarp.2014.69080

127. Oudin, L., Hervieu, F., Michel, C., Perrin, C., Andréassian, V., Anctil, F., & Loumagne, C. (2005). Which potential evapotranspiration input for a lumped rainfall–runoff model? Part 2—towards a simple and efficient potential evapotranspiration model for rainfall–runoff modelling. *Journal of Hydrology, 303*(1–4), 290–306. https://doi.org/10.1016/j.jhydrol.2004.08.026

128. Orsini, F., Kahane, R., Nono-Womdim, R., & Gianquinto, G. (2013). Urban agriculture in the developing world: A review. *Agronomy for Sustainable Development*, *33*(4), 695–720. https://doi.org/10.1007/s13593-013-0143-z

129. Qadir, M., Drechsel, P., Cisneros, B. J., Kim, Y., Pramanik, A., Mehta, P., & Olaniyan, O. (2020). *Global and regional potential of wastewater as a water, nutrient and energy source*. *Natural Resources Forum*, *44*(1), 40–51. https://doi.org/10.1111/1477-8947.12187

130. Orsini, F., Kahane, R., Nono-Womdim, R., & Gianquinto, G. (2013). Urban agriculture in the developing world: A review. *Agronomy for Sustainable Development*, *33*(4), 695–720. https://doi.org/10.1007/s13593-013-0143-z

131. Pénzes, J., Hegedűs, L. D., Makhanov, K., & Túri, Z. (2023). Changes in the patterns of population distribution and built-up areas of the rural–urban fringe in post-socialist context—a Central European case study. *Land, 12*, 1682. https://doi.org/10.3390/land12091682

132. Pontius Jr., R. G. (2000). Quantification error versus location in comparison of categorical maps. *Photogrammetric Engineering & Remote Sensing*, *66*(8), 1011–1016. Retrieved from https://www.asprs.org/wp-content/uploads/pers/2000journal/august/2000_aug_1011-1016.pdf

133. Pásztor, L., Laborczi, A., Bakacsi, Z., Szabó, J., & Illés, G. (2018). Compilation of a national soil-type map for Hungary by sequential classification methods. *Geoderma*, *311*, 93–108. https://doi.org/10.1016/j.geoderma.2017.04.018

134. Pontius, R. G., Jr. (2022). *Metrics that make a difference*. Springer Nature. https://scholar.google.com/scholar?q=Pontius+Jr%2C+R.G.%2C+2022.+Metrics+That+Make+a+Difference.+Springer+Nature+Switzerland+AG:+Cham,+Switzerland.+ISBN-10:+3030707644

135. Pontius, R. G., Jr., & Millones, M. (2011). Death to kappa: Birth of quantity disagreement and allocation disagreement for accuracy assessment. *International Journal of Remote Sensing*, *32*(15), 4407–4429. https://doi.org/10.1080/01431161.2011.552923

136. Poleman, H. (2018). Assessing access to green areas in Europe's cities. In *A walk to the park? Assessing access to green areas in Europe's cities* (Working Paper). European Commission, DG for Regional and Urban Policy. https://ec.europa.eu/regional_policy/en/information/publications/working-papers/2018/a-walk-to-the-park-assessing-access-to-green-areas-in-europe-s-cities

137. Padma, S., & Sanjeevi, S. (2014). Jeffries Matusita based mixed-measure for improved spectral matching in hyperspectral image analysis. *International Journal of Applied Earth Observation and Geoinformation*, *32*, 138–151. https://doi.org/10.1016/j.jag.2014.04.001

138. Pregun, C. Z. (2022). Dynamics of self-regulatory processes in a lowland river due to seasonal changes in certain hydro-ecological and water quality factors. *Ecological Engineering*, *178*, Article 106595. https://doi.org/10.1016/j.ecoleng.2022.106595

139. Pulighe, G., & Lupia, F. (2020). Food first: COVID-19 outbreak and cities lockdown a booster for a wider vision on urban agriculture. *Sustainability*, *12*(12), 5012. https://doi.org/10.3390/su12125012

140. Paranychianakis, N. V., Salgot, M., Snyder, S. A., & Angelakis, A. N. (2015). Water reuse in EU states: Necessity for uniform criteria to mitigate human and environmental risks. *Critical Reviews in Environmental Science and Technology*, *45*(13), 1409–1468. https://doi.org/10.1080/10643389.2014.955629

141. Patle, P., & Sharma, A. (2025). *A novel coupled hydrological model-water accounting framework for quantification of water resources and agricultural production*. *Journal of Hydrology*, *661*(Part B), Article 133676. https://doi.org/10.1016/j.jhydrol.2025.133676

142. Pontius Jr, R. G., & Millones, M. (2011). Death to kappa: Birth of quantity disagreement and allocation disagreement for accuracy assessment. *International Journal of Remote Sensing*, *32*(15), 4407–4429. https://doi.org/10.1080/01431161.2011.552923

143. Parsons, L. A., Shindell, D., Tigchelaar, M., Zhang, Y., & Spector, J. T. (2021). Increased labor losses and decreased adaptation potential in a warmer world. *Nature Communications*, *12*(1), 7286. https://doi.org/10.1038/s41467-021-27328-y

144. Pénzes, J., Hegedűs, L. D., Makhanov, K., & Túri, Z. (2023). Changes in the patterns of population distribution and built-up areas of the rural–urban fringe in post-socialist context—A Central European case study. *Land*, *12*, 1682. https://doi.org/10.3390/land12091682

145. Qingyan, S., Chuiyu, L., Hui, G., Lingjia, Y., Xin, H., Tao, Q., Chu, W., Qinghua, L., Bo, Z., & Zepeng, L. (2021). Study on hydrologic effects of land use change using a distributed hydrologic model. *Water*, *13*(4), 447. https://doi.org/10.3390/w13040447

146. Q. Zhou, H. Tollerud, C. Barber, K. Smith, D. Zelenak Training data selection for annual land cover classification for the land change monitoring, assessment, and projection (LCMAP) initiative Remote Sens., 12 (4) (2022), p. 699,10.3390/rs12040699

147. Qin, Q., Xu, D., Hou, L., Shen, B., & Xin, X. (2021). Comparing vegetation indices from Sentinel-2 and Landsat 8 under different vegetation gradients based on a controlled grazing experiment. *Ecological Indicators*, *133*, Article 108363. https://doi.org/10.1016/j.ecolind.2021.108363

148. Roy, D. P., Wulder, M. A., Loveland, T. R., & Woodcock, C. E. (2014). Landsat-8: Science and product vision for terrestrial global change research.

Remote Sensing of Environment, 145, 154–172. https://doi.org/10.1016/j.rse.2014.02.001

149. Ramier, D., Berthier, E., & Andrieu, H. (2011). The hydrological behavior of urban streets: Long-term observations and modelling of runoff losses and rainfall–runoff transformation. *Hydrological Processes, 25*(14), 2161–2178. https://doi.org/10.1002/hyp.7968

150. Rahman, Z. A., Al Kafy, A., Saha, M., Rahim, A. A., Almulhim, A. I., Rahman, S. N., Fattah, M. A., Rahman, M. T., Kalaivani, S., Faisal, A. A., & Rakib, A. A. (2022). Assessing the impacts of vegetation cover loss on surface temperature, urban heat island and carbon emission in Penang city, Malaysia. *Building and Environment, 222*, 109335. https://doi.org/10.1016/j.buildenv.2022.109335

151. Roy, D. P., Kovalskyy, V., Zhang, H. K., Vermote, E. F., Yan, L., Kumar, S. S., & Egorov, A. (2016). Characterization of Landsat-7 to Landsat-8 reflective wavelength and normalized difference vegetation index continuity. *Remote Sensing of Environment, 185*, 57–70. https://doi.org/10.1016/j.rse.2015.12.024

152. Rogerson, C. M. (2010). In search of urban agriculture in South Africa. *Cities*, *27*(1), 38–45. https://doi.org/10.1016/j.cities.2009.10.005

153. Resh, H. M. (2013). *Hydroponic food production: A definitive guidebook for the advanced home gardener and the commercial hydroponic grower* (7th ed.). CRC Press.

154. Rajalakshmi, M., Manoj, V. R., & Manoj, H. (2022). Comprehensive review of aquaponic, hydroponic, and recirculating aquaculture systems. *Journal of Experimental Biology and Agricultural Sciences*, 10(6), 1266–1289. https://doi.org/10.18006/2022.10(6).1266.1289

155. Mustapha, M. R., Lim, H. S., & Mat Jafri, M. Z. (2010). Comparison of neural network and maximum likelihood approaches in image classification. *Journal of Applied Sciences, 10*(22), 2847–2854. https://doi.org/10.3923/jas.2010.2847.2854

156. Rembold, F., Atzberger, C., Rojas, O., & Savin, I. (2013). Using low resolution satellite imagery for yield prediction and yield anomaly detection. *Remote Sensing, 5*(11), 5572–5573. https://doi.org/10.3390/rs5041704

157. Strategy 24. (2023). *Debrecen fenntartható városfejlesztési stratégiája 2021–2027: Stratégiai munkarész*. Hajdú-Bihar Megyei Közigazgatási Portál.

Retrieved from https://hbmo.hu/portal/wp-content/uploads/2023/12/01B_eloterj.mell._DMJV-FVS-2021-27-strategiai-munkaresz.pdf

158. Szilassi, P. (2017). Magyarországi kistájak felszínborítás változékonysága és felszínborítás mozaikosságuk változása. *Tájökológiai Lapok, 15*(2), 131–138. https://doi.org/10.56617/tl.3612

159. Sajjad, H., Mubeen, M., & Karuppannan, S. (2022). Land use and land cover (LULC) change analysis using TM, ETM+ and OLI Landsat images in Okara District, Punjab, Pakistan. *Physics and Chemistry of the Earth, Parts A/B/C, 126*, 103117. https://doi.org/10.1016/j.pce.2022.103117

160. Stehman, S. V. (2014). Estimating area and map accuracy for stratified random sampling when the strata are different from the map classes. *International Journal of Remote Sensing*, *35*(17), 4923–4939. https://doi.org/10.1080/01431161.2014.930207

161. , W. D., Yim, J. S., & Lee, J. S. (2024). Assessing land cover classification accuracy: Variations in dataset combinations and deep learning models. Remote Sensing, 16(14), 2623. https://doi.org/10.3390/rs16142623

162. Specht, K., Siebert, R., Hartmann, I., Freisinger, U. B., Sawicka, M., Werner, A., & Dierich, A. (2014). Urban agriculture of the future: An overview of sustainability aspects of food production in and on buildings. *Agriculture and Human Values*, *31*(1), 33–51. https://doi.org/10.1007/s10460-013-9448-4

163. Stehman, S. V. (2014). Estimating area and map accuracy for stratified random sampling when the strata are different from the map classes. International Journal of Remote Sensing, 35(17), 4923–4939. https://doi.org/10.1080/01431161.2014.930207

164. Safari, F., De Smedt, F., & Moreda, F. (2012). WetSpa model application in the Distributed Model Intercomparison Project (DMIP2). *Journal of Hydrology, 418–419*, 78–89. https://doi.org/10.1016/j.jhydrol.2009.04.001

165. Settembre, G., Taggio, N., Del Buono, N., Esposito, F., Di Lauro, P., & Aiello, A. (2024). A land cover change framework analyzing wildfire-affected areas in bitemporal PRISMA hyperspectral images. *Mathematics and Computers in Simulation, 229*, 855–866. https://doi.org/10.1016/j.matcom.2024.10.034

166. Su, Y., Zhao, J., Wang, M., Chen, R., Shao, M., & Lu, Z. (2025). Ecological stability in watershed: What to measure and how to measure it.

Ecological Frontiers, In Press, Corrected Proof. https://doi.org/10.1016/j.ecofro.2025.04.010

167. Su, M., Guo, R., Chen, B., Hong, W., Wang, J., Feng, Y., & Xu, B. (2020). Sampling strategy for detailed urban land use classification: A systematic analysis in Shenzhen. *Remote Sensing, 12*(9), 1497. https://doi.org/10.3390/rs12091497

168. Sandu, M. A., & Virsta, A. (2015). Applicability of MIKE SHE to simulate hydrology in Argesel River catchment. *Agricultural and Agricultural Science Procedia, 6*, 517–524. https://doi.org/10.1016/j.aaspro.2015.08.135

169. Szilassi, P. (2017). Magyarországi kistájak felszínborítás változékonysága és felszínborítás mozaikosságuk változása [Land cover variability and mosaic change of small regions in Hungary]. *Tájökológiai Lapok, 15*(2), 131–138. https://doi.org/10.56617/tl.3612

170. STRATEGY 24. (2023). *Debrecen fenntartható városfejlesztési stratégiája 2021–2027: Stratégiai munkarész* [Debrecen Sustainable Urban Development Strategy 2021–2027: Strategic section]. Hajdú-Bihar Megyei Közigazgatási Portál. https://hbmo.hu/portal/wp-content/uploads/2023/12/01B_eloterj.mell._DMJV-FVS-2021-27-strategiai-munkaresz.pdf

171. Shi, F., & Li, M. (2021). Assessing land cover and ecological quality changes under the new-type urbanization from multi-source remote sensing. *Sustainability, 13*(21), 11979. https://doi.org/10.3390/su132111979

172. S. Talukdar, P. Singha, S. Mahato, Shahfahad, S. Pal, Y.-A. Liou, A. Rahman Land-use land-cover classification by machine. learning classifiers for satellite observations—a review Remote Sens, 12 (2020), p. 1135, 10.3390/rs12071135

173. S. Kim, J. Kim, H. Kang, W.S. Jang, K.J. Lim Analysis of water balance changes and parameterization reflecting soil characteristic in a hydrological simulation program-FORTRAN model Water MDPI, 14 (6) (2022), 10.3390/w14060990

174. Somlyai, I., Berta, C., Nagy, S. A., Dévai, G., Ács, É., Szabó, L. J., Nagy, J., & Grigorszky, I. (2019). Heterogeneity and anthropogenic impacts on a small lowland stream. *Water, 11*(10), Article 2002. https://doi.org/10.3390/w11102002

175. Schueler, T. (editor). “Impact of suspended and deposited sediment.” Watershed Protection Techniques. Vol. 2, no.3, pp. 443. February 1997a

176. Sucozhañay, A., Pesántez, J., Guerrero-Coronel, R., Guerrero-Coronel, R., Peña, D., & Célleri, R. (2024). Rainwater harvesting as a sustainable solution for the production of urban hydroponic crops. *Water Reuse*, 14(2), 177–189. https://doi.org/10.2166/wrd.2024.151

177. Soil and Water Conservation Society (SWCS). (2003). *Conservation implications of climate change: Soil erosion and runoff from cropland* (SWCS Report). https://www.swcs.org/static/media/cms/Climate_changefinal_112904154622.pdf

178. Srivastav, A. L., Madhav, S., Bhardwaj, A. K., & Jones, E. V. (2022). Urban water crisis and management: Strategies for sustainable development. In *Current Directions in Water Scarcity Research* (Vol. 6). Elsevier. ISBN: 9780323918381

179. Smerdon, B. D., Allen, D. M., Grasby, S. E., & Berg, M. A. (2009). An approach for predicting groundwater recharge in mountainous watersheds. *Journal of Hydrology*, *365*(3–4), 156–172. https://doi.org/10.1016/j.jhydrol.2008.11.023

180. Schott, J. R. (2002). *Remote sensing: Active and passive systems and applications* (1st ed.). Oxford University Press. (Chapter 13: Image classification). https://scholar.google.com/scholar_lookup?title=Remote%20Sensing%3A%20Active%20and%20Passive%20Systems%20and%20Applications&publication_year=2002&author=J.R.%20Schott

181. Town of Buckeye Public Works Department. (2007). *Storm water drainage system design manual* (p. 70). Buckeye, AZ: Town of Buckeye, Engineering Division.

182. Talha, M., Farrukh, A. B., Sajid, G., & Hamza, Z. (2023). ADU-Net: Semantic segmentation of satellite imagery for land cover classification. *Advances in Space Research, 72*(5), 1780–1788. https://doi.org/10.1016/j.asr.2023.05.007

183. Tarawally, M., Wenbo, X., Weiming, H., Mushore, T. D., & Kursah, M. B. (2019). Land use/land cover change evaluation using Land Change Modeller: A comparative analysis between two main cities in Sierra Leone. *Remote Sensing Applications: Society and Environment, 16*, 100262. https://doi.org/10.1016/j.rsase.2019.100262

184. Tallis, H. T., Ricketts, T., Guerry, A. D., Wood, S. A., Sharp, R., Nelson, E., Ennaanay, D., Wolny, S., Olwero, N., Vigerstol, K., Pennington, D., Mendoza, G., Aukema, J., Foster, J., Cameron, D., Arkema, K., Lonsdorf, E., Kennedy, C., Verutes, G., Kim, C. K., Lacayo, M. (2013). A modeling suite developed by the Natural Capital Project to support environmental decision making. In *InVEST 2.5.6 User's Guide* (p. 347)https://scholar.google.com/scholar?q=Tallis%2C%20H.T.%2C%20Ricketts%2C%20T.%2C%20Guerry%2C%20A.D.%2C%20Wood%2C%20S.A.%2C%20Sharp%2C%20R.%2C%20Nelson%2C%20E.%2C%20Ennaanay%2C%20D.%2C%20Wolny%2C%20S.%2C%20Olwero%20N.%2C%20Vigerstol%2C%20K.%2C%20Pennington%2C%20D.%2C%20Mendoza%2C%20G.%2C%20Aukema%2C%20J.%2C%20Foster%2C%20J.%2C%20Cameron%2C%20D.%2C%20Arkema%2C%20K.%2C%20Lonsdorf%2C%20E.%2C%20Kennedy%2C%20C.%2C%20Verutes%2C%20G.%2C%20Kim%2C%20C.K.%2C%20Guannel%2C%20G.%2C%20Papenfus%2C%20M.%2C%20Toft%2C%20J.%2C%20Marsik%2C%20M.%2C%20Bernhardt%2C%20J.%2C%20Griffin%2C%20R.%2C%20Glowinski%2C%20K.%2C%20Chaumont%2C%20N.%2C%20Perelman%2C%20A.%2C%20Lacayo%2C%20M.%2C%202013.%20A%20Modeling%20Suite%20Developed%20By%20The%20Natural%20Capital%20Project%20to%20Support%20Environmental%20Decision%20Making%2C%20In%20InVEST%202.5.6%20User%27s%20Guide.%20Stanford%20CA%2C%20347.

185. Turc, L. (1961). Water requirements assessment of irrigation, potential evapotranspiration: Simplified and updated climatic formula. *Annales Agronomiques*, *12*, 13–49.

186. Tucker, C. J. (1979). Red and photographic infrared linear combinations for monitoring vegetation. *Remote Sensing of Environment*, *8*(2), 127–150. https://doi.org/10.1016/0034-4257(79)90013-0

187. Timothée,S.-S.–Rodolphe,C.–Matthieu,F.(2018): The shape of watersheds.Nature Communicationsvolume9, Articlenumber:3791 (2018)

188. Tony, V. M. S., & Jorge, R. (2022). On the quality of the drainage network cartographic representation. *Ecological Indicators*, *143*, Article 109350. https://doi.org/10.1016/j.ecolind.2022.109350

189. Thomaier, S., Specht, K., Henckel, D., Dierich, A., Siebert, R., Freisinger, U., & Sawicka, M. (2015). Farming in and on urban buildings: Present practice

and specific novelties of Zero-Acreage Farming (ZFarming). *Renewable Agriculture and Food Systems*, *30*(1), 43–54. https://doi.org/10.1017/S1742170514000143

190. T. Zhang, J. Su, Z. Xu, Y. Luo, J. Li Sentinel-2 satellite imagery for urban land cover classification by optimized random forest classifier Appl. Sci., 11 (2021), p. 543, 10.3390/app11020543

191. Talukdar, S., Singha, P., Mahato, S., Shahfahad, Pal, S., Liou, Y.-A., & Rahman, A. (2020). Land-use land-cover classification by machine learning classifiers for satellite observations—A review. *Remote Sensing*, *12*(7), 1135. https://doi.org/10.3390/rs12071135

192. Tamás, J., Nagy, A., Buday-Bódi, E., Gálya, B., Nistor, S., & Fehér, J. (2019). *Guideline - Application of the process oriented spatial decision support tools: Methods in urban hydrology for middle-sized cities in CEE based on the reference sites* (p. 93). University of Debrecen. ISBN: 978-963-490-162-4

193. University Corporation for Atmospheric Research, COMET® Program. (2010). *Runoff processes: International edition*. Retrieved from https://www.meted.ucar.edu/hydro/basic_int/runoff/navmenu.php

194. UNESCO, OMM, & AISH. (1974). *Design of water resources projects with inadequate data: Proceedings of the Madrid Symposium* (Vol. 1). UNESCO. https://unesdoc.unesco.org/ark:/48223/pf0000013828

195. USGS. (2016). *Earth Explorer*. https://earthexplorer.usgs.gov/

196. Urbancsek, J. (1960). Az alföldi artézi kutak fajlagos vízhozama és abból levonható vízföldtani és ősföldrajzi következtetések. *Hidrológiai Közlöny, 40*(5), 398–403.https://scholar.google.com/scholar_lookup?title=Az%20alf%C3%B6ldi%20art%C3%A9zi%20kutak%20fajlagos%20v%C3%ADzhozama%20%C3%A9s%20abb%C3%B3l%20levonhat%C3%B3%20v%C3%ADzf%C3%B6ldtani%20%C3%A9s%20%C5%91sf%C3%B6ldrajzi%20k%C3%B6vetkeztet%C3%A9sek&publication_year=1960&author=J.%20Urbancsek

197. United Nations. (2022). *World urbanization prospects: The 2022 revision*. Department of Economic and Social Affairs, Population Division. https://population.un.org/wup/

198. United Nations. (2005). *World urbanization prospects: The 2005 revision*. Department of Economic and Social Affairs, Population Division.

199. Várallyay, G. Y., & Molnár, S. (1989, July). The agro-topographical map of Hungary. In *14th World Conference ICA/ACI*, Budapest (pp. 221–225). *Hungarian Cartographical Studies*. Retrieved from https://scholar.google.com/scholar_lookup?title=The%20agro-topographical%20map%20of%20Hungary.%20Hungarian%20Cartographical%20Studies&publication_year=1989&author=G.Y.%20V%C3%A1rallyay&author=S.%20Moln%C3%A1r

200. Vrebos, D., Vansteenkiste, T., States, J., Willems, P., & Meire, P. (2014). Water displacement by sewer infrastructure in the Grote Nete catchment, Belgium, and its hydrological regime effects. *Hydrology and Earth System Sciences, 18*, 1119–1136. https://doi.org/10.5194/hessd-10-7425-2013

201. Widiyanti, R., Sari, R. P., & Rahmanto, F. (2022). Greywater reuse for soilless cultivation using bioretention systems: A sustainable approach. Desalination, 221(1-3), 66-79. https://doi.org/10.1016/j.desal.2008.03.048

202. Weng, Q., & Lu, D. (2008). A sub-pixel analysis of urbanization effect on land surface temperature and its interplay with impervious surface and vegetation coverage in Indianapolis, United States. *International Journal of Applied Earth Observation and Geoinformation, 10*(1), 68–83. https://doi.org/10.1016/j.jag.2007.05.002

203. Wakode, H. B., Baier, K., Jha, R., & Azzam, R. (2018). *Impact of urbanization on groundwater recharge and urban water balance for the city of Hyderabad, India*. *International Soil and Water Conservation Research, 6*(1), 51–62. https://doi.org/10.1016/j.iswcr.2017.10.003

204. Wu, T., Chen, Z., Zhou, S., Huang, R., Xing, P., Li, S., Qiao, R., & Wu, Z. (2025). Joint evaluation of urban built environment's driving patterns on urban heat island (UHI) and urban moisture island (UMI). Sustainable Cities and Society, 122, 106450. https://doi.org/10.1016/j.scs.2025.106450

205. Welle,P.I.–Woodward,D.(1986): Engineering hydrology-time of concentration. Technical note 4, US Department of Agriculture, Soil Conservation Service, Pennsylvania

206. Wong, Y. H. T., Habibah, M. A. B. H. M., & Choy, W. W. (2022). Urban Heat Island Mitigation: GIS-Based Analysis for a Tropical City Singapore. *International Journal of Environmental Research and Public Health, 19*(11917). https://doi.org/10.3390/ijerph191911917

207. Xu, X., Long, D., Li, X., Wang, Y., Zhao, F., & Cui, Y. (2024). Unveiling lake ice phenology in Central Asia under climate change with MODIS data and a two-step classification approach. *Remote Sensing of Environment, 301*, Article 113955. https://doi.org/10.1016/j.rse.2023.113955

208. Yong, M., & Lim, K. H. (2020, December 5). *Urban Heat Islands: Beating the Heat with Multi-Modal Spatial Analysis*. arXiv. https://doi.org/10.48550/arXiv.2012.03049

209. Yonaba, R., Koïta, M., Mounirou, L. A., Tazen, F., Queloz, P., Biaou, A. C., Niang, D., Zouré, C., Karambiri, H., & Yacouba, H. (2021). Spatial and transient modelling of land use/land cover (LULC) dynamics in a Sahelian landscape under semi-arid climate in northern Burkina Faso. *Land Use Policy, 103*, 105305. https://doi.org/10.1016/j.landusepol.2021.105305

210. Yan, X., Li, J., Smith, A. R., Yang, D., Ma, T., & Su, Y. (2023). Rapid land cover classification using a 36-year time series of multi-source remote sensing data. *Land*, *12*(12), Article 2149. https://doi.org/10.3390/land12122149

211. Zhang, K., Cao, C., Chu, H., Zhao, L., Zhao, J., & Lee, X. (2023). Increased heat risk in wet climate induced by urban humid heat. *Nature, 617*(7962), 738–742. https://doi.org/10.1038/s41586-023-05911-1

212. Kavzoglu, T., & Mather, P. M. (2000). Using feature selection techniques to produce smaller neural networks with better generalization capabilities. In Proceedings of the IGARSS 2000. IEEE 2000 International Geoscience and Remote Sensing Symposium: Taking the Pulse of the Planet: The Role of Remote Sensing in Managing the Environment (Vol. 7, pp. 23–31). IEEE. https://doi.org/10.1109/IGARSS.2000.860339

213. Z.Zhu,A.L.Gallant,C.E.Woodcock,B.Pengra,P.Olofsson,T.R.Loveland,S. Jin,D.Dahal,L.Yang,R.F.Auch; Optimizing selection of training and auxiliary data for operational land cover classification for the LCMAP initiative ISPRS J. Photogramm. Remote Sens., 122 (2016), pp. 206-221, 10.1016/j.isprsjprs.2016.11.004

214. Zhao, S., Tu, K., Ye, S., Tang, H., Hu, Y., & Xie, C. (2023). Land use and land cover classification meets deep learning: A review. *Sensors, 23*(21), 8966. https://doi.org/10.3390/s23218966

215. Zezza, A., & Tasciotti, L. (2010). Urban agriculture, poverty, and food security: Empirical evidence from a sample of developing countries. *Food Policy*, *35*(4), 265–273. https://doi.org/10.1016/j.foodpol.2010.04.007

216. Z. Xie, Y. Chen, D. Lu, G. Li, E. Chen Classification of land cover, forest, and tree species classes with ZiYuan-3 multispectral and stereo data Remote Sens.,11 (2) (2019), p.164,10.3390/rs11020164

217. Zhou, Q., Tollerud, H., Barber, C., Smith, K., & Zelenak, D. (2022). Training data selection for annual land cover classification for the Land Change Monitoring, Assessment, and Projection (LCMAP) initiative. *Remote Sensing*, *12*(4), 699. https://doi.org/10.3390/rs12040699

218. Zhu, Z., Gallant, A. L., Woodcock, C. E., Pengra, B., Olofsson, P., Loveland, T. R., Jin, S., Dahal, D., Yang, L., & Auch, R. F. (2016). Optimizing selection of training and auxiliary data for operational land cover classification for the LCMAP initiative. *ISPRS Journal of Photogrammetry and Remote Sensing*, *122*, 206–221. https://doi.org/10.1016/j.isprsjprs.2016.11.004

219. Dams, J., Dujardin, J., Reggers, R., Bashir, I., Canters, F., & Batelaan, O. (2013). Mapping impervious surface change from remote sensing for hydrological modelling. *Journal of Hydrology*, *485*, 84–95. https://doi.org/10.1016/j.jhydrol.2012.09.045

220. Bakacsi, Z., Laborczi, A., Szabó, J., Takács, K., & Pásztor, L. (2014). Proposed correlation between the legend of the 1:100,000 scale geological map and the FAO code system for soil parent material. *Agrokémia és Talajtan, 63*(2), 189–202. https://doi.org/10.1556/agrokem.63.2014.2.3

11. APPENDIX

Table 15. List of L8 datasets used in this study.

Year	Season	L8 Product Identifier L1	Acquisition time
2013	Summer	LC08_L1TP_186027_20130809_20200912_02_T1	2013.08.09 9:22
2013	Winter	LC08_L1TP_186027_20140116_20200912_02_T1	2014.01.16 9:21
2014	Summer	LC08_L1TP_186027_20140609_20200911_02_T1	2014.06.09 9:20
2014	Winter	LC08_L1TP_186027_20150220_20200909_02_T1	2015.02.20 9:20
2015	Winter	LC08_L1TP_186027_20150220_20200909_02_T1	2015.02.20 9:20
2015	Summer	LC08_L1TP_186027_20150612_20200909_02_T1	2015.06.12 9:19
2015	Summer	LC08_L1TP_186027_20150815_20200908_02_T1	2015.08.15 9:20
2016	Winter	LC08_L1TP_186027_20160207_20200907_02_T1	2016.02.07 9:20
2016	Summer	LC08_L1TP_186027_20160630_20200906_02_T1	2016.06.30 9:20
2017	Winter	LC08_L1TP_186027_20170225_20200905_02_T1	2017.02.25 9:20
2017	Summer	LC08_L1TP_186027_20170804_20200903_02_T1	2017.08.04 9:20
2018	Winter	LC08_L1TP_186027_20171226_20200902_02_T1	2017.12.26 9:20
2018	Summer	LC08_L1TP_186027_20180807_20200831_02_T1	2018.08.07 9:19
2019	Winter	LC08_L1TP_186027_20190215_20200829_02_T1	2019.02.15 9:20
2019	Summer	LC08_L1TP_186027_20190607_20200828_02_T1	2019.06.19 9:20

Table 16. List of S2 MSI and L8 OLI sensor datasets utilised in this research

		Growth Season	Product Identifier	Acquisition time UTC
Landsat-8	2018	June	LC08_L1TP_186027_20180620_20200831_02_T1	2018/06/20 09:20
		July	LC08_L1TP_186027_20180706_20200831_02_T1	2018-07-06 09:20
		August	LC08_L1TP_186027_20180823_20200831_02_T1	2018-08-23 09:20
		September	LC08_L1TP_186027_20180908_20200831_02_T1	2018-09-08 09:20
	2020	June	LC08_L1TP_186027_20200625_20200823_02_T1	2020-06-25 09:20
		July	LC08_L1TP_186027_20200711_20200912_02_T1	2020-07-11 09:20
		August	LC08_L1TP_186027_20200828_20200906_02_T1	2020-08-28 09:20
		September	LC08_L1TP_186027_20200913_20200919_02_T1	2020-09-13 09:20
	2022	June	LC09_L1TP_186027_20220623_20230410_02_T1	2022-06-23 09:20
		July	LC09_L1TP_186027_20220725_20230406_02_T1	2022-07-25 09:20
		August	LC08_L1TP_186027_20220818_20220824_02_T1	2022-08-18 09:21
		September	LC09_L1TP_186027_20220911_20230329_02_T1	2022-09-11 09:20
Sentinel-2	2018	June	S2A_MSIL1C_20180619T094031_N0500_R036_T34TET_20230811T190137	2018-06-19 09:40
		July	S2B_MSIL1C_20180714T094029_N0500_R036_T34TET_20230820T012645	2018-07-14 09:40
		August	S2A_MSIL1C_20180828T094031_N0206_R036_T34TET_20180828T121318	2018-08-28 09:40
		September	S2B_MSIL1C_20180919T093029_N0500_R136_T34TET_20230820T025309	2018-09-19 09:30:
	2020	June	S2A_MSIL1C_20200628T094041_N0500_R036_T34TET_20230506T074207	2020-06-28 09:40:
		July	S2A_MSIL1C_20200705T093041_N0500_R136_T34TET_20230530T081333	2020-07-05 09:30
		August	S2B_MSIL1C_20200829T093039_N0209_R136_T34TET_20200829T105201	2020-08-29 09:30
		September	S2B_MSIL1C_20200921T094039_N0209_R036_T34TET_20200921T111126	2020-09-21 09:40
	2022	June	S2A_MSIL1C_20220628T094041_N0400_R036_T34TET_20220628T113959	2022-06-28 09:40
		July	S2B_MSIL1C_20220720T092559_N0400_R136_T34TET_20220720T101237	2022-07-20 09:25

August	S2B_MSIL1C_20220819T092549_N0400_R136_T34TET_20220819T101112	2022-08-19 09:25
September	S2B_MSIL1C_20220928T093039_N0400_R136_T34TET_20220928T101405	2022-09-28 09:30:

Source: ESA and NASA.

Table 17. Crop coefficients (K_c) for the main types of vegetation of Debrecen land use and LC categories.

LC categories based on references	Crop coefficients (K_c) based on references	LC categories of Debrecen	Crop coefficients (K_c) for Debrecen
Urban and Built-up	0.001	Sealed surface	0.001
Orchards/Vineyards	0.7	Area with crop Cover	0.783
Mixed vegetation cover	1		
Cropland (Row Crops)	0.65		
Wooded Grassland	1	Lawns and pasture	0.833
Grazing Pasture	0.65		
Pasture	0.85		
Urban and Built-up	0.001	Semi sealed surface	0.26
Bare Ground	0.001		
Wooded Grassland	1		
Open Shrubland	0.398		
Evergreen Needle Leaf Forest	1	Forest	1
Evergreen Broadleaf Forest	1		
Bare Ground	0.001	Bare ground	0.001
Open Water and < 2 m depth	1.2	Surface water bodies	1.2
Open Water and > 5 m depth	1		
Stagnant Water	1.4		

Source: Tallis et al. 2013

12. ACKNOWLEDGEMENT

First and foremost, I thank God Almighty for His endless blessings, strength, and guidance throughout my PhD journey. Without His grace, I would not have reached this point.

I am deeply grateful to my supervisor, Prof. Dr. Attila Nagy, for his unwavering support, insightful guidance, and continuous encouragement, which have been instrumental in shaping my academic and professional growth. I also extend my sincere thanks to Prof. Dr. Tamás János for his valuable academic input and mentorship.

I wish to express my heartfelt appreciation to Dr. Jung András and Dr. Péter Riczu, the reviewers of my dissertation, for their thoughtful evaluation and constructive feedback, which have enriched the final version of this work.

My sincere thanks go to the Institute of Water and Environmental Management, Faculty of Agricultural and Food Sciences and Environmental Management, University of Debrecen, for providing institutional support and a research environment that fostered my development. I am also grateful for the financial and academic support provided by the RRF-2.3.1-21-2022-00008 project, which played a significant role in the successful completion of this research.

Finally, I would like to thank my beloved family Baba essedik, Choubi, lhajja, Oussama, Roa, Amal, Wahid, Jasmouna, Lotfi, Zikou, Youba, Saadoun for their unconditional love and support throughout this journey, and a very special thanks to my sweet Adrienn Touta, whose love, patience, and encouragement have meant the world to me and to Ammi Dasti.

13. STATEMENTS

STATEMENT

I wrote this thesis in the framework of the University of Debrecen Food Sciences Doctoral School for the purpose of obtaining a doctoral degree (Ph.D.) at the University of Debrecen.

Debrecen, 7 January 2026.

.....

Signature of the candidate

STATEMENT

I hereby certify that the doctoral candidate Douraied Guizani has carried out his work under my supervision within the framework of the above-mentioned Doctoral School between 2021-2026. The candidate has made a decisive contribution to the results of the thesis through his independent creative work, and the thesis is the candidate's independent work. I recommend that the thesis be accepted.

Debrecen, 7 January 2026.

.....

Signature of the supervisor(s)